POLYKETONE SYTNHESIS, POST-POLYMERIZATION FUNCTIONALIZATION AND PER-AND POLYFLUORINATED ALKYL SUBSTANCE ADSORPTION

A Dissertation
Submitted to the
Temple University Graduate Board

In Partial Fulfilment
of the Requirements for the Degree of
DOCTOR OF PHILOSOPHY

---

by
Thomas R. Boller, Jr.
May 2023

Examining Committee Members:

Dr. Graham E. Dobereiner, Thesis Advisor, Department of Chemistry
Dr. Ann M. Valentine, Department of Chemistry
Dr. Stephanie L. Wunder, Department of Chemistry
Dr. Marc A. Ilies, External Member, School of Pharmacy, Temple University

ABSTRACT

This thesis focuses largely on the synthesis, application, and degradation of olefin-based polymers. The metal-catalyzed copolymerization of olefin and carbon monoxide to form polyketones and its associated mechanism are of central concern. The role of the metal catalyst counter-anion and its associated coordination strength are of interest during the copolymerization, as it is theorized that such coordination strength may disrupt polymer-metal chelate formation and improve overall catalyst activity if balanced correctly. To achieve the balanced counter-anion coordination strength, novel imidazolyl-phenyl (IMP) anions with variable functionality were paired with palladium catalysts and used in the copolymerization. Polymerizations of 1-hexene and carbon monoxide with palladium-IMP systems showed no variability as anion coordination strength was varied, however when allyl glycidyl ether is implemented as the olefin results indicate a potential anion dependence for polymerization.

The degradation of polyketones through a pathway of post-polymerization modification is also studied. Akrotek PK-VM polyketones were successfully altered to polyoximes by addition of hydroxylamine. The conversion of polyketone carbonyl groups to oxime functionality caused a change in crystallinity as observed by differential scanning calorimetry and a decreased degradation temperature through thermal gravimetric analysis. Further functionalization to polyamides via a Beckmann rearrangement was unsuccessful, however polyoximes and their potential for aqueous metal chelation was studied for possible other applications. It was demonstrated through UV-vis analysis that polyoximes may have some capability to chelate to aqueous copper (ii) species, however the degree to which the residual solvent plays in this chelation is still unclear.

Applications of olefin-based polymers centered around the use of waste plastics such as polyethylene as adsorbents for per- and poly-fluorinated substances (PFAS) in water ways. Initial studies focused on the effects of plastic surface area and its relation to PFAS adsorption. Successful experimental design and implementation of appropriate characterization techniques were achieved. Additional research demonstrated the effects PFAS have on the morphology of lipid vesicles. Specifically, the interactions with the phospholipid bilayers. PFAS is found to have a measurable effect on the phase transition temperature of lipid vesicles and the overall stability of the bilayer.

DEDICATION

This thesis is dedicated to my loving parents Tom and Kara Boller, to my brother Christopher, and fiancé Leonie, whose unrelenting support and guidance have led me to this achievement.

ACKNOWLEDGEMENTS

In the past five years I have had one of the greatest experiences in terms of academic growth and personal development in my life. I would like to thank my advisor Dr. Graham Dobereiner for making it possible. Graham has always been available to help, listen, and advise in times of need. He has been a guiding light through this often-foggy maze of research and a pristine role model for all students. I would also like to thank Dr. Ann Valentine for serving on my committee and for her work keeping the department running. I would like to thank Dr. Stephanie Wunder for serving on my committee and giving me critical advice pertaining to polymers and lipids. Thank you to Dr. Marc Ilies for serving as my external committee member and giving valuable insight into this thesis. I would also like to thank Dr. Charles DeBrosse for his mentorship and guidance with complex spectral problems and insight into my research. His expertise in NMR usage and maintenance makes him an integral part of the department and I am thankful to have had the honor of learning all that I have from him over the years. Thank you to all of the Dobereiner lab members both past and present. I am so happy to have been surrounded by lab mates who would drop anything to help out or give great advice on challenging problems. I would also like to acknowledge all of the undergraduate researchers I have had the opportunity to mentor. Tyler, Shannon, Shen and Sam: thank you for your contribution to this work and I hope you find success in your careers, wherever they may take you. Of all my experiences at Temple, I am most grateful for the friends I have made here. The graduate students in the chemistry department have been welcoming and friendly since day one of my first year and quickly made the initially overwhelming city of Philadelphia a second home for me. Specifically, I will always cherish my time with Dr. Alex Gardner, Justin Steets and Scott

Witte. We have been on many adventures together and I look forward to where each of our futures lead.

Most importantly I would like to thank my family, without whom I would not be able to accomplish this achievement. My mother Kara and father Tom have been supportive of me throughout my life and have ensured I make it through both good times and bad and I owe everything to them. Chris, you have always been a reliable, trustworthy, smart, and funny person and I am glad to call you my brother. You may be the younger one, but I see you as an exemplary brother. Lastly, but of great importance, I would like to thank my fiancé Leonie. You have supported me through the best and roughest times of my career. You've offered advice, given counsel, and have shown unwavering love and support through this journey from day one. I could not ask for someone better in my life, thank you for everything.

TABLE OF CONTENTS

LIST OF TABLES

Table **Page**

LIST OF FIGURES

Figure **Page**

CHAPTER 1

COUNTER-ANION EFFECTS ON TRANSITION METAL CATALYST ACTIVTIY DURING POLYKETONE COPOLYMERIZATION

1.1 Introduction

1.1.1 Polyketone Background

Polyketones are a versatile class of polymer known for their high tensile strength, as well as strong chemical- and physical resistance.[1, 2, 3] Applications include injection molding to form gears or other plastic parts,[4] fire resistant foams,[5] and films and coatings.[6, 7] Commonly, polyketones are synthesized by the copolymerization of an olefin and carbon monoxide (CO) to create either perfectly alternating or random copolymers[8] (Figure 1.1).

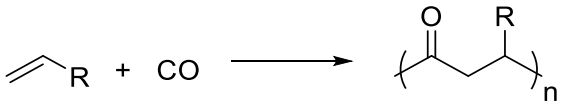

Figure 1.1: Copolymerization of olefin and carbon monoxide to make polyketones.

1.1.2 Metal Catalysts and Associated Ligands

Typically, such reactions are catalyzed by square planar cationic metal complexes with a d^8 electron configuration and an oxidation state of +2.[9] The most common metals used are nickel,[10, 11] rhodium,[12, 13] and palladium.[14, 15, 16] Typically, a bidentate ligand will accompany the metal with amines or phosphines as the chelating groups.[16, 17, 18, 19] The active catalyst has two vacant coordination sites, one from which the polymer chain will grow and the other, for incoming monomer which is to be incorporated into the chain

(Figure 1.2).[9] Therefore, pre-catalysts will most often possess two ancillary ligands opposite the bidentate chelate which can easily be dissociated.

1.1.3 Counter-Anions and Effects on Catalysis

The cationic catalysts are typically paired with weakly coordinating anions. Coordination strength of the anion impacts catalysis in multiple ways. Anions that prefer the outer coordination sphere will not compete with monomer for binding,[9, 20] while more strongly coordinating anions may form discrete bonds to the metal[21, 22] and block incoming monomers. However, very weakly coordinating anions may not effectively stabilize unsaturated cationic intermediates, initiating premature decomposition.[23] (Figure 1.3) Indeed, altering the coordination strength of counter-anion in the copolymerization of olefin and carbon monoxide affects the reaction rate.[9, 24, 25] Though comprehensive studies are lacking, early research and patents suggest that a counter-anion of weaker coordination strength is preferred for best results.[9]

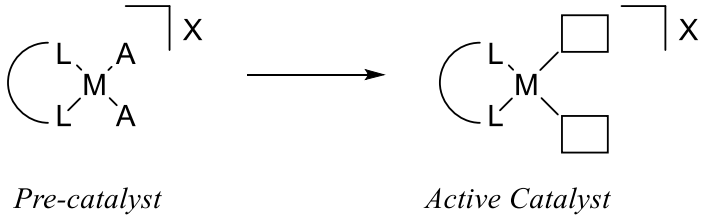

Figure 1.2: General pre-catalyst and active catalyst forms used in olefin carbon monoxide copolymerization. Bidentate ligand is denoted by "L" and ancillary ligands by "A". Blank boxes represent the vacant coordination sites.

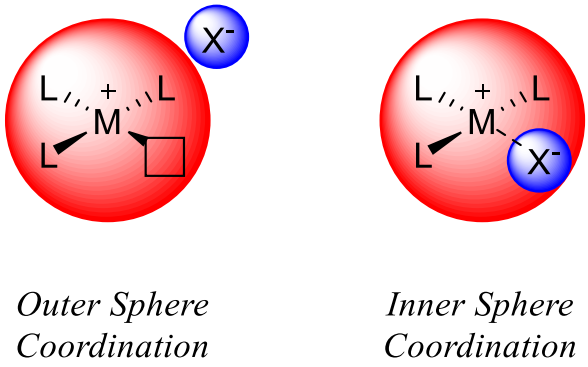

Figure 1.3: Possible coordination modes of counter-anion and metal cation complex. Metal is denoted by "M", ligands by "L" and counter-anion by "X".

Solvent is yet another factor affecting rate, as solvent molecules may compete with monomer for the vacant site on the metal complex. Small molecular solvents of high polarity like methanol or ethanol are likely exhibit stronger coordination to the metal cation, whereas more sterically encumbered polar solvents like *tert*-butyl alcohol exhibit a weaker binding.[26] Factors such as metal identity, bidentate ligand type, counter-anion coordination ability and solvent, all contribute to overall catalyst activity and therefore impact the polymerization. Changing variables in this process is therefore a delicate balancing act that - if tweaked correctly - produces a polymer of desirable properties.

1.1.4 Mechanism of Polyketone Copolymerization

The overall mechanism of the copolymerization of olefin and carbon monoxide is generally well understood, though the rate-determining step and identities of individual species remain elusive.[27] Three main steps of the polymerization cycle are initiation, propagation, and termination.[9] Initiation involves activating the metal species to begin the polymerization process. This may be done by either addition of methanol or olefin to the metal species, producing either a carbomethoxy species or a metal hydride.[9] Two

competing initiation mechanisms, in conjunction with two termination mechanisms, creates polymers with three possible end group combinations: the keto-ester, diester and diketone (Figure 1.4).[9]

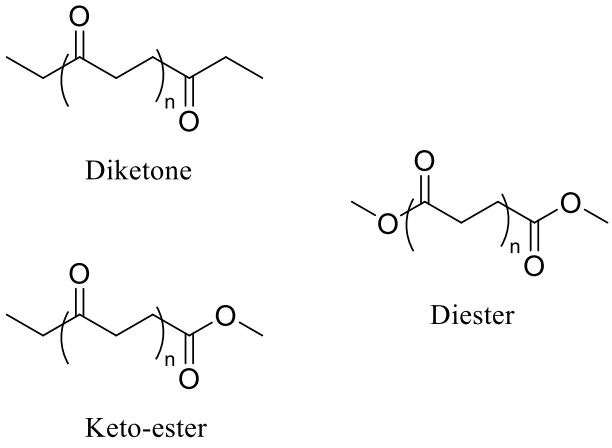

Figure 1.4: Possible polymer end groups following initiation and termination steps.

Propagation follows the initiation and involves the alternating insertion of olefin and carbon monoxide to the metal species. Double insertions of carbon monoxide do not occur due to thermodynamic unfavorability.[28, 29] Likewise, double insertions of olefin are also not observed, because the more strongly coordinating carbon monoxide is unlikely to be displaced by an olefin.[9, 30] As the polymer chain grows during propagation, there is a competition for the vacant metal site between counter-anion, solvent, and monomer. There is another possibility during propagation specifically: intramolecular chelation of a carbonyl group on the polymer chain (Figure 1.5).[31] Chelation may stabilize the metal species in between coordination of monomer, prevent binding of coordinating solvents, and prohibit double olefin insertions, thus maximizing the overall rate of copolymerization.[9] However, if the carbonyl does not dissociate for the incoming monomer, it may hinder catalyst activity. There are two chelation possibilities: a less stable

six atom ring formation in which the chelate may be more easily displaced (gamma chelate), and a stronger five atom ring structure (beta chelate) (Figure 1.5).[9] Coordination of the olefin can occur with the functional group alpha or beta to the metal, which may result in the orientation of the olefin being head-to-head or head-to-tail within the resulting polymer.[9]

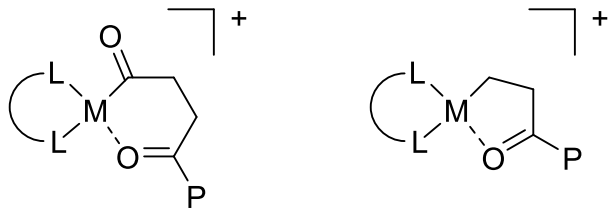

Gamma Chelate *Beta* Chelate

Figure 1.5: Possible chelation modes of polyketone carbonyl group to metal catalyst. "P" signifies the growing polymer chain.

Chain termination is the third and final portion of the polymerization cycle and is thought to follow two possible mechanisms. The first is protonolysis of the metal-polymer bond which produces a diketone end functionality, and the second being alcoholysis, producing the ester functionality (Figure 1.6).[9] Each cycle is competitive at higher temperatures,[9] and therefore polyketones may be produced with mixed end group functionalities.

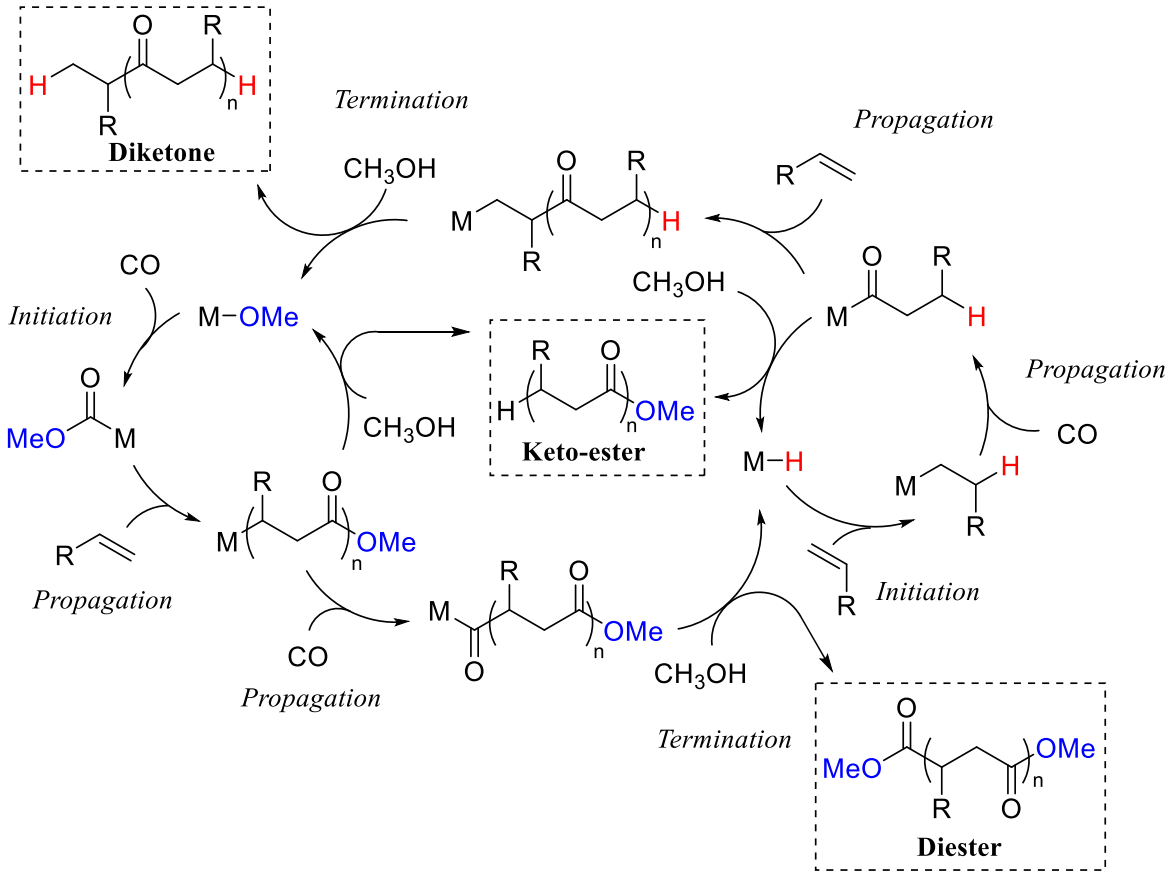

Figure 1.6: Mechanism for the metal catalyzed copolymerization of olefin and carbon monoxide with three possible polymer end group combinations. Adapted from Drent, E.; Budzelaar, P. H. M. Chem. Rev. 1996, 96, 663-681.

1.1.5 Project Goals

Although the mechanism of metal catalyzed polyketone polymerization is generally well understood, the aforementioned phenomenon of carbonyl chelation during the propagation step remains an area of interest. The balance between maintaining a chelate, which stabilizes the metal cation in between monomer coordination, and dissociation, which allows an incoming monomer to propagate polymerization, depends on substrate, solvent, and counter-anion. Modifying catalyst activity, and therefore polymer properties,

depends in part on controlling access to the metal's coordination site. The work discussed herein is based on the proposal that counter-anion strength can be tuned such that it is weak enough to encourage chelation in between monomer incorporation, but strong enough to displace other competitive binding modes (Figure 1.7). Previous studies within the Dobereiner Lab investigated the effect Lewis acid additives have on metal catalyst activity during the polymerization of polyketones. It was found that increased activity was observed upon addition of Tris(pentafluorophenyl)borane (BCF) which resulted in high polymer molecular weights and yield. Conversely, the use of triflate additives resulted in catalyst poisoning and lower polymer yields and molecular weight.[32] The observation of such effects suggest that counter-anion identity may also impact polymerization activity.

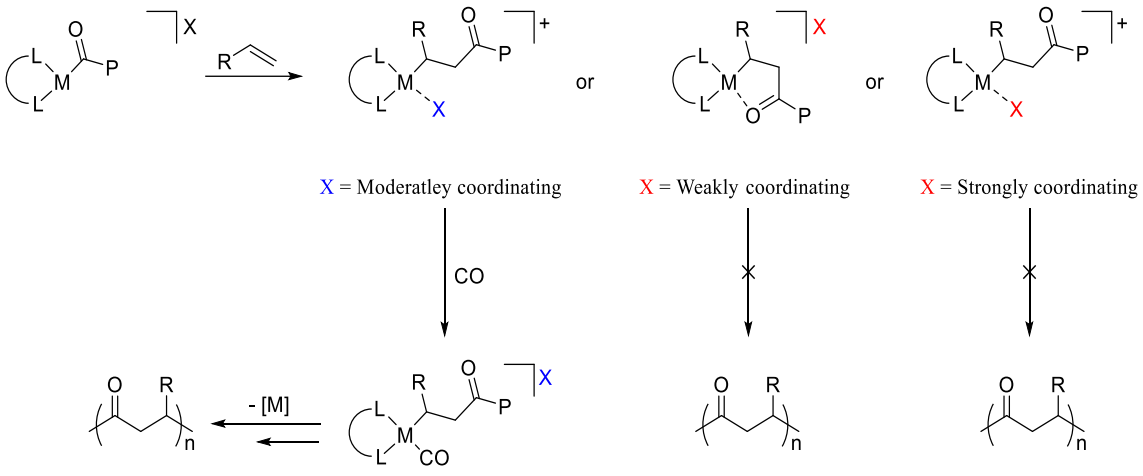

Figure 1.7: Possible effects of differing anion strength on catalyst polymerization activity.

To test the hypothesis that catalyst activity can be tuned through modifying anion coordination strength, anions of varying metal affinity are needed. The imidazolyl-phenyl (IMP) anions of the Dobereiner group allow for precise tuning of coordinating ability while keeping steric volume relatively constant.[33] These anions serve as useful counter-anions

for catalysis due to their large size, making them effective at charge dispersion. Anion tuning is achieved by modifying the phenyl ring with functionality of varying electron donating or withdrawing capabilities ("R" in Figure 1.8). Therefore, these species may serve as the ideal counter-anions to probe the role of counter-anion binding in the polymerization of olefin and carbon monoxide.

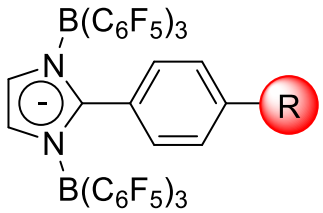

IMP

Figure 1.8: Imidazolyl-phenyl (IMP) anions. The variable functional group is depicted by "R".

The main interest of this work is to investigate the impact of IMP anions on the polymer resulting from palladium catalyzed copolymerization of olefin and carbon monoxide, with the hypothesis that catalyst activity and therefore polymer properties will be affected when anion coordination strength is altered. As the functionality on the IMP anion is changed to more or less electron donating character, the catalyst activity is inferred through the resulting polyketone yield, molecular weight, and polydispersity.

1.2 Results and Discussion

1.2.1 Catalyst Development

For the initial copolymerization studies the palladium catalyst precursor [(dppp)Pd(*N*,*N*-dimethylbenzylamine)][X] (dppp = 1,3-Bis(diphenylphosphino)propane), (X = counter-anion) described by Schwarz and coworkers[34] was paired with the following

anions with the identity IMP-R which were synthesized following literature procedure (Figure 1.9).[33]

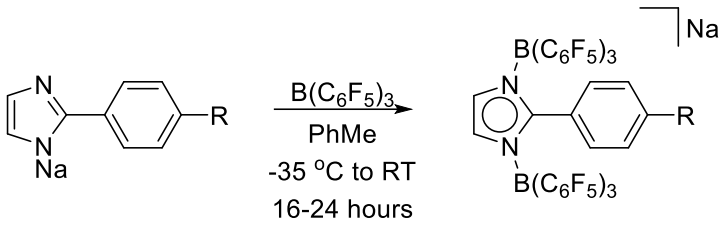

Figure 1.9 Synthesis of imidazolyl-phenyl (IMP) anions.

IMP-H (**1**), IMP-CF_3 (**2**), and IMP-CO_2Me (**3**) Where IMP is the imidazolyl-phenyl group and R is the phenyl group functionality (Figure 1.8). Complexes [(dppp)Pd(C,P-tri(orthotolyl)phosphine][X] were also synthesized in accordance with the literature[34] and paired with anions: IMP-H (**4**), IMP-CF_3 (**5**), IMP-CO_2Me (**6**) and IMP-$N(CH_3)_2CO$ (**7**). Following trials of these catalysts, palladium complexes with only one bidentate were used using the procedure outlined by Dekker and coworkers.[35] The cation configuration $[(dppp)Pd(CH_3)(CH_3CN)]^+$ was paired with IMP anions consisting of functionality: R = H (**8**), R = CF_3 (**9**), R = CO_2Me (**10**), R = $N(CH_3)_2CO$ (**11**), R = NO_2 (**12**). The same cation was also paired with a $[\{3,5\text{-}(CF_3)_2C_6H_3\}_4B]^-$ ($BAr^F{}_4^-$) anion (**13**). Lastly, the metal complex $[(dppp)Pd(CH_3CN)_2][(BF_4)_2]$ described by Chein and coworkers[36] was also used (Figure 1.10).

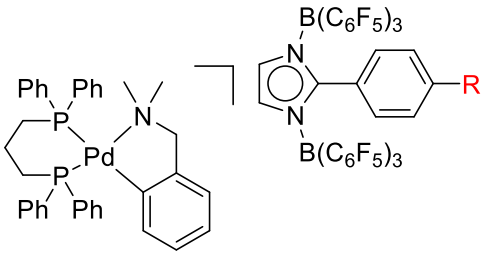

(**1**) R = H, (**2**) R = CF_3,
(**3**) R = CO_2Me

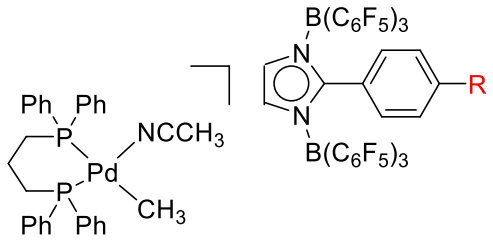

(**8**) R = H, (**9**) R = CF_3,
(**10**) R = CO_2Me,
(**11**) R = $N(CH_3)_2CO$,
(**12**) R = NO_2,

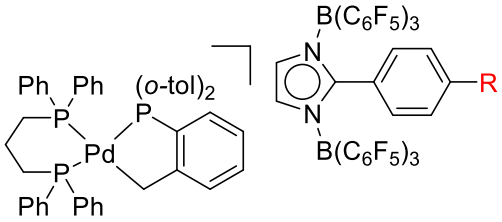

(**4**) R = H, (**5**) R = CF_3
(**6**) R = CO_2Me, (**7**) R = $N(CH_3)_2CO$

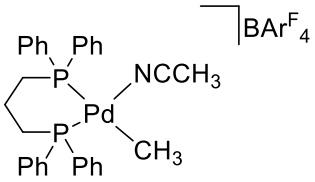

13

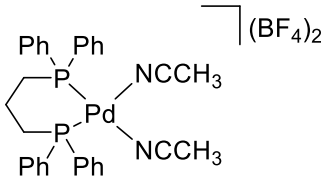

14

Figure 1.10: Palladium catalysts and their associated counter-anions used in the copolymerization of olefin and carbon monoxide.

1.2.2 Copolymerization of 1-Hexene and Carbon Monoxide

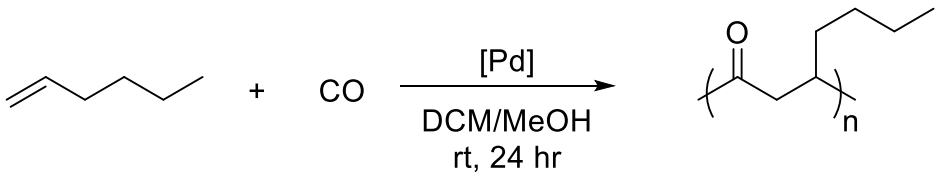

Figure 1.11: Copolymerization of 1-hexene and carbon monoxide by palladium catalyst.

Polyketones were made by copolymerization of carbon monoxide and 1-hexene (Figure 1.11). The rationale for using 1-hexene for this study is in part because of its liquid

state at room temperature and its lack of functionality, eliminating unwanted side reactions with the catalyst. Reactions were run with each catalyst in dichloromethane (DCM), with some methanol added to activate the catalyst. Upon recovery of the resulting polyketone and removal of the metal catalyst, molecular weight data was obtained by gel permeation chromatography (GPC). Molecular weight average (M_w) and molecular number average (M_n) are both recorded along with the polydispersity index (Đ). This data, along with polymer yield (calculated by assuming the polymer is made entirely of perfectly alternating monomers) was used to estimate catalyst activity (Table 1.1). Catalysts **1**-**3**, which contain the bidentate dimethylbenzylamine ligand, yielded trace amounts of polymer that were insufficient for GPC analysis. Therefore, molecular weights are unknown for these polymers. Similarly, catalysts **4-7,** which contain the bidentate κ^2-(C,P)-triorthotolylphosphine ligand, produce little to no polymer. It may be that the dimethylbenzylamine and triorthotolylphosphine ligands are too tightly bound to the metal center and do not dissociate, and therefore polymerization cannot occur.

Catalyst	Yield (%)	M_w (kDa)	M_n (kDa)	Đ
1	0.1	-	-	-
2	0.3	-	-	-
3	0.1	-	-	-
8[a]	33	20.6	14.3	1.5
9[b]	47	22.7	16.0	1.4
10[b]	33	28.0	18.7	1.5
11[b]	26	27.3	19.7	1.4
12[a]	37	23.5	16.0	1.4
13[a]	34	26.5	18.6	1.4
14	30	38.6	26.1	1.5

Table 1.1: 1-hexene/carbon monoxide copolymer yield and molecular weight data. [a]Averaged over two separate experiments, [b]averaged over three separate experiments. No polymer was observed for catalysts 4-7. Đ = polydispersity index (Mw/Mn).

Catalysts **8-14** can more easily make two coordination sites available (through dissociation of labile acetonitrile (MeCN) and/or protonolysis of Pd-CH_3) and show good polymerization activity, but molecular weights observed for differing cation/anion pairs are similar to one another. Lower yield, albeit higher M_w and M_n, were achieved with **14** (paired with the more coordinating BF_4 anion). As functionalization on the IMP anion is changed from electron donating to withdrawing, it was expected that coordination to the metal would become stronger or weaker and therefore alter the polymer yields and molecular weights. This, however, is not observed. Catalyst **9**, which has the CF_3-derived

IMP anion - among the most weakly coordinating anions known - displays similar activity to catalyst **11,** which has an IMP anion derived with a highly coordinating -CO-N$(CH_3)_2$ group. IMP functionalization does not appear to influence polymer yield or properties.

The IMP anions themselves may not have adequate coordination strength in the reaction medium (DCM) to affect the catalyst activity. The steric bulk of the anions themselves may prevent a close inner sphere interaction in this coordination environment, thereby preventing the anions from displacing any chelate or other species in a catalyst vacant site. Insufficient coordination may also impact catalyst stability, where the unsaturated palladium center is reduced and deactivated. Pd black was in fact observed to ultimately occur in all cases in varying amounts, although it is unclear at this stage if decomposition rate is impacted by anion.

1.2.3 Copolymerization of Allyl Glycidyl Ether and Carbon Monoxide

Polyketones synthesized by the copolymerization of carbon monoxide and allyl glycidyl ether (AGE) as the olefin were also studied (Figure 1.12). AGE was chosen in part due to its ease of polymerization under the same conditions as 1-hexene/CO polymerizations. In addition to a change in olefin monomer, the reaction solvent in some instances was changed to benzene. This decrease in solvent polarity is theorized to decrease the charge separation in solution and therefore increase the extent of cation/anion interactions. For CO/AGE copolymerization, the same cation/anion catalyst species were tried, in the hopes that activity difference between anion functionalization would be apparent. Such a difference in activity may be apparent in olefin monomers which compete less with the counter-anion for the catalyst coordination site. In addition to the previous catalysts, the cation $[(dppp)Pd(CH_3)(CH_3CN)]^+$ was paired with a benzyl-imidazolyl

(BIM) anion, **15** (Figure 1.13). This anion has a more delocalized charge in comparison to the typical IMP anion.

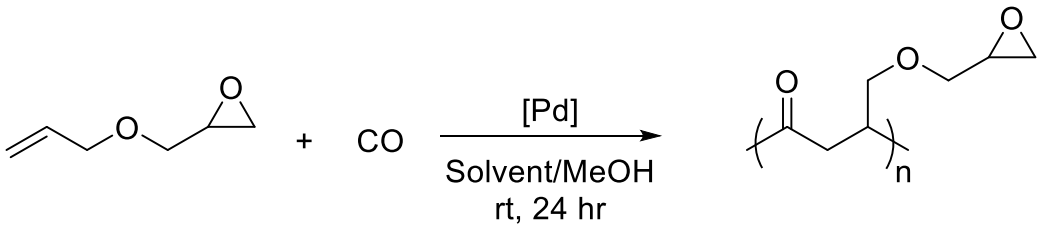

Figure 1.12: Palladium catalyzed copolymerization of allyl glycidyl ether and carbon monoxide.

Catalyst	Yield (%)	M_w (kDa)	M_n (kDa)	Đ
8	7.2	5.2	3.8	1.4
9	1.1	15.5	11.6	1.3
10[a]	27.8	17.2	8.7	2.3
13[b]	2.0	-	-	-
14	-	-	-	-
15[c]	24.3	52.1	19.7	2.7

Table 1.2: Allyl glycidyl ether/carbon monoxide copolymerization yield and molecular weight data. [a]Averaged over three separate experiments. [b]Reaction done in DCM. [c]Averaged over two separate experiments.

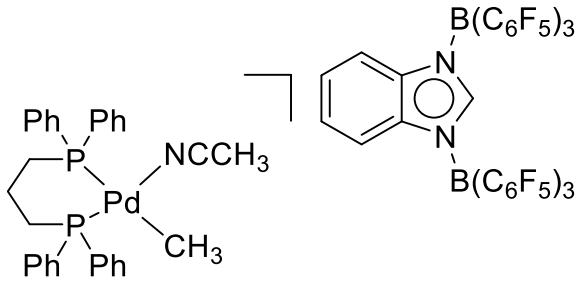

15

Figure 1.13: Palladium cation paired with benzyl-imidazolyl anion.

Unlike 1-hexene/CO copolymerization, for AGE/CO copolymers, the polymer yield and properties depend on the catalyst used (Table 1.2). A trial with catalyst **14** produced little to no polymer. Catalyst **13** produced minimal amounts of polymer insufficient for molecular weight to be determined via GPC, perhaps due to facile catalyst decomposition when paired with the very weakly coordinating $BAr^{F}_{4}^{-}$ anion. Catalyst **8** (IMP-H) produced 7% yield of low molecular weight polymer, whereas polymerization with catalyst **9** (IMP-CF_3) was extremely low yielding yet higher in molecular weight. Like $BAr^{F}_{4}^{-}$, the IMP-CF_3 anion may be too weakly coordinating, and the catalyst may be decomposing before any significant amount of polymer is produced. Unfortunately, further reactions with catalyst **9** produced no polymer at all. Here, a very low rate of initiation could be leading to irreproducibility. Trace deactivating contaminants may be harmless when concentrations are far lower than the concentration of active catalyst, but a low rate of initiation reduces active catalyst concentration and increases susceptibility to trace contaminants.

Both catalysts **10** (IMP-CO_2Me) and **15** (BIM) produce polymers with modest yields and higher molecular weights compared with the rest of the catalysts, though

polydispersity is higher in each case. Higher polydispersity indicates a larger distribution of molecular weights as seen by GPC (Figure 1.14). The counter-anion ester group on **10** is more coordinating than the trifluoromethyl group on **9** due to the greater delocalization effects of fluorine.[37] Therefore, the anion of catalyst **10** may be the optimal coordination strength for this polymerization reaction.

Anion effects are more apparent in AGE/CO copolymerization than 1-hexene/CO, probably due to the nature of solvent. With the AGE/CO reaction, benzene could be used as solvent because polar AGE monomer keeps the catalyst soluble. The resulting benzene/AGE reaction medium is probably more non-polar than DCM/1-hexene, making

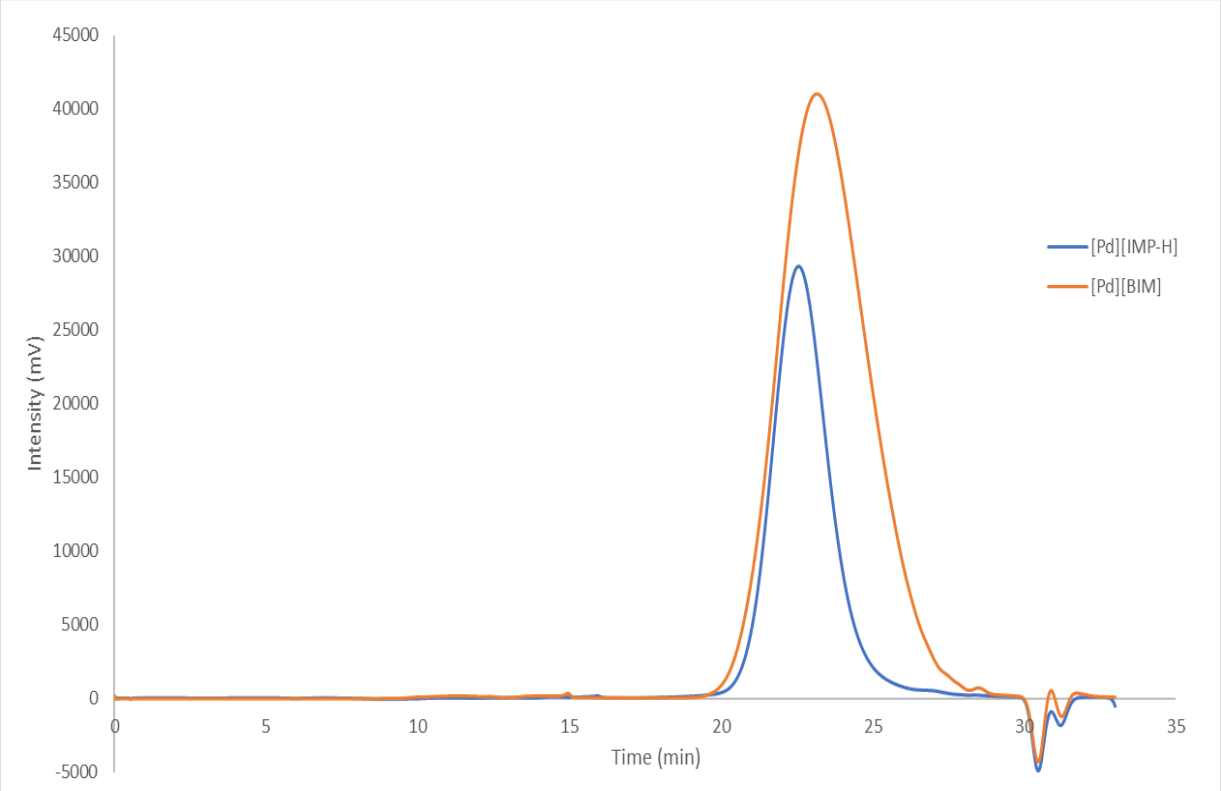

Figure 1.14: GPC trace of polymers produced by catalyst 8 (blue) and by catalyst 15 (orange).

cation/anion interactions stronger. Unfortunately, DCM had to be used in 1-hexene copolymerization, because the catalyst has poor solubility in the benzene/hexene mixture.

Some of the poor yields and high polydispersity of polymers produced may be explained by functionality on the olefin. The epoxide group may be non-innocent during polymerization, opening and causing cross linking between polymer chains, or leading to olefin homo-polymerization and therefore higher polydispersity (Figure 1.15). Allyl glycidyl ether homo-polymers are in fact known and are typically polymerized by anionic initators.[38] It may be possible for methanol to initiate this event, but such species are difficult to observe in ^{1}H NMR spectra.

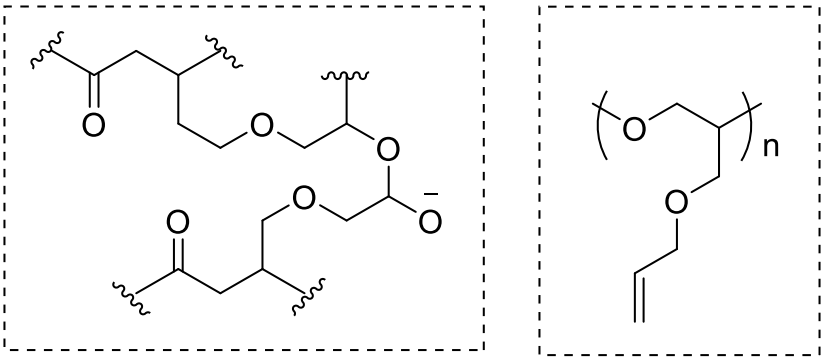

Figure 1.15: (Left) potential cross linking of epoxide groups. (Right) allyl glycidyl ether homo-polymerization.

1.3 Conclusion

The mechanism of metal catalyzed olefin and carbon monoxide copolymerization to form polyketones is generally well understood, though there is still uncertainty about the effect of competition between monomer, solvent, and anion for coordination sites prior to the propagation step. This work focused on the strength of the counter-anion coordination

and what effect it has on the metal cation's activity and therefore the resulting polymer properties.

It was hypothesized that by comparing catalyst activity with a series of anions of varying coordination strength, an optimal anion for copolymerization could be identified. The hypothesis was tested by pairing palladium catalysts with the tunable IMP anion library, polymerizing two different olefins with carbon monoxide, and analyzing the resulting polyketone yield and molecular weight to infer catalyst activity.

Polymers produced with 1-hexene as the olefin showed no relationship between catalyst activity and anion coordination strength. The anion/cation interactions were probably too weak to modify reactivity in the polar DCM medium required to maintain reaction homogeneity. When allyl glycidyl ether (AGE) was used as the olefin, weaker coordinating anions such as IMP-CF_3 and $BAr^F{}_4^-$ produced little or no polymer in comparison to anions of greater coordination strength. Although there may be an influence of anion coordination on AGE/CO copolymerization activity, the AGE epoxide is prone to side reactions or cross-linking that complicate the interpretation of any anion/catalysis relationship. Future work will explore monomers that share the polarity of AGE but avoid the high reactivity of the epoxide moiety.

1.4 Experimental

1.4.1 General Methods

All preparations or reactions, which were noted to be air- or moisture-sensitive, were performed in a glove box under nitrogen atmosphere or using Schlenk techniques. Chemicals were purchased commercially unless otherwise noted and no additional

purification methods were taken. Solvents used in inert atmosphere were degassed by a solvent purification system and dried using molecular sieves. ^{1}H and ^{13}C NMR spectra were collected on a Bruker AVIII-500 or a Bruker AV400 spectrometer. All NMR spectra were referenced to residual protio-solvent. Polymer molecular weight analysis was conducted on a Shimadzu LC 20-AT chromatograph with three 300 x 7.5 mm Agilent PolarGeL® columns (two M, one L) at an oven temperature of 30 °C and flow rate of 0.5 mL/min with acetone as the mobile phase. Molecular weight was determined by use of a refractive index detector calibrated with polymethyl methacrylate standards (200-71,800 Da). IR spectra were collected on a Thermo Scientific Nicolet is5 ATR-FTIR spectrophotometer. Copolymerization with carbon monoxide was conducted in a 100 mL Parr Instrument Co 4590 Micro stirred reactor. IMP/BIM anions and compounds **1**-**13** were synthesized in the Dobereiner laboratory in accordance with literature procedure[33]. The yield of polymers was found by finding the mol percent of the recovered polymer, then dividing by the initial mass of the olefin (Equation 1.1 and Equation 1.2).

$$mol\ \% = \frac{Molar\ Mass\ Olefin}{Molar\ Mass\ Olefin + Molar\ Mass\ CO} \quad (\mathbf{1.1})$$

$$\%\ yield\ = \frac{Mass\ of\ Polymer}{Initial\ Mass\ of\ Olefin} \times 100 \quad (\mathbf{1.2})$$

1.4.2 Synthesis of $[Pd(CH_3CN)_4][(BF_4)_2]$ (16)

Procedure was followed according to literature precedent.[36] In a glove box: nitrosonium tetrafluoroborate (4.67 mmol, 542 mg) was dissolved in acetonitrile in a Schlenk flask. Palladium sponge (2.33 mmol, 248.5 mg) was added, and the vessel was sealed and taken outside the box to react under nitrogen atmosphere on a Schlenk line. Solution was stirred at room temperature overnight to afford the tetrakis acetonitrile

compound $[Pd(CH_3CN)_4][(BF_4)_2]$. The solution was then purified in the glove box by filtration through a glass frit to remove unreacted palladium, then concentrated to less than half its original volume. The solution was next layered with diethyl ether which precipitated the tetrakis compound as a yellow solid which was further dried under vacuum. ^{1}H NMR: (500 MHz, CD_3CN) Bound acetonitrile: δ 2.15 ppm (s).

1.4.3 Synthesis of [(dppp)Pd(CH$_3$CN)$_2$][(BF$_4$)$_2$] (14)

Procedure was followed according to literature precedent.[36] In a glove box: catalyst **16** (0.525 mmol, 233 mg) and diphenylphosphinopropane (0.525mmol, 216 mg) were dissolved in acetonitrile at room temperature then stirred for 24 hours. The solution was concentrated to less than half its original volume then layered with diethyl ether. After the solution was decanted, the yellow precipitate was washed further with ether and dried under vacuum. ^{1}H NMR: (500 MHz, CD_3Cl) δ 7.68 (dd, 8H), 7.49 (m, 12H), 2.94 (s, 4H), 2.31 (m, 2H), 1.87 (s, 6H).

1.4.4 Synthesis of 1-Hexene/Carbon Monoxide Copolymers

The general procedure for the synthesis of 1-hexene/CO copolymers is modified from Rieger and coworkers[39] and is as follows: in a glove box, a stock solution of catalyst:olefin ratio of 0.001:1 was created in dichloromethane or benzene. 0.150 equivalents of methanol with respect to olefin were added, and the solution was divided equally into three vials equipped with a septum cap and pierced with a needle. The solutions were sealed in a Parr reactor then taken out of the glove box and pressurized with carbon monoxide at 500 psi. The vessel was left to stir at room temperature for 24 hours, after which the reactor was opened, and the solutions were individually passed through a silica

plug using ethyl acetate as the eluent. Filtered solutions were then concentrated via rotary evaporation then redissolved with minimal amounts of dichloromethane and layered with methanol. The resulting polymer was precipitated out as a translucent gel and dried under vacuum. ^{1}H NMR: (500 MHz, $CDCl_3$) δ 2.91 (br), 2.65 (br), 2.39 (br), 1.79 (br), 1.58 (br), 1.26 (br), 1.05 (br), 0.89 (br). 212.8 ^{13}C NMR: (126 MHz, $CDCl_3$) δ 212.8, 45.7, 30.2, 22.8, 14.3. IR: C=O (1702 cm^{-1}).

1.4.5 Synthesis of Allyl Glycidyl Ether/Carbon Monoxide Copolymers

In a glove box: a stock solution of catalyst:olefin ration of 0.001:1 was created in benzene. 0.150 equivalents of methanol were added, and the solution was divided equally into three portions, equipped with a septum line cap, and pierced with a needle. The solutions were then sealed in a Parr reactor and removed from the glove box, then pressurized with carbon monoxide at 500 psi and left to react at room temperature for 24 hours. The resulting solutions were passed through a silica plug using ethyl acetate as the eluent then concentrated via rotary evaporation. A minimal amount of dichloromethane was added then layered with methanol. The resulting polymer was precipitated out as a clear gel and dried under vacuum. ^{1}H NMR: (500 MHz, $CDCl_3$) δ 3.71 (br), 3.52 (br), 3.31 (br), 3.20 (br), 3.09 (br), 2.89 (br), 2.76 (br), 2.55 (br). ^{13}C NMR: (126 MHz, $CDCl_3$) δ 209.5, 128.5, 71.9, 50.7, 46.6, 44.2. IR: C=O (1702 cm^{-1}).

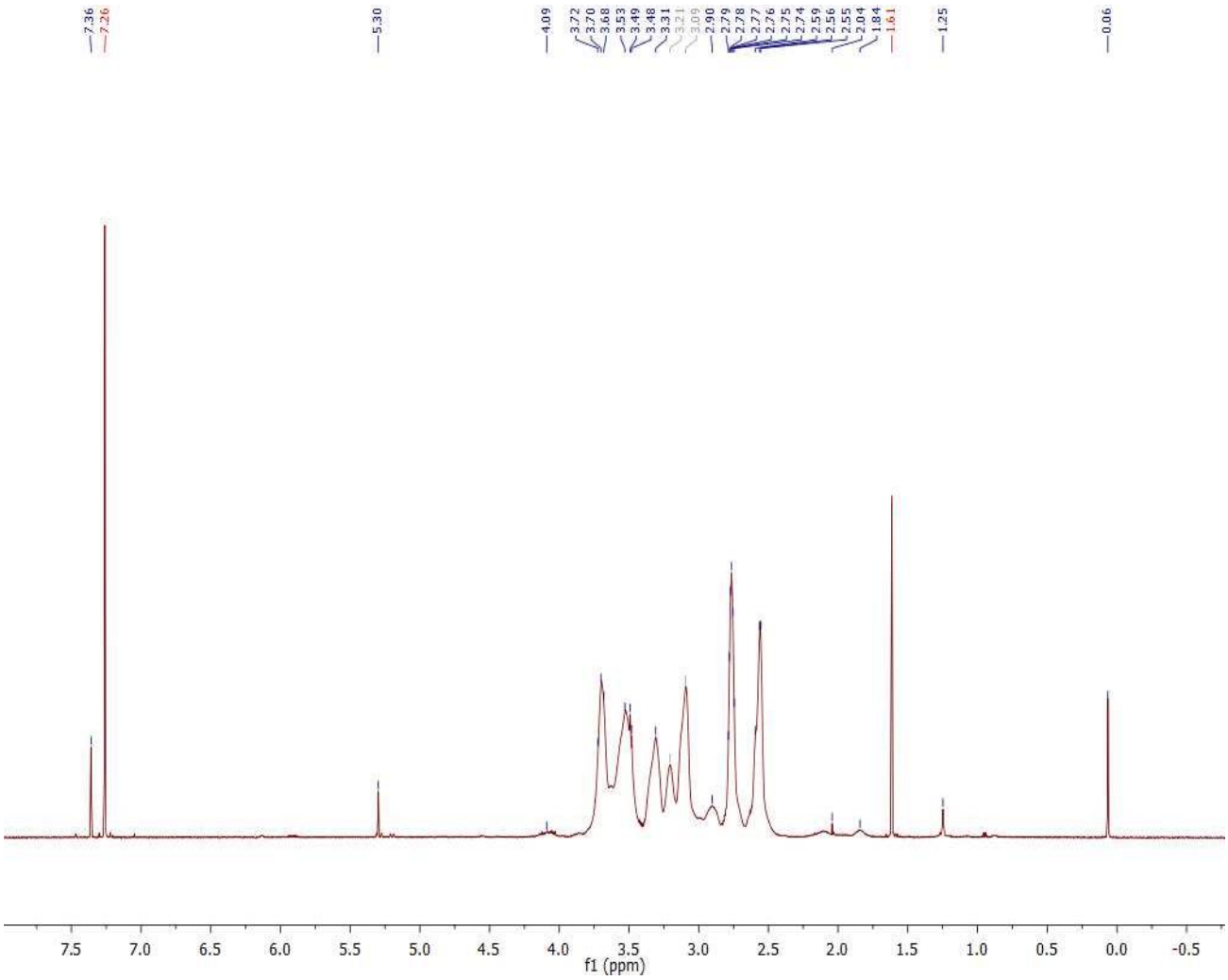

Figure 1.16: ^{1}H NMR spectra of allyl glycidyl ether/carbon monoxide copolymer (500 MHz, $CDCl_3$).

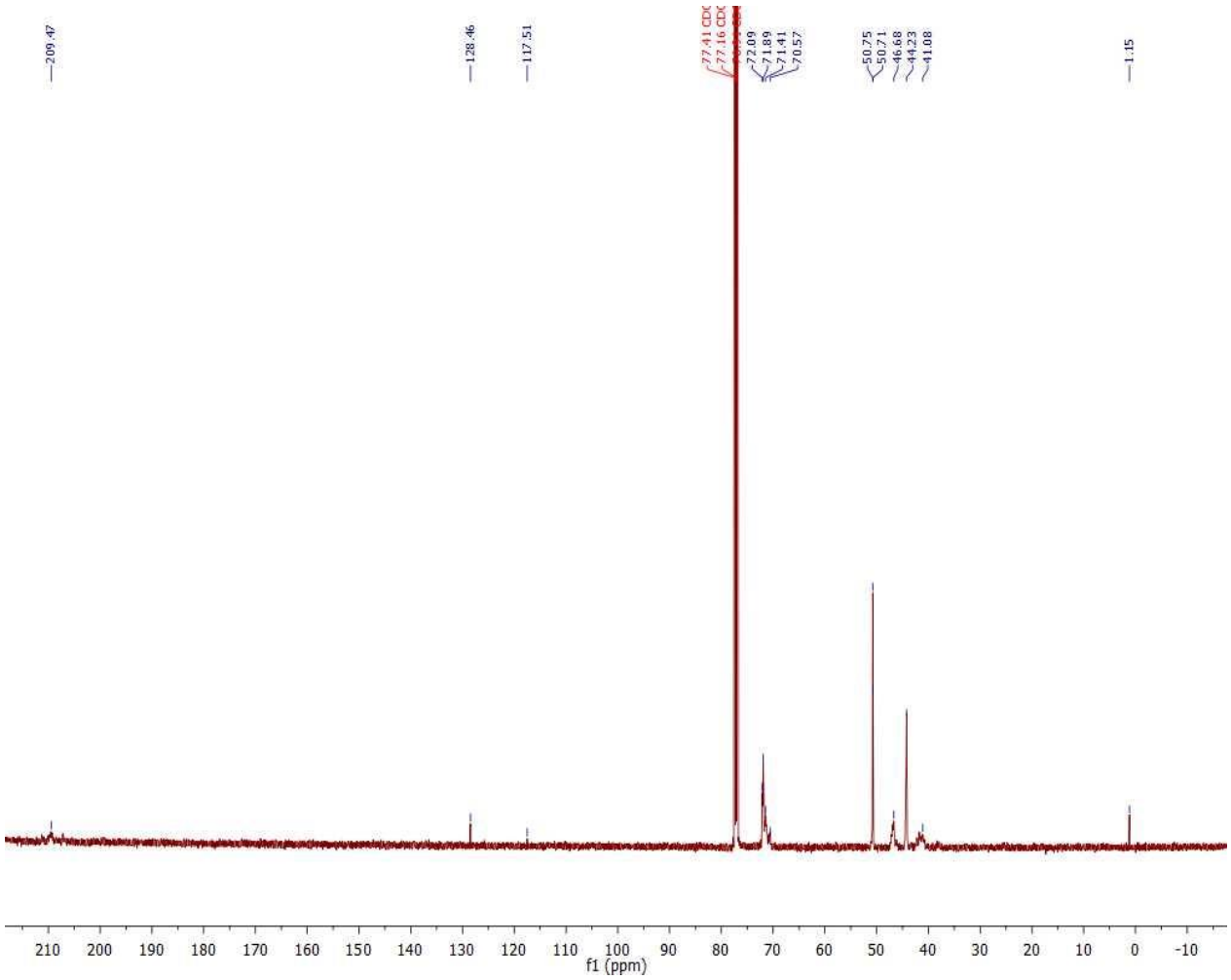

Figure 1.17: ^{13}C NMR spectra of allyl glycidyl ether/carbon monoxide copolymer (500 MHz, $CDCl_3$).

2

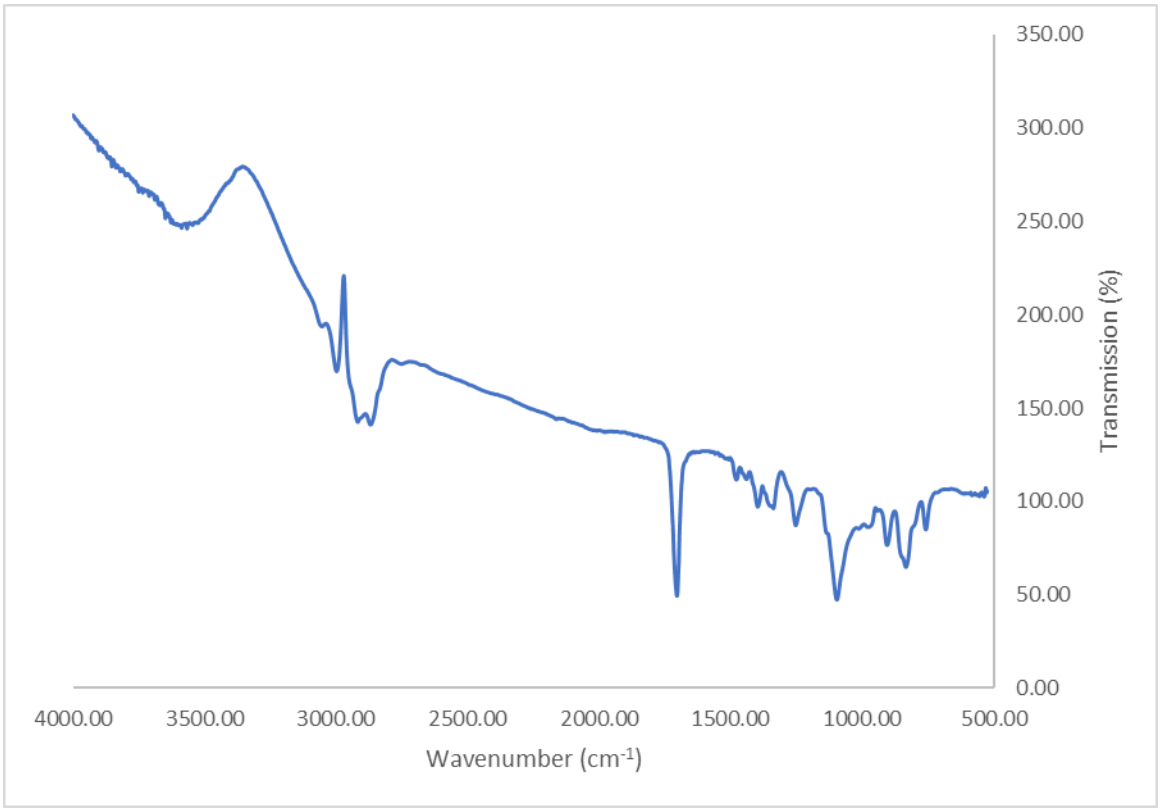

Figure 1.18: IR spectra of allyl glycidyl ether/carbon monoxide copolymer.

1.5 References Cited

(1). Brubaker, M. M.; Coffman, D. D.; Hobin, H. H. Synthesis and Characterization of Ethylene/Carbon Monoxide Copolymers, A New Class of Polyketones. *J. Am. Chem. Soc.*, **1952**, *74*, 1509-1515.

(2). DeVito, S.; Ciardelli, F.; Ruggeri, G.; Chiantore, O.; Moro, A. Thermal Degradation of Ethylene–Carbon Monoxide Alternating Copolymer Under Inert Atmosphere. *Polym. Int.*, **1998**, *45*, 353-365.

(3). Sommazzi, A.; Garbassi, F. Olefin-Carbon Monoxide Copolymers. *Prog. Polym. Sci.*, **1997**, *22*, 1547-1605.

(4). LaVerne, L. Advances in Engineering Plastics. *Advanced Materials & Processes*, **1997**, *152* (6), 29

(5). George, E.R.; Reimer, J. Recent Advances in Flamesprayed Thermoplastic Powder Coatings. *Process in Organic Coatings*, **1993**, *22*, 195-199.

(6). Vavasori, A.; Ronchin, L. Polyketones: Synthesis and Applications. *Encyclopedia of Polymer Science and Technology*, **2017**, 1.

(7). Zhang, L.; Lin, Y.; Cheng, L.; Yang, Z.; Matsuyama, H. A comprehensive Fouling- and Solvent Resistant Aliphatic Polyketone Membrane for High-Flux Filtration of Difficult Oil-in-Water Micro- and Nanoemulsions. *Journal of Membrane Science*, **2019**, *58*, 48-58.

(8). Suarez, E. J. G.; Godard, C.; Ruiz, A.; Claver, C. Alternating and Non-Alternating Pd-Catalyzed Co- and Terpolymerisation of Carbon Monoxide and Alkenes. *Eur. J. Inorg. Chem.*, **2007**, 2582-2593.

(9). Drent, E.; Budzelaar, P. H. M. Palladium-Catalyzed Alternating Copolymerization of Alkenes and Carbon Monoxide. *Chem. Rev.*, **1996**, *96*, 663-681.

(10). Reppe, W.; Magin, A. U.S. Pat. 3,984,388. *Chem. Abstr.*, **1952**, *46*, 6413.

(11). Klabunde, U.; Ittel, S. D. Nickel Catalysis for Ethylene Homo- and Co-polymerization. *J. Mol. Catal.,* **1987**, *41*, 123-124.

(12). Iwashita, Y.; Sakuraba, M. Alternating Oligermerization of Ethylene and Carbon Monoxide Catalyzed by Rhodium Carbonyl. *Tetrahedron Letters,* **1971**, *26*, 2409-2412.

(13). Sen, A.; Brumbaugh, J. S. Rhodium(I) Catalyzed Cooligomerization of Carbon Monoxide with Ethylene Direct Evidence for a Single Mode of Stepwise Chain Growth. *J. Organometal. Chem.* **1985**, *279*, C5-C10.

(14). Gough, A. British Pat. 1,081,304, 1967; *Chem. Abstr.* **1967**, *67*, 100569.

(15). Chen, S.; Pan, R.; Chen, M.; Liu, Y.; Chen, C.; Lu, X. Synthesis of Nonalternating Polyketones Using Cationic Disphospazane Monoxide-Palladium Complexes. *J. Am. Chem. Soc.* **2021**, *143*, 10743-10750.

(16). Drent, E.; Broekhoven, J.A.M.; Doyle, M. J. Efficient Palladium Catalysts for the Copolymerization of Carbon Monoxide with Olefins to Produce Perfectly Alternating Polyketones. *J. Org. Organometal. Chem.* **1991**, *417*, 235-251.

(17). Cavinato, G.; Toniolo, L. Carbonylation of Ethene Catalyzed by Pd(II)-Phosphine Complexes. *Molecules*. **2014**, *19*, 15116-15161.

(18). Axet, M. R.; Amoroso, F.; Bottari, G.; D'Amora, A.; Zangrando, E.; Faraone, F.; Drommi, D.; Saporita, M.; Carfagna, C.; Natanti, P.; Seragila, R.; Milani, B. Application of Chiral Amine-Imine Ligands in Palladium-Catalyzed Polyketone Synthesis: Effect of Ligand Backbone on the Polymer Stereochemistry. *Organometallics*. **2009**, *28*, 4464-4474.

(19). Brookhart, M.; Wagner, M. I. Synthesis of Stereoblock Polyketone through Ancillary Ligand Exchange. *J. Am. Chem. Soc.* **1996**, *118*, 7219-7220.

(20). Koehn, R. Oligio- and Polymerization of Olefins. *Comprehensive Inorganic Chemistry II (Second Edition)*. **2013**, *6*, 127-154.

(21). Strauss, S. H. The Search for Larger and More Weakly Coordinating Anions. *Chem. Rev.* **1993**, *93*, 927-942.

(22). Macchioni, A. Ion Pairing in Transition-Metal Organometallic Chemistry. *Chem. Rev.* **2005**, *105*, 2039-2073.

(23). Molinos, E.; Brayshaw, S. K.; Kociok-Koehn, G.; Weller, A. S. Cationic Rhodium Mono-phosphine Fragments Partnered with Carborane Monoanions [closo-CB11H6X6] − (X = H, Br). Synthesis, Structures and Reactivity with Alkenes. *Dalton Trans.* **2007**, 4829-4844.

(24). Drent, E. Eur. Pat. Appl. 220,767, 1985; *Chem. Abstr.* **1987**, *107*, 39199.

(25). Drent, E.; Kragtwijk, E.; Pello, D. H. L. Eur. Pat. Appl. 495-547, 1992; *Chem. Abstr*. **1992**, *117*, 150570.

(26). Sen, A. Mechanistic Aspects of Metal-Catalyzed Alternating Copolymerization of Olefins with Carbon Monoxide. *Acc. Chem. Res.* **1993**, *26*, 303-310.

(27). Bianchini, C.; Meli, A.; Oberhauser, W. Catalyst Design and Mechanistic Aspects of the Alternating Copolymerization of Ethene and Carbon Monoxide by Diphosphine-modified Palladium Catalysis. *Dalton Trans*. **2003**, 2627-2635.

(28). Chen, J. T.; Sen, A. Mechanism of Transition-metal-catalyzed Double Carbonylation Reactions. Synthesis and Reactivity of Benzoylformyl Complexes of Palladium(II) and Platinum(II). *J. Am. Chem. Soc.* **1984**, *106* (5), 1506-1507.

(29). Sen, A.; Chen, J. T.; Vetter, W. M.; Whittle, R. R. Synthesis, Characterization, and Reactivity of Alpha-ketoacyl Complexes of Platinum(II) and Palladium(II). Crystal Structures of Trans-Pt(PPh3)2(Cl)(COCOPh) and Cis-Pt(PPh3)2(COPh)(CO2Me). *J. Am. Chem. Soc.* **1987**, *109* (1), 148-156.

(30). Rix, F. C.; Brookhart, M. Energetics of Migratory Insertion Reactions in Pd(II) Acyl Ethylene, Alkyl Ethylene, and Alkyl Carbonyl Complexes. *J. Am. Chem. Soc.* **1995**, *117* (3), 1137-1138.

(31). Brookhart, M.; Rix, F. C.; DeSimone, J. M. Palladium(II) Catalysts for Living Alternating Copolymerization of Olefin and Carbon Monoxide. *J. Am. Chem. Soc.* **1992**, *114*, 5895-5897.

(32). Samples, E. M. (2019). *Synthesis of 1,4-Polyketones and Enantioselective Polyester Catalyst Development Using Molecular Lego Scaffolds*. Doctoral Dissertation, Temple University. Tuscholarshare. http://dx.doi.org/10.34944/dspace/3503

(33). Wozniak, D. I.; Hicks, A. J.; Sabbers, W. A.; Dobereiner, G. E. Imidazolyl-phenyl (IMP) Anions: A Modular Structure for Tuning Solubility and Coordinating Ability. *Dalton Trans.* **2019**, *48*, 14138-14155.

(34). Schwarz, J.; Herdtweck, E.; Herrmann, W. A. Highly Efficient Monocationic Palladacycles of Chelating Diphosphines in C2H4/CO Copolymerization. *Organometallics*, **2000**, *19*, 3154-3160.

(35). Dekker, P. C. M. G.; Elsevier, C. J.; Vrieze, K. Influence of Ligands and Anions on the Rate of Carbon Monoxide Insertion into Palladium-Methyl Bonds in the Complexes (P-P)Pd(CH_3)Cl and [(P-P)Pd(CH_3)(L)]$^+$ $SO_3CF_3^-$ (P-P = dppe, dppp, dppb, dppf; L = CH_3CN, PPh_3). *Organometallics*, **1992**, *11*, 1598-1603.

(36). Zhao, A. X.; Chien, J. C. W. Palladium Catalyzed Ethylene-carbon Monoxide Alternating Copolymerization. *J. Polym. Sci., Part A: Polym. Chem.,* **1992**, *30* (13), 2735-2747.

(37). Strauss, S. H. The Search for Larger and More Weakly Coordinating Anions. *Chem. Rev.* **1993**, *93*, 927-942.

(38). Hu, Z.; Fan, X.; Zhang, G. Synthesis and Characterization of Glucose-grafted Biodegradable Amphiphilic Glycopolymers P(AGE-glucose)-*b*-PLA. *Carbohydrate Polymers*, **2010**, *79* (1), 119-124.

(39). Abu-Surrah, A.; Rieger, B. High Molecular Weight 1-Olefin/Carbon Monoxide Copolymers: A New Class of Versatile Polymers. *Topics in Catalysis*, **1999**, *7*, 165-177.

CHAPTER 2

POST-POLYMERIZATION FUNCTIONALIZATION OF INDUSTRIAL POLYKETONES AND POTENTIAL APPLICATIONS

2.1 Introduction

2.1.1 Background

As of 2018 there were 27 million tons of plastic in landfills across the United States, accounting for approximately 18.5% of all solid waste.[1] Of these plastics worldwide, approximately 80% are thermoplastic polymers.[2] Known for their tunable transition temperatures and chemical resistance,[3] thermoplastics are molded for applications including food or material packaging,[4] high-stress-enduring parts in automobiles,[5] and electronic chip manufacturing.[6] Value in essential areas is undoubtedly the cause of their exponential growth in usage.[7] With the enormous volume of plastic generated, it is imperative that methods to safely dispose of, or reuse, these materials be developed.

Thermoplastic polymers are either crystalline, amorphous, or semi-crystalline. Crystalline polymers are rigid and possess high impact strength like high density polyethylene or polypropylene, whereas amorphous materials are flexible and randomly ordered.[3] Semi-crystalline polymers share properties of both crystalline and amorphous polymers (Figure 2.1).[3]

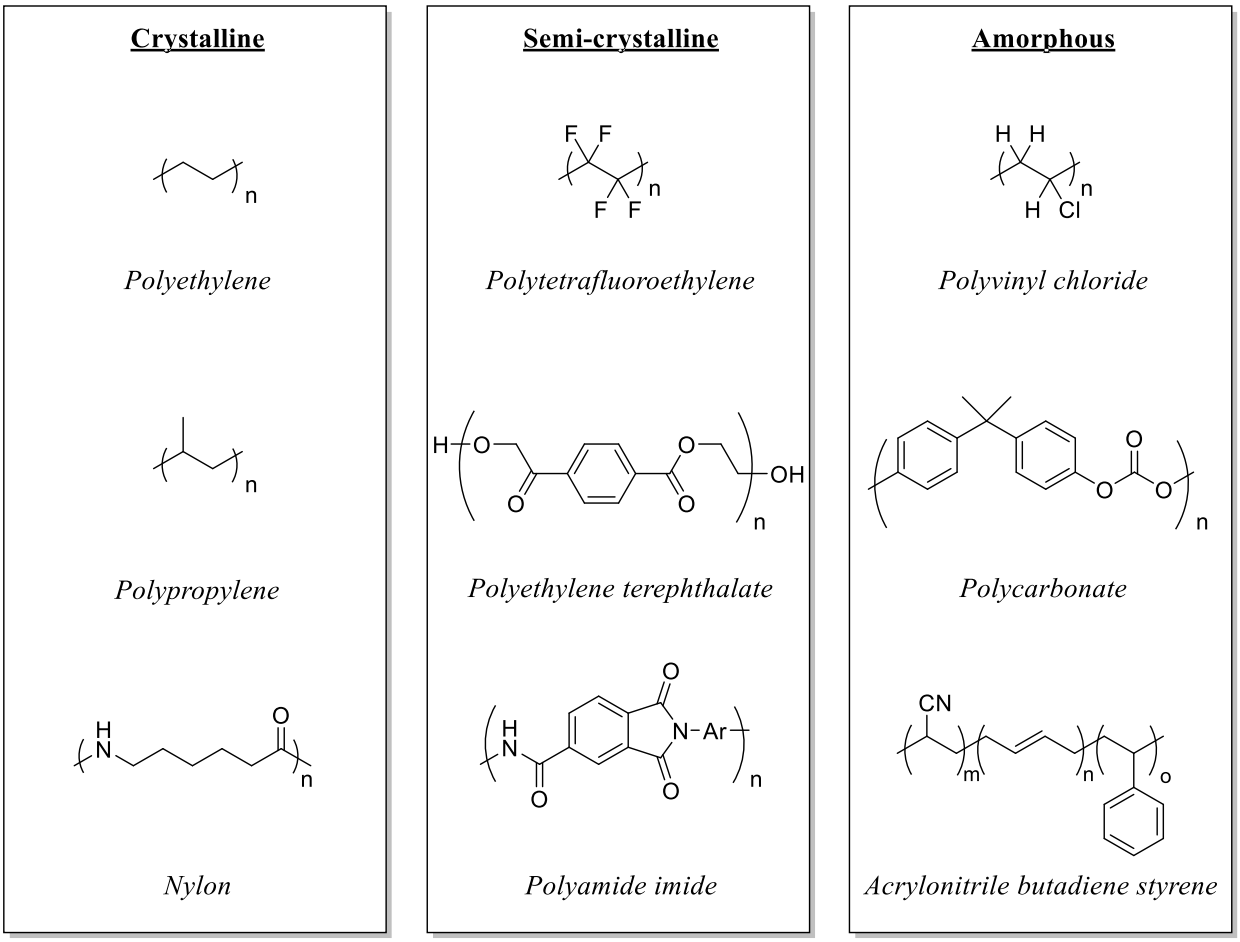

Figure 2.1: Examples of crystalline, semi-crystalline and amorphous thermoplastic polymers.

2.1.2 Plastic Recycling Methods

Recycling thermoplastic materials is often difficult as result of the same qualities which make them desirable. For instance, secondary recycling, which involves melting and remolding plastic waste, can typically only be performed two or three times on a material due to a decrease of plastic strength as a result of thermal degradation.[8] After these plastics have been reused the maximum amount of times they may be placed in a land fill, which

presents the issue of soil contamination.[9] They may also be incinerated for energy reclamation, though this produces harmful pollutants such as dioxins.[10]

One promising solution to the accumulation of plastic waste is chemical recycling, which involves the depolymerization of polymer chains to shorter-chained oligomers or monomers in order to be used in a different application.[3, 11] Such a process would minimize the amount of waste produced, and the recovered monomers could be used to prepare plastics with the strength and durability of the original material. Unfortunately, research into this topic is underdeveloped and chemical recycling is not widely used. Currently known methods require high energy inputs or expensive and exotic metal catalysts.[12] The only two chemolysis methods to have reached prominence are glycolysis-like degradation[13, 14] and methanolysis.[3, 15] Hydrolysis methods are also used, however these may require high reaction temperatures (Figure 2.2).[16] Furthermore, such methods are typically only suited for condensation polymers. Polyolefins and polyketones are significantly more difficult to degrade chemically.

2.1.3 Degradation of Polyketones

Polyketones, which contain carbonyl functional groups and a hydrocarbon backbone, are significantly more difficult to depolymerize than condensation polymers. Polyketones degrade through irradiation by gamma rays[18] or ultraviolet[19, 20] but these processes are not controlled and run the risk of generating undesirable side products due to free radical formation. It is essential that a method which depolymerizes polyketones does so effectively and in a controlled manner, and it would be preferable if it can be applied to other thermoplastics that share similar structure or functionality.

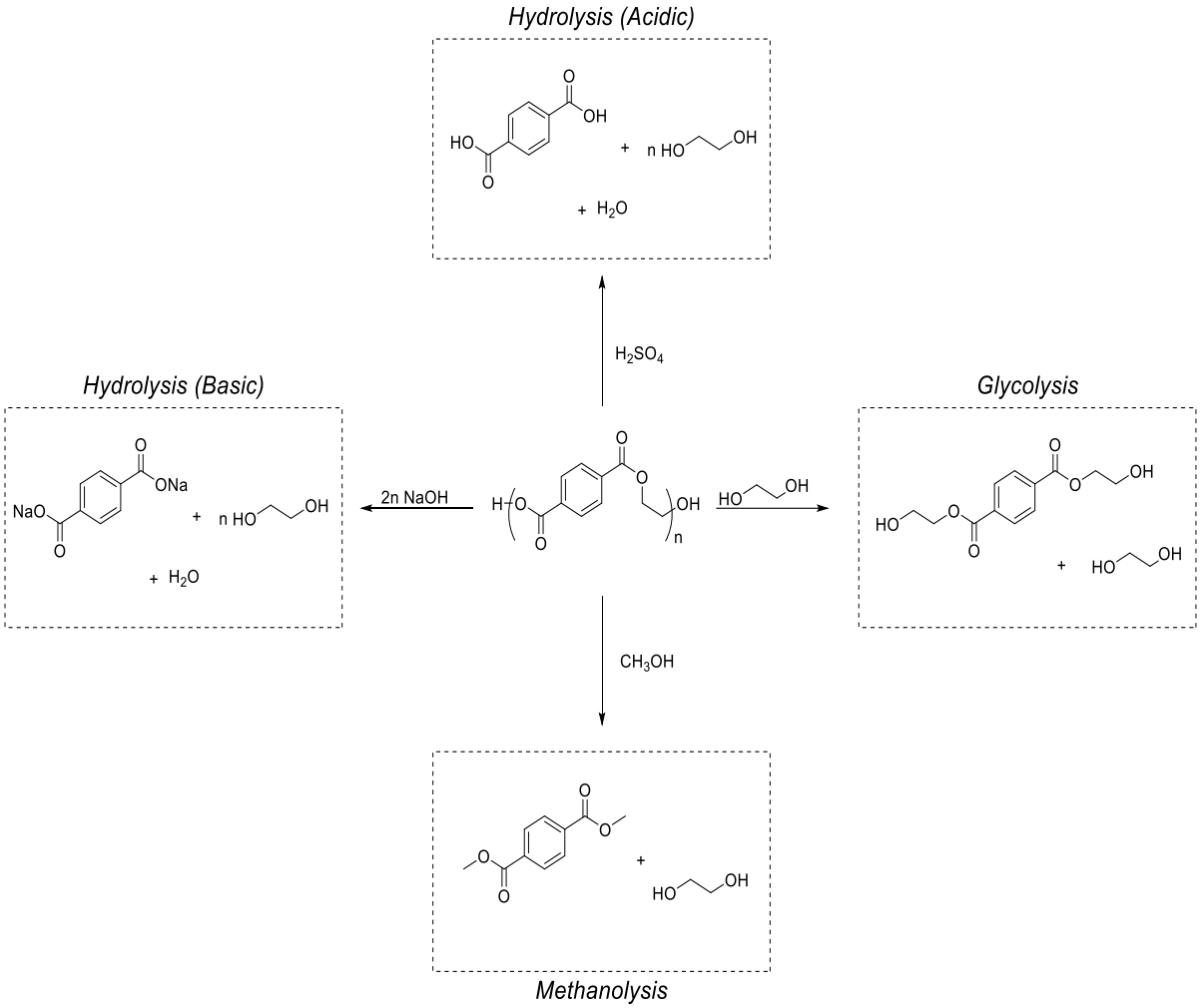

Figure 2.2: Commonly used chemical recycling methods for the degradation of polyethylene terephthalate.

One method for the degradation of polyketones requires post-polymerization modification, where reaction of polymer functional groups change the physical or chemical properties of the existing polymer. For chemical recycling, the modifications could facilitate subsequent controlled degradation reactions; alternatively, modifications may change properties to allow the polymer to be used in a different application entirely (Figure 2.3). Examples of the latter include use of the Paal-Knorr reaction on aliphatic polyketones

for application in luminescence,[21] anion exchange membranes,[22] and coatings.[23] Some instances of controlled depolymerization of polyketones have in fact been demonstrated, however these typically contain built-in segments on the monomer which allow for reversibility[24, 25] or thermal induced depolymerization.[26] Processes which incorporate or alter existing functionality post-polymerization for chemical recycling are an underdeveloped area in plastics research.

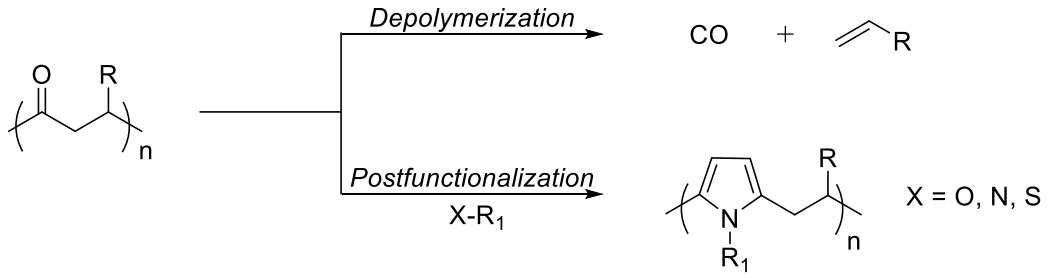

Figure 2.3: General scheme for the depolymerization and post-polymerization functionalization of 1,4-polyketones.

2.1.4 Polyoximes: Applications and Synthesis

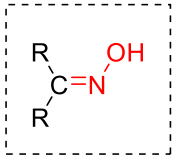

Figure 2.4: Oxime functional group.

Oximes are a common chemical functionality consisting of a carbon-nitrogen double bond with a pendant hydroxyl group on the nitrogen atom (Figure 2.4). This unique structure induces electron delocalization in the sp^2 carbon which allows for higher

resistance towards hydrolysis.[27, 28] As such, this functionality is commonly found within bio conjugates where it is used as a linker to form larger biomolecular constructs which are resistant to physiological conditions.[27] Oxime functionality have also found use as cross-linking agents in larger polymeric structures,[29, 30] exchangeable bond units in vitrimers,[31] and self-healing polymers.[32, 33] The functional diversity of the oxime group makes it an ideal platform for the modification of polymers with the purpose of tuning chemical or physical properties.

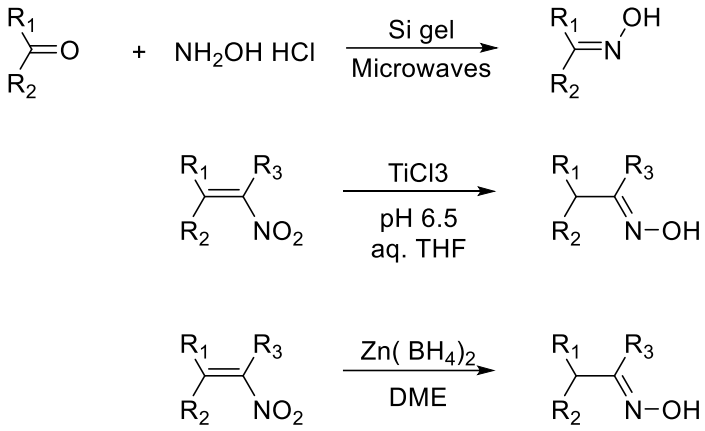

Figure 2.5: Common synthetic routes for the synthesis of oxime functionality.

A variety of synthetic routes exist for oxime synthesis, the most prominent include oximation of a carbonyl by hydroxylamine,[34] and reduction of corresponding nitro compounds using reductants such as titanium (III) chloride,[35] or zinc borohydride[36] (Figure 2.5). For the synthesis of polyoximes, the previous methods may therefore be applied through post-polymerization functionalization to polymers containing the specified functionalities. Alternativity, polyoximes polymers can be synthesized by the copolymerization of monomers containing oxime functionality,[37] though this appears to be a lesser implemented route.

2.1.5 Project Goals

The focus of this project is the development of methods for post-polymerization functionalization of polyketones, either to facilitate chemical recycling, or to prepare a material with novel properties suitable for application in different fields. Since the carbonyl group of the polyketone backbone is selected as the primary target for functionalization, the reactions investigated are centered around ketone chemistry. The polyketone of choice for post-polymerization functionalization attempts is the PK-VM Natural 4774 line of polyketones made by Akrotek® (Figure 2.6). These polyketones possess high impact strength, are resistant to solvent and acid/base exposure and degrade at high temperatures. As such, these polymers find application in injection molding to form plastic parts typically used in the automotive industry.[38]

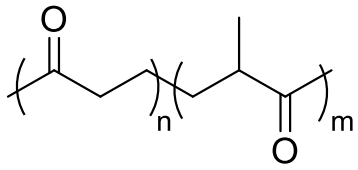

1

Figure 2.6: Akrotek® PK-VM 4774 polyketone.

Since the selected polymer possesses chemical inertness as well as thermal and stress resistance, it poses a significant challenge for current chemical recycling methods. A series of post-polymerization reactions are studied and the avenues for depolymerization or reapplication are explored for the ultimate purpose of chemical recycling of this polymer and future application to others like it.

2.2 Results and Discussion

2.2.1 Post-Polymerization Functionalization of Polyketone to Polyoxime

Post-polymerization modification of polyketone carbonyls could improve solubility of the polymer and enable subsequent depolymerization by providing a site of greater reactivity. As a starting point we chose a procedure of Lu and coworkers,[39] who converted polyketones to polyoximes by use of aqueous hydroxylamine to replace carbonyl groups with oxime groups. A modified version of this procedure was followed, which included swelling the polyketone pellets in dimethylformamide (DMF) at 150 °C rather than refluxing them in toluene due to the later solvent having no effect on the solubility of the polyketone pellets. The resulting solution was then reacted with methanol and aqueous hydroxylamine at room temperature for five days to yield PK-VM polyoximes (**2**) as a yellow powder (Figure 2.7).

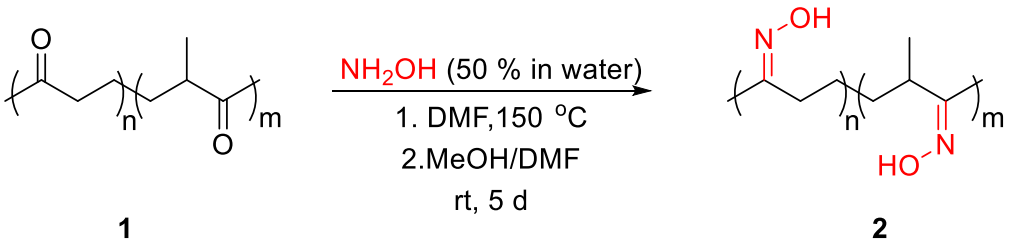

1 **2**

Figure 2.7: Reaction of Akrotek® 4774 PK-VM polyketones with aqueous hydroxylamine to form polyoximes.

Oxime functionality was confirmed by observing the N-OH proton in the ^{1}H NMR spectra (Figure 2.8, A) and the C=N functionality through ^{13}C NMR (Figure 2.8, B). No NMR spectra were obtained for the parent PK-VM polyketone due to its insolubility in common NMR solvents at room temperature.

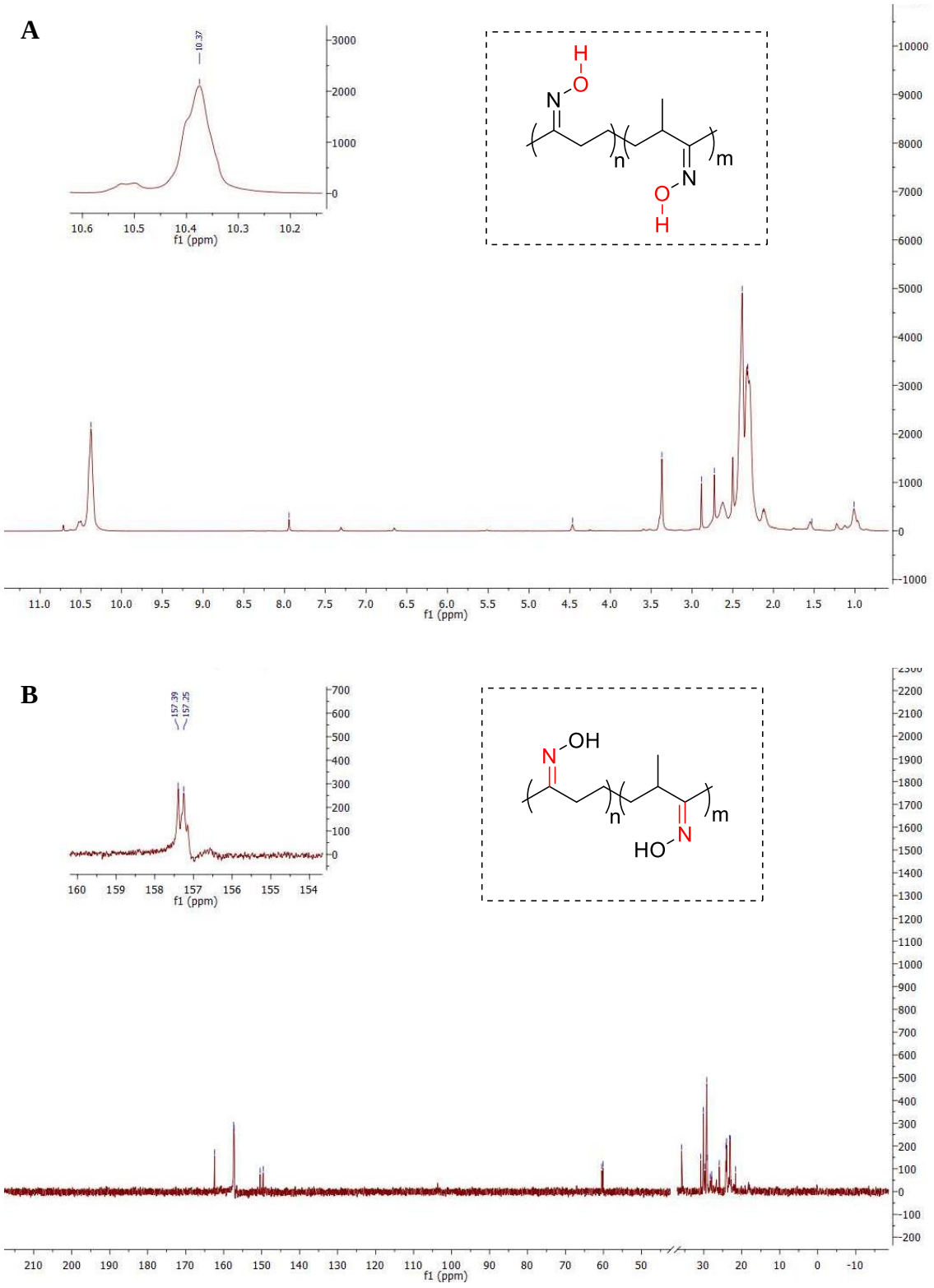

Figure 2.8: (A) ^{1}H NMR spectra of polyoxime with hydroxyl proton inset at 10.37 ppm. (B) ^{13}C NMR spectra of polyoxime with imine bond shown in inset at 157 ppm. (Solvent: DMSO- d^{6}).

Infrared spectra of the solid polyketone and polyoxime products were compared (Figure 2.9). The strong and sharp carbonyl stretch seen at 1689 cm^{-1} for the polyketone sample is not seen in the polyoxime spectrum. Instead, a large broad peak observed at 3200 cm^{-1} can be attributed to a oxime O-H stretch. A peak at approximately 1600 cm^{-1} is likely the C=N functionality. Though this potential imine peak is less clearly identified due to a large amount of noise.

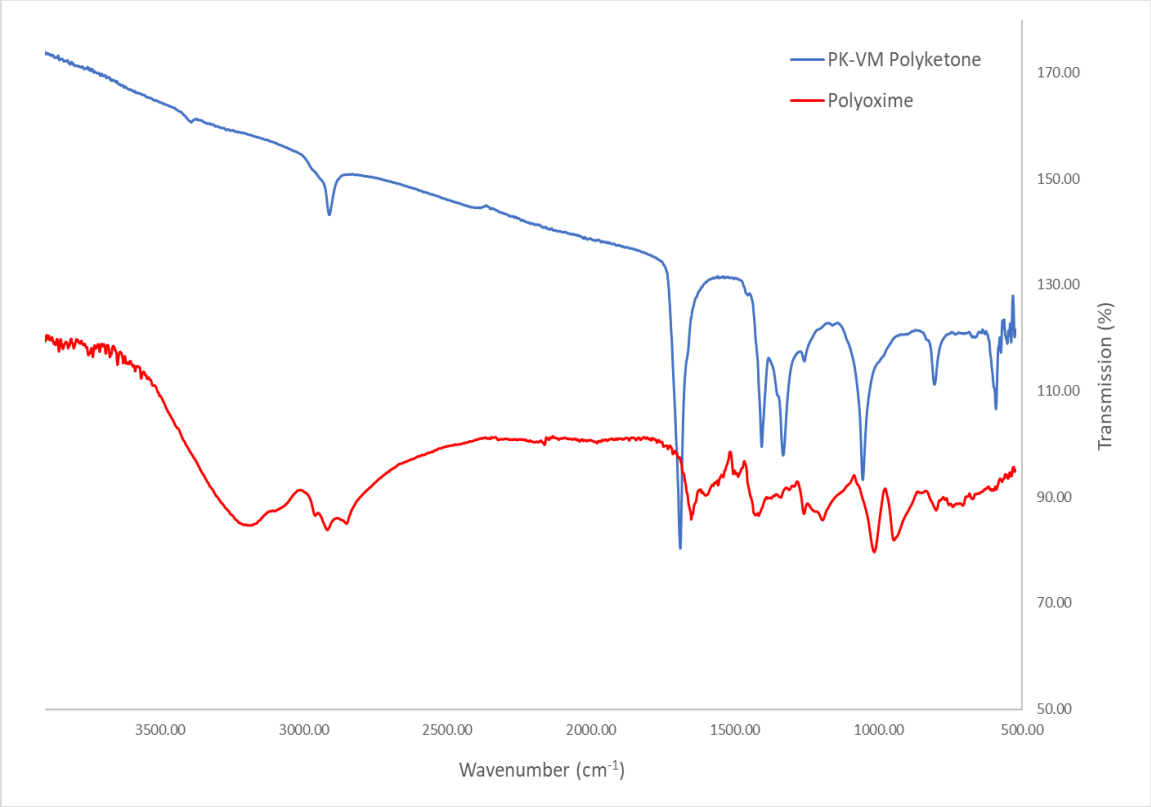

Figure 2.9: Infrared spectra of PK-VM polyketone (blue) and the polyoxime product (red).

The solubility of the polymer improved in DMSO after the functionalization from carbonyl to oxime. DMSO is suitable for NMR analysis, however it is a poor work-up solvent due to its high boiling point. GPC analysis is also difficult in DMSO as the mobile phase resulting from the high viscosity. It was found that refluxing in xylenes (139 °C) does dissolve the polyoxime thus this solvent was selected for GPC analysis. The molecular weight obtained for this post-functionalized polymer is very low, though dispersity is almost an ideal value of 1.0 (Table 2.1).

M_w (kDa)	M_n (kDa)	Đ (M_w/ M_n)
1.4	1.6	1.2

Table 2.1: Molecular weight data of polyoxime. Xylenes used as a mobile phase along with polymethyl methacrylate standards.

2.2.2 Thermal Analysis

In addition to NMR and infrared spectroscopy, the PK-VM polyketones and post-functionalized polyoxime thermal degradation points and morphology were contrasted through thermogravimetric analysis (TGA) and differential scanning calorimetry (DSC) respectively. TGA shows that upon heating, the PK-VM polyketone begins degradation at approximately 355 °C and sharply declines to a loss of 50% of its mass at approximately 393 °C (Figure 2.10). This sharp decline in mass is expected as it is characteristic of a semicrystalline polyketone.[40, 41] The polyoxime however, degrades at almost half the temperature that the original polyketone degrades at (Figure 2.10).

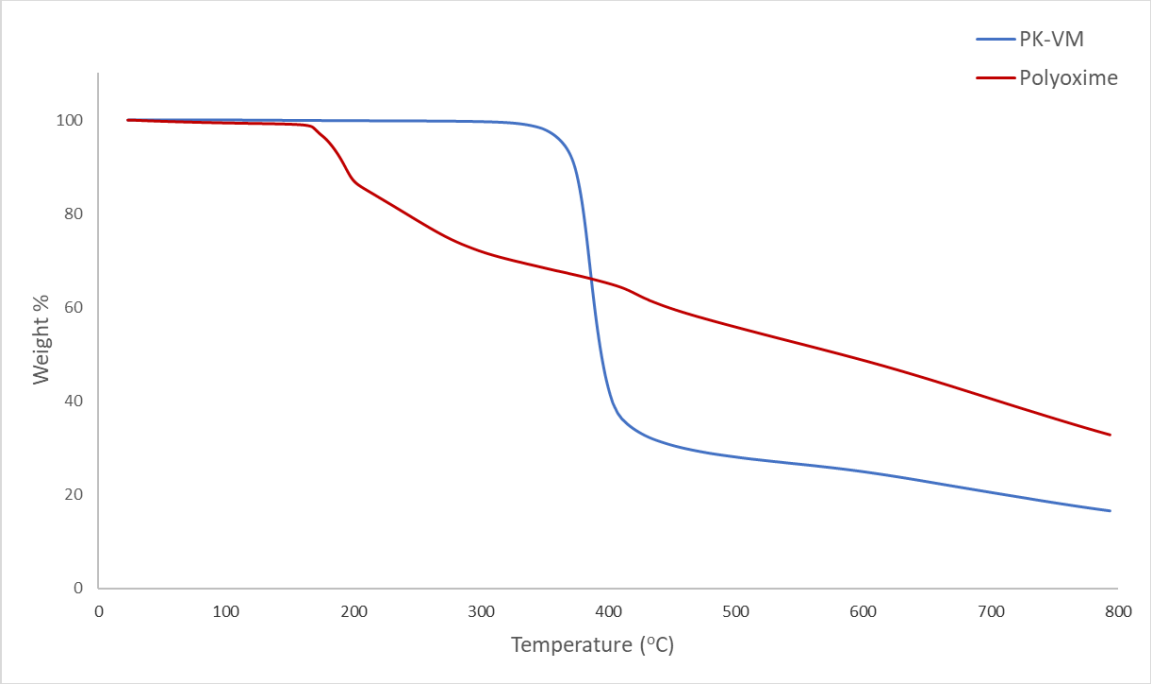

Figure 2.10: Thermogravimetric analysis of PK-VM polyketone (blue) and polyoxime yielded from post-functionalization of polyketone (red).

Beginning at approximately 168 °C, the polyoxime does not lose 50% of its original mass until 570 °C and mass declination is over a gradual slope rather than a sharp drop. This finding seems to indicate a change in polymer morphology after the post-polymerization functionalization from ketone to oxime. Additionally, the thermal stability has clearly decreased which may be beneficial for chemical recycling applications.

A deeper analysis by DSC gives insight into the potential alteration of polymer morphology after functionalization. Again, the PK-VM polyketone precursor and its functionalized polyoxime product are compared. When observing the first heating cycle

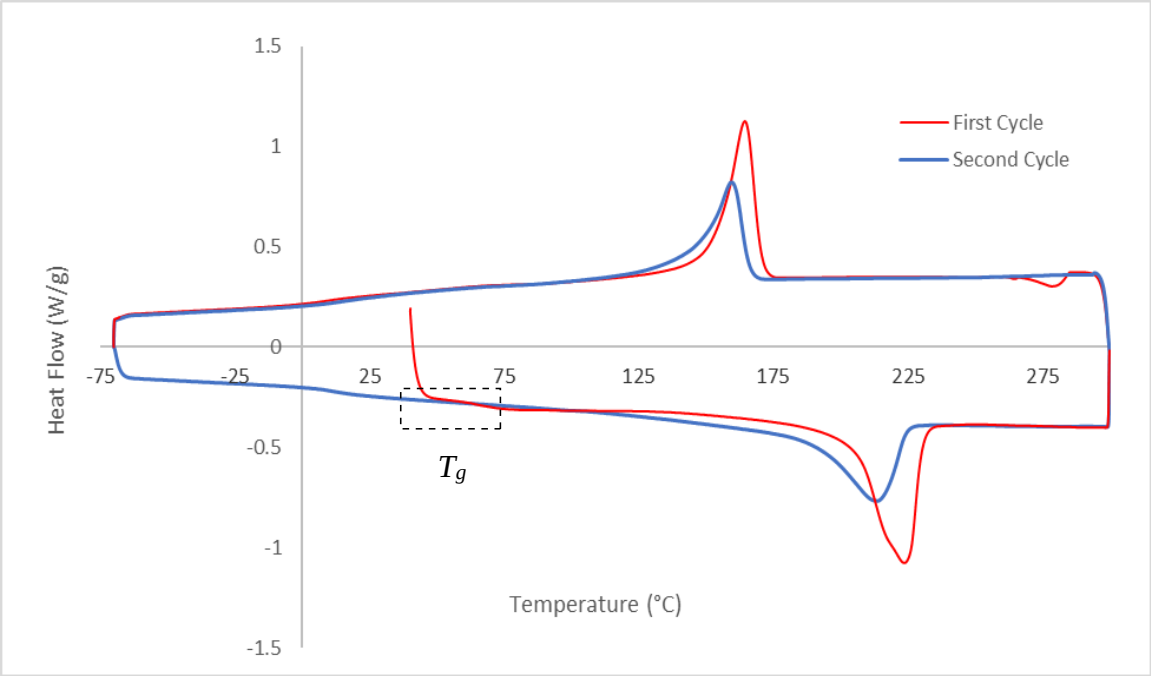

Figure 2.11: Differential scanning calorimetry reading for PK-VM polyketone. The first heating/cooling cycle is shown in red and the second, in blue.

for the polyketone, a glass transition temperature can be observed at approximately 63 °C to 75 °C (Figure 2.11). Following this, a melt is observed at approximately 224 °C in the first cycle and 214 °C in the second. Upon cooling, the polyketone then undergoes crystallization at 165 °C in the first heating cycle and 160 °C in the second. These results are expected and indicate what is likely a semi-crystalline polymer.[42] In contrast, the polyoxime obtained from the functionalization of this polyketone does not show these characteristics. In both heating and cooling cycles there are no observable melting or crystallization points (Figure 2.12). It should be noted that in this case a maximum temperature of 150 °C was chosen based on the observed degradation point found in thermogravimetric analysis, therefore no phase transitions are likely to be observed past this window. Such an absence may be indicative of an amorphous polymer. The

morphology has clearly been altered after post-polymerization functionalization of carbonyl groups.

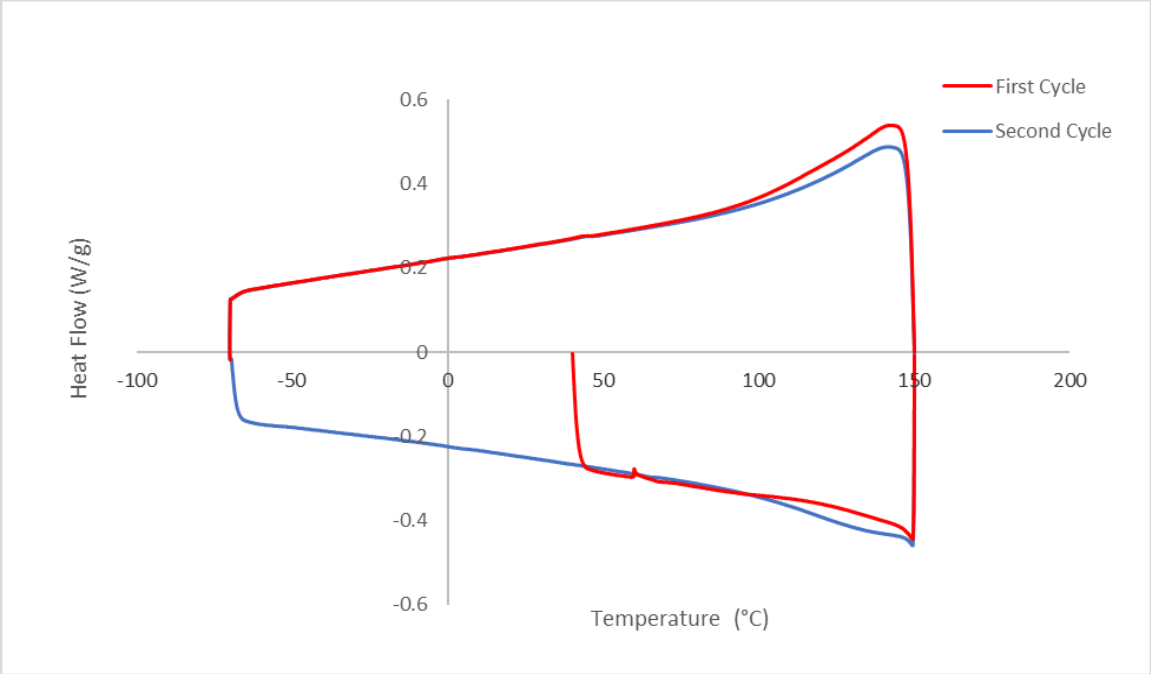

Figure 2.12: Differential scanning calorimetry reading for the oxime functionalized PK-VM polymer. The first heating/cooling cycle is shown in red and the second, in blue.

2.2.3 Functionalization Attempts of PK-VM Polyoxime

In addition to the post-polymerization functionalization of the PK-VM polyketones, the resulting polyoximes were envisioned to undergo additional functionalization to enable the process of depolymerization to individual monomers. One method to achieve this goal involved the transformation of the oxime groups on the polymer to amide functionality via the intramolecular Beckmann rearrangement (Figure 2.13). This process has been demonstrated by Michel and coworkers in their studies of intramolecular rearrangements of polyketones.[43] Once the polyoxime was functionalized to polyamide, it was proposed

that this polymer would then be able to undergo degradation via exposure to hydrochloric or formic acid to yield its respective carboxylic acid and diamine monomers. Such a process has in fact been demonstrated on the polyamide Nylon.[44, 45] Other methods of degradation for such a polyamide like UV exposure or pyrolysis are also possible however these present the same issues discussed earlier.[46] Therefore, this transformation is promising due potential reclamation and reuse of monomers after depolymerization.

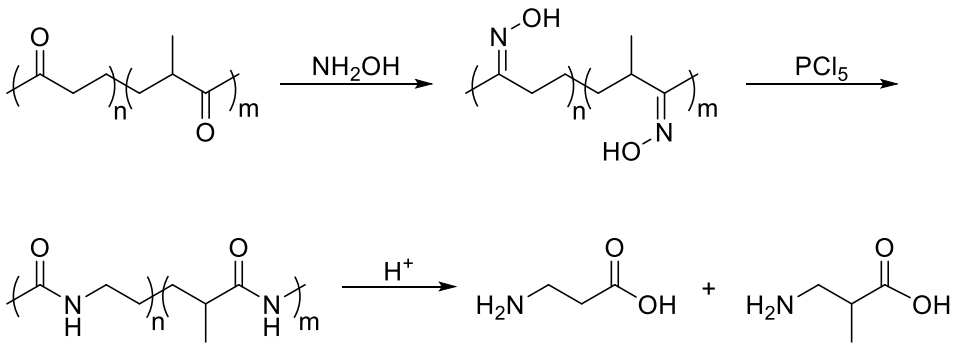

Figure 2.13: Post-polymerization functionalization of PK-VM polyketone to polyoxime. The Beckmann rearrangement is proposed to yield polyamides then exposed to acid degradation to yield amine/carboxylic acid monomers.

A modified version of the procedure outlined by Michel and coworkers was implemented due to poor solubility of the polymer in chloroform.[43] The polymer was dissolved in DMSO as the solvent, then subjected to phosphorous pentachloride (PCl_5). However, no evidence suggesting the formation of an amide was observed. Other oxidants such as phosphorus pentoxide (P_2O_5) were also used but yielded similar outcomes. One potential explanation for these results is the possibility that the oxidant is reacting with the solvent instead of the polymer. Unfortunately, the reaction solvent choice is limited due to restricted solubility of the polyoxime, and there is no other inert polar solvent known at this time. Rather than a full depolymerization of the polymer, the transformation to

polyoxime has at the very least lowered the thermal degradation point of the polymer therefore making recycling an easier possibility for this material.

2.2.4 Application of PK-VM Polyoximes: Aqueous Metal Chelation

The potential application of the synthesized polyoxime in other areas was also explored. One such area polyoximes have been utilized is in the water purification process. Specifically, these polymers have been used as heterogenous chelating agents to bind metal ions in aqueous solutions in order to remove potentially toxic substances from water supplies.[47, 48, 49] Therefore, PK-VM polyoximes were investigated as to their applications in this area as well. A series of metal ions of oxidation state +2, whose identity include copper, cobalt, nickel, manganese, iron and chromium, and their possible chelation abilities to the polymer were investigated (Figure 2.14).

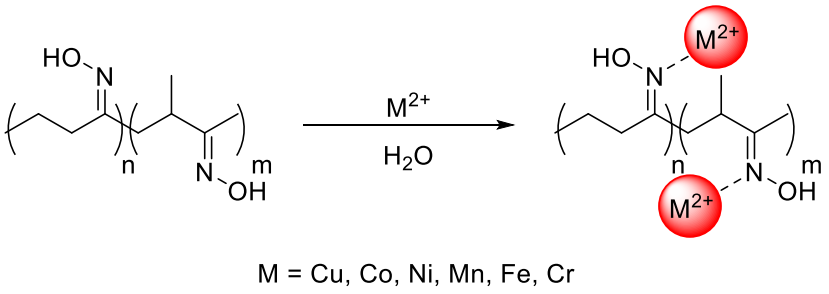

Figure 2.14: Possible metal chelation to PK-VM polyoximes in aqueous medium.

To measure the potential chelation ability of the polyoximes, the concentration of the aqueous metal solution was determined before and after exposure to the polymer. Any difference in metal concentration was attributed to chelation to the polymer. Solution concentration was measured by use of UV-Vis spectrophotometry, with concentration determined from absorption using standards and the Beer-Lambert law. When 100 mg of

polyoxime was used, the aqueous metal filtrate had an absorbance of 0.462 (Table 2.2) at λ_{max} = 808 nm (Figure 2.15). Standard solutions of the copper (II) chloride salt had the same λ_{max} = 808 nm. Assuming a linear relationship between concentration and absorbance, the amount of copper remaining in the filtrate after exposure to 100 mg polymer was determined to be 33.97 mg/5 mL, implying 6.03 mg of copper was bound to the 100 mg polymer sample.

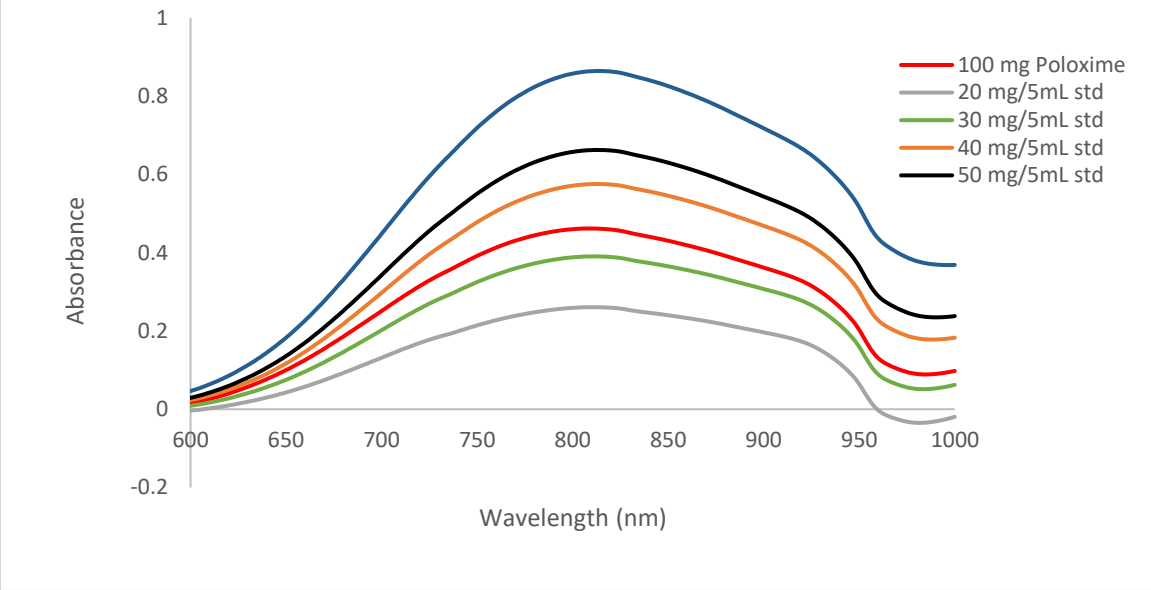

Figure 2.15: Combined UV-Vis spectra of copper standards and metal ion solution after exposure to 100 mg of polyoxime.

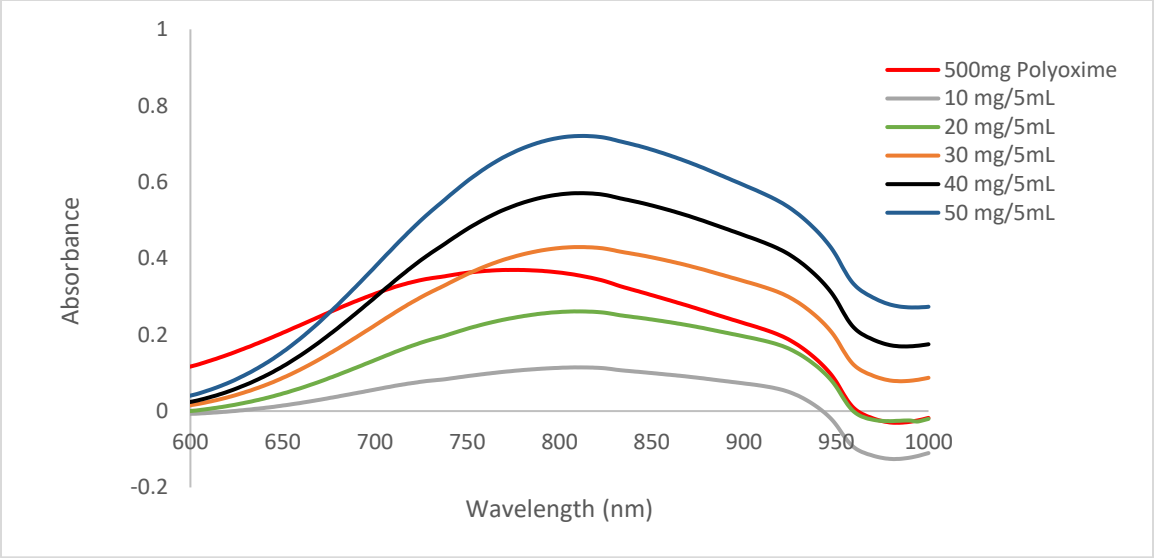

Figure 2.16: Combined UV-Vis spectra of copper standards and metal ion solution after exposure to 500 mg of polyoxime.

When 500 mg of polyoxime is used, UV-Vis results indicate a max absorption of 0.3698 at λ_{max} = 778 nm (Figure 2.16). Here, λ_{max} has shifted from the copper standards (808 nm). Using the max absorption values of the standards, the amount of copper remaining in the filtrate solution was determined to 26.8 mg which implies 13.2 mg would be retained to the polymer (Table 2.2).

Clearly with these two instances, the amount of copper present in the final solution decreases as polymer amount is increased. Whether this may be attributed to polymer chelation, or some other factor is difficult to determine. Fluctuation of the oxime proton or imine carbon shift as a result of copper coordination is difficult to monitor since the copper ions may not be bound to the polymer for long before precipitation, if even bound at all. Furthermore, since the polyoximes were synthesized in DMF, it may be the case that residual amounts of this solvent present within the polymer are acting as the chelating agent. A control experiment was conducted which contained two polyoximes: one in which

the polymer was spiked with DMF during the work-up process and the other which was washed copiously with dichloromethane and dried under vacuum until all observable traces of DMF were removed. The sample which contained DMF showed a higher absorbance and therefore a greater amount of copper retention was determined compared to the clean polyoxime when used in the same copper chelation experiments (Table 2.2). This may suggest that DMF plays a role in the binding of copper, though this does not rule out any chelation ability of the polymer itself. With the data on hand at present, it is unclear what degree residual solvent within the polyoxime plays in the chelation of copper ions in aqueous solutions.

Polymer	**Cu^{2+} Retained (mg)**	**Filtrate Abs Max**
Polyoxime (100 mg)	6.03	0.462
Polyoxime (500 mg)	13.2	0.370
DMF Spiked Polyoxime	8.1	0.435
Clean Polyoxime	1.4	0.541

Table 2.2: Amount of copper theoretically retained by polyoxime via chelation along with the corresponding max absorption.

Since the polyoxime appears to bind copper, chelation of other metals was also considered. It had been previously found that generally polyoximes have a higher uptake for copper ions though other metals are also observed to chelate to a lesser degree.[47, 49] In our instance, aqueous cobalt, nickel, manganese, iron, and chromium did appear to exhibit

the same degree of chelation as copper. These results do not rule out any chelation ability of the polymer towards these metals, however. The use of UV-Vis for the determination of metal concentration is simple and quantitative, but sample range is limited to colored solutions. Another technique such as atomic absorption spectroscopy may provide better information on metal concentration. Furthermore, the ligation environment around the metal ion itself may also play a factor in chelation. Further chelation studies on the metals listed above may be more conclusive if other metal species are implemented.

2.3 Conclusion

This project explored the ability of a commercial polyketone to undergo post-polymerization functionalization with two possible uses in mind: to facilitate depolymerization routes, and to change chemical or physical properties. PK-VM 4774 polyketones supplied from Akrotek® underwent functionalization to polyoximes by reaction with hydroxylamine.

We hypothesized that the resulting polyoxime could transform to polyamides via the Beckmann rearrangement, which could then be depolymerized into the respective carboxylic acid and amine-containing monomers. Although complete depolymerization was unsuccessful, the polyoximes have a lower degradation temperature than the parent polyketones, which be explored in future work targeting the degradation and chemical recycling of thermoplastics.

The polyoxime was investigated for metal chelation in aqueous media. Results obtained by UV-Vis spectrophotometry suggest that metal concentration in solutions after exposure to the polyoxime decreased by a small amount, relative to the initial metal

solution before any polymer addition. Though residual solvent appears to play some role in the efficiency of the chelation. The chelation ability of the polymer towards other metal species cannot be conclusively determined at this time.

2.4 Experimental

2.4.1 General Methods

All preparations or reactions which are noted to be air- or moisture sensitive were performed in a glove box under nitrogen atmosphere or using Schlenk techniques. Chemicals were purchased commercially unless otherwise noted and no additional purification methods were taken. Solvents used in inert atmosphere were degassed by a solvent purification system and dried using molecular sieves. ^{1}H and ^{13}C NMR spectra were collected on a Bruker AVIII 500 or a Bruker AV400 spectrometer. All NMR samples were referenced to a residual protio-solvent. Polymer molecular weight analysis was conducted on a Shimadzu LC 20-AT chromatograph with three 300 x 7.5 mm Agilent PolarGeL® columns (two M, one L) at an oven temperature of 30 °C and flow rate of 0.5 mL/min. Tetrahydrofuran or acetone were used as eluent unless noted otherwise. Molecular weight was determined by use of a refractive index detector calibrated with polymethyl methacrylate standards (200-71,800 Da). IR spectra were collected on a Thermo Scientific Nicolet is5 ATR-FTIR spectrophotometer. Differential scanning calorimetry was conducted on a TA Instruments Discovery DSC 250. Thermogravimetric analysis was conducted on a TA Instruments Discovery 550 TGA. UV-Vis spectra were obtained on a Shimadzu UV-1800 spectrophotometer.

2.4.2 Post-polymerization Functionalization of Polyketones to Polyoximes

PK-VM 4774 Natural polyketones were purchased from Akrotek® as plastic pellets. 500 mg of polymer was added to a vial containing 5 mL of DMF, then heated at 150 °C until the pellets melted into the solvent. The solution was removed from heat and an additional 5 mL of DMF was added along with 6 mL of hydroxylamine (50% in water) and 10 mL of methanol. The solution was stirred at room temperature for five days, after which 25 mL of water was added and a white precipitate formed immediately. The solution was filtered and the solid washed with water, methanol and DCM then dried under vacuum overnight to yield the polyoxime product (**2**). ^{1}H NMR: (500 MHz, DMSO-d_6) δ 10.37 (br), 2.62 (br), 2.38 (br), 2.32 (br), 2.12 (br), 1.54 (br), 1.22 (br), 1.13 (br), 1.01 (br). ^{13}C NMR: (126 MHz, DMSO-d_6) 157.39, 157.29, 150.39, 149.60, 60.43, 60.14, 30.83, 30.10, 29.72, 29.23, 29.03, 25.91, 24.17, 24.01, 23.18, 23.03, 21.61. IR: 3200 cm^{-1} (N-OH).

2.4.3 Procedure for Beckmann Rearrangement of Polyoximes

The procedure was modified from that described by Michel and coworkers.[43] 250 mg of the polyoxime was dissolved in 6 mL of DMSO, 2.0 g of PCl_5 was dissolved separately in 6 mL of chloroform. The polymer solution was placed on an ice bath and once solution temperature reached 0 °C, the PCl_5 was added dropwise while stirring. After 30 minutes, the reaction was poured into a separatory funnel packed with ice then diluted with water. A brown precipitate formed and was collected. The organic layer was isolated and dried over $MgSO_4$ then concentrated to reveal a yellow oil. ^{1}H NMR and IR analysis of both the brown precipitate and the yellow oil indicated no presence of a polyamide.

2.4.4 Polyoxime Metal Ion Chelation

The general procedure for polyoxime metal ion chelation in aqueous medium is described as follows: A calibration curve was created by dissolving the metal salt hydrates ($CuCl_2 \cdot 2H_2O$, $NiCl_2 \cdot 6H_2O$, $Co(OAc)_2 \cdot 4H_2O$, $FeSO_4 \cdot 7H_2O$, $MnCl_2 \cdot 4H_2O$, $CrCl_2$) in DI water to the appropriate concentrations in 5 mL volumetric flasks. The metal solution was created by dissolving 40 mg of metal ion hydrate in 5 mL of water then passing it over the 100 or 500 mg of the polyoxime which was packed into a Schlenk frit. After being passed through the frit packed with polyoxime, the metal ion solution was collected and UV-Vis absorption was recorded along with the series of standards of known concentration. The maximum absorption for each standard and the filtered metal solution for copper as the metal is shown in Table 2.3. The concentration of each standard's max absorption was then plotted with respect to concentration (Figure 2.17).

Sample	Concentration (mg/5mL)	Max Absorption	λ Max (nm)
Standard 1	10	0.11447	809
Standard 2	20	0.26117	808
Standard 3	30	0.42963	811
Standard 4	40	0.57086	812
Standard 5	50	0.72072	813
Filtered Solution	33.98	0.36977	778

Table 2.3: Max absorption values for copper standard solutions and solution after exposure to polyoxime along with corresponding wavelengths.

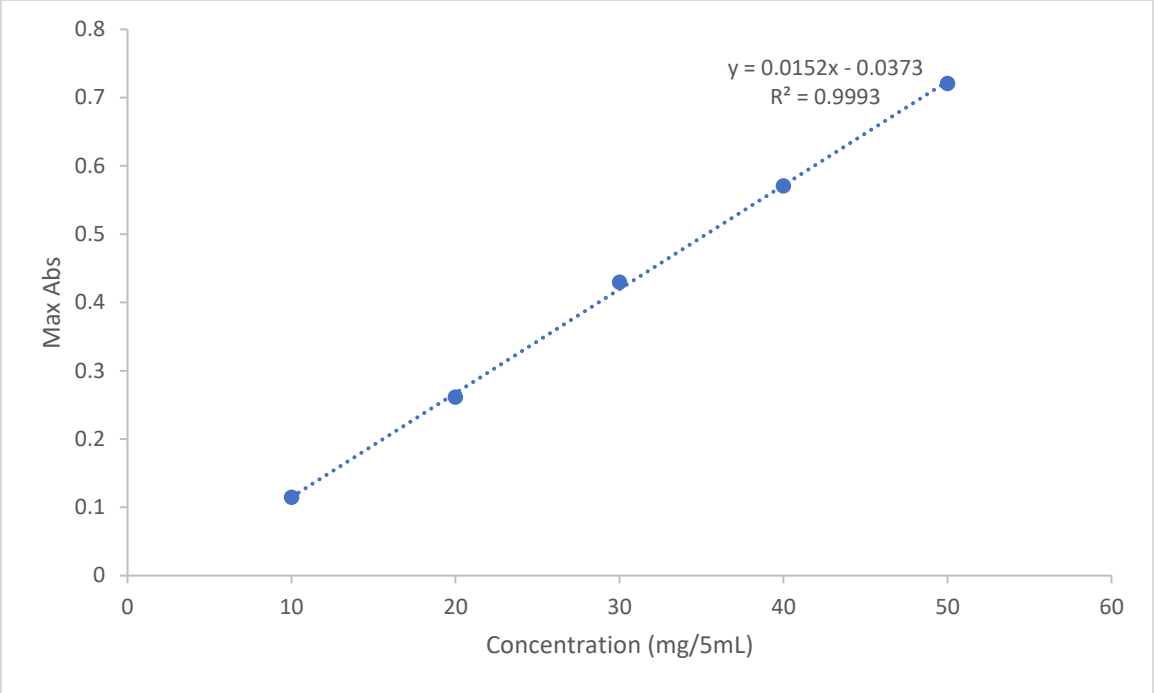

Figure 2.17: Calibration curve plotted from copper ion standards listed in Table 2.3 with max absorption as a function of concentration.

Concentration of the filtered metal ion solution was determined by use of the Beer-Lambert law (Equation 2.1). Where A is absorbance, ε is the molar absorptivity, b is the width of the cell (1 cm), and C is the concentration.

$$A = \varepsilon bC \qquad \textbf{(2.1)}$$

A modified version may be written setting equation 1 equal to the slope-intercept form of a straight line (Equation 2.2). Where the slope m is equal to $\varepsilon(b)$ and x equal to concentration (Equation 2.3).

$$y = mx + b \qquad \textbf{(2.2)}$$

$$A = (\varepsilon b)C + b \qquad \textbf{(2.3)}$$

To find the concentration of the filtered solution, max absorbance for the sample was substituted into Equation 3 as y, the slope value of 0.0152 from the calibration curve was used for εb and 0.0373 for the y intercept b. Solving for x gives a concentration value of 33.98 mg/5mL (Table 2.3), or 33.98 mg of copper out of an initial 40 mg implying a difference of 6.02 mg.

2.5 References Cited

(1). Environmental Protection Agency, *Plastics: Material-Specific Data*. **2023**, https://www.epa.gov/facts-and-figures-about-materials-waste-and-recycling/plastics-material-specific-data

(2). Morici, E.; Carroccio, S. C.; Bruno, E.; Scarfato, P. Filippone, G.; Dintcheva, N. T. Recycled (Bio)Plastics and (Bio)Plastic Composites: Trade Opportunity in a Green Future. *Polymers*, **2022**, *14*, 2038.

(3). Grigore, M. E. Methods of Recycling, Properties and Applications of Recycled Thermoplastic Polymers. *Recycling*, **2017**, *2* (4), 24.

(4). Geyer, R.; Jambeck, J. R.; Law, K. L. Production, Use, and Fate of All Plastics Ever Made. *Science Advances*, **2017**, *3*, e1700782.

(5). Patil, A.; Patel, A.; Purohit, R. An Overview of Polymeric Materials for Automotive Applications. *Materials Today: Proceedings*, **2017**, *4*, 3807-3815.

(6). Giri, K.; Tsao, C. Recent Advances in Thermoplastic Microfluidic Bonding. *Micromachines*, **2022**, *3*, 486.

(7). Nguyen, H. T. H.; Qi, P.; Rostagno, M.; Feteha, A.; Miller, S. A. The Quest for High Glass Transition Temperature Bioplastics. *J. Mater. Chem. A.*, **2016**, *6* (20), 9298-9748.

(8). Singh, N.; Hui, D.; Singh, R.; Ahuja, I. P. S.; Feo, L.; Fraternali, F. Recylcing of Plastic Solid Waste: A State of the Art Review and Future Applications. *Composites Part B*, **2017**, *115*, 409-422.

(9). Teuten, E. L.; Saquing, J. M.; Knappe, D. R. U.; Barlaz, M. A.; Jonsson, S.; Bjorn, A.; Rowland, S. J.; Thompson, R. C.; Galloway, T. S.; Yamashita, R.; Ochi, D.; Watanuki, Y.; Moore, C.; Viet, P. H.; Tana, T. S.; Prudente, M.; Boonyatumanond, R.; Zakaria, M. P.; Akkhavong, K.; Ogata, Y.; Hirai, H.; Iwasa, S.; Mizukawa, K.; Hagino, Y.; Imamura, A.; Saha, M.; Takada, H. Transport and Release of Chemicals from the Environment and to Wildlife. *Phil. Trans. R. Soc. B.*, **2006**, *364*, 2027-2045.

(10). Shibamoto, T.; Yasuhara, A.; Katami, T. Dioxin Formation from Waste Incineration. *Rev. Environ. Contam. Toxicol.*, **2007**, *190*, 1-41.

(11). Ragaert, K.; Delva, L.; Geem, K. V. F. Mechanical and Chemical Recycling of Solid Plastic Waste. *Waste Management*, **2017**, *69*, 24-58.

(12). Rahimi, A.; Garcia, J. M. Chemical Recycling of Waste Plastics for New Materials Production. *Nature Reviews*, **2017**, *1* (0046).

(13). Chen, C.; Chen, C.; Lo, Y.; Mao, C.; Liao, W. Studies of Glycolysis of Poly(ethylene terephthalate) Recycled from Postconsumer Soft-Drink Bottles. I. Influences of Glycolysis Conditions. *J. Appl. Polym. Sci.*, **2001**, *80*, 943-948.

(14). Chen, J.; Chen, L. The Glycolysis of Poly(ethylene terephthalate). *J. Appl. Polym. Sci.*, **1999**, *73*, 35-40.

(15). Paszun, D.; Spychaj, T.; Chemical Recycling of Poly(ethylene terephthalate). *Ind. Eng. Chem. Res.* **1997**, *36* (4), 1373-1383.

(16). Sinha, V.; Patel, M. R.; Patel, J. V. PET Waste Management by Chemical Recycling: A Review. *J. Polym. Environ.* **2010**, *18*, 8-25.

(17). Miao, Y.; Jouanne, A. V.; Yokochi, A. Current Technologies in Depolymerization Process and the Road Ahead. *Polymers*. **2021**, *13*, 449.

(18). Golodkov, O. N.; Ol'khov, Y. A.; Allayarov, S. R.; Grakovich, P. N.; Belov, G. P.; Ivanov, L. F.; Kalinin, L. A.; Dixon, D. A. The Effect of γ-Irradiation on Laser Ablation of Polyketone. *Radiation Chemistry*. **2013**, *47* (3), 77-82.

(19). Arrington, K. J.; Waugh, J. B.; Radzinski, S. C.; Matson, J. B. Photo- and Biodegradable Thermoplastic Elastomers: Combining Ketone-Containing Polybutadiene with Polylactide Using Ring Opening Polymerization and Ring-Opening Metathesis Polymerization. *Macromolecules*, **2017**, *50*, 4180-4187.

(20). Reeves, J. A.; Allegrezza, M. L.; Konkolewicz, D. Rise and Fall: Poly(phenyl vinyl ketone) Photopolymerization and Photodegradation under Visible and UV Radiation. *Macromol. Rapid Commun.*, **2017**, *38*, 1600623.

(21). Du, C.; Cheung, C. S.; Zheng, H.; Donghui, L.; Du, W.; Gao, H.; Liang, G.; Gao, H. Bathochromic-Shifted Emissions by Postfunctionalization of Nonconjugated Polyketones. *ACS Appl. Mater. Interfaces*, **2021**, *13*, 59288-59297.

(22). Zhou, Y.; Zhou, L.; Feng, C.; Wu, X.; Bao, R.; Liu, Z.; Yang, M.; Yang, W. Direct Modification of Polyketone Resin for Anion Exchange Membrane of Alkaline Fuel Cells. *Journal of Colloid and Interface Science*, **2019**, *556*, 420-431.

(23). Toncelli, C.; Schoonhoven, M.; Broekhuis, A. A.; Picchioni, F. Paal-Knorr Kinetics in Waterborne Polyketone-based Formulations as Modulating Cross-Linking Tool in Electrodeposition Coatings. *Materials & Design*, **2016**, *108*, 718-724.

(24). Xiong. W.; Chang, W.; Shi, D.; Yang, L.; Tian, Z.; Wang, H.; Zhang, Z.; Zhou, X.; Chen, E.; Lu, H. Geminal Dimethyl Substitution Enables Controlled Polymerization of Penicillamine-Derived b-Thiolactones and Reversed Depolymerization. *Chem.*, **2020**, *6*, 1831-1843.

(25). Gandini, A.; The Furan/Maleimide Diels-Alder Reaction: A Versatile Click-Unclick Tool in Macromolecular Synthesis. *Progress in Polymer Science*, **2013**, *38* (1), 1-29.

(26). Bertini, F.; Audisio, G.; Kiji, J. Thermal Degradation of Alternating Styrene-Carbon Monoxide Copolymers. *Journal of Analytical and Applied Pyrolysis*, **1999**, *49*, 31-42.

(27). Ulrich, S.; Boturyn, D.; Marra, A.; Renaudet, O.; Dumy, P. Oxime Ligation: A Chemoselective Click-Type Reaction for Accessing Multifunctional Biomolecular Constructs. *Chem. Eur. J.*, **2014**, *20*, 34-41.

(28). Kalia, J.; Raines, R. T. Hydrolytic Stability of Hydrazones and Oximes. *Angew. Chem. Int. Ed.*, **2008**, *47*, 7523-7526.

(29). Hardy, H. G.; Lin, P.; Schmidt, C. E. Biodegradable Hydrogels Composed of Oxime Crosslinked Poly (Ethylene Glycol), Hyaluronic Acid and Collagen: A Tunable Platform for Soft Tissue Engineering. *Journal of Biomaterials Science, Polymer Edition*, **2015**, *26* (3), 143-161.

(30). Ghosh, S.; Cabral, J. D.; Hanton, L. R.; Moratti, S. C. Strong Poly(Ethylene Oxide) Based Gel Adhesives Via Oxime Cross-Linking. *Acta Biomaterialia*, **2016**, *29*, 206-214.

(31). He, C.; Shi, S.; Wang, D.; Helms, B. A.; Russell, T. P. Poly(Oxime-Ester) Vitrimers with Catalyst-Free Bond Exchange. *J Am. Chem. Soc.*, **2019**, *141*, 13753-13757.

(32). Fu, D.; Pu. W.; Wang, Z.; Lu, X.; Sun, S.; Yu, C.; Xia, H. A Facile and Dynamic Crosslinked Healable Poly(Oxime-Ureathane) Elastomer with High Elastic Recovery and Recyclability. *Journal of Materials Chemistry A*, **2018**, *6* (37), 18154-18164.

(33). Cai, Y.; Li, C.; Yang, Y.; Li, H.; Wang, Y.; Zhang, Q. Self-Healable and Reprocessable Cross-Linker Poly(Urea-Urethane) Elastomers with High Mechanical Performance Based on Dynamic Oxime-Carbamate Bonds. *Ind. Eng. Chem. Res.*, **2021**, *60*, 13585-135593.

(34). Hajipour, A. R.; Mellakpour S. E.; Imanzadeh, G. A Rapid and Convenient Synthesis of Oximes in Dry Media under Microwave Irradiation. *Journal of Chemical Research Synopses*, **1999**, 23 (3), 228-229.

(35). Sera, A.; Fukumoto, S.; Tamura, M.; Takabatake, K. Titanium(III) Chloride Mediated Reduction of 1-Nitro-2-Phenylethenes. *Bull. Chem. Soc. Jpn.*, **1991**, *64*, 1787-1791.

(36). Ranu, B. C.; Chakraborty, R. Reduction of Conjugated Nitroalkenes with Zinc Borohydride. A Mild Method for Converting Monosubstituted Nitroalkenes to Nitroalkanes and Disubstituted Ones to Oximes. *Tetrahedron*, **1992**, *48* (25), 5317-5322.

(37). Liu, W.; Zhang, C.; Zhang, H.; Zhao, N.; Yu, Z.; Xu, J. Oxime-Based and Catalyst-Free Dynamic Covalent Polyurethanes. *J. Am. Chem. Soc.*, **2017**, *139*, 8678-8684.

(38). Akro-Plastic, PK- Polyketone PK: *Akrotek® PK-VM Natural (4774)*. **2023**, https://akro-plastic.com/productfilter/details/4774/

(39). Lu, S.; Paton, R. M.; Green M. J.; Lucy, A. R. Synthesis and Characterization of Polyketoximes Derived from Alkene-Carbon Monoxide Copolymers. *European Polymer Journal*, **1996**, *32* (11), 1285-1288.

(40). Shrivastava, A. 1 – Introduction to Plastics Engineering. In *Plastics Design Library*, Shrivastava, A., William Andrew Publishing, **2018**, 1-16.

(41). Banihashemi, A.; Akhlaghinia, B. New Heat Stable Polyethers, Polyketones and Polysulfones. *Macromol. Chem. Phys.*, **1999**, *200*, 2284-2293.

(42). Porras, C.; Alcantar, P.; Solis, V.; Guerra, E.; Balderrama, C. I.; Martinez, I. C.; Leos, M. Z. Application of Differential Scanning Calorimetry (DSC) and Modulated Differential Scanning Calorimetry (MDSC) in Food and Drug Industries. *Polymers*, **2019**, *12*, 5.

(43). Michel, R. H.; Murphey, W. A. Intramolecular Rearrangements of Polyketones. *Journal of Polymer Science*, **1961**, *55*, 741-751.

(44). Hosino, K. Studies on Synthetic Fibers. Decomposition and Synthesis of "Nylon". *Bull. Chem. Soc. Jpn.*, **1943**, *18* (3), 97-104.

(45). Shukala, S. R.; Harad, A. M.; Mahato, D. Depolymerization of Nylon 6 Waste Fibers. *J. Appl. Polym. Sci.*, **2006**, *100*, 186-190.

(46). Achhammer, B. G.; Reinhart, F.W.; Kline, G. M. Mechanism of the Degradation of Polyamides. *Journal of Research of the National Bureau of Standards*, **1951**, *46* (5), 391-421.

(47). Colella, M. B.; Siggia, S.; Barnes, R. M. Poly(acrylamidoxime) Resin for Determination of Trace Metals in Natural Waters. *Anal. Chem.*, **1980**, *52*, 2347-2350.

(48). Hammad, E. M.; Mubarak, M. S. Chelation Properties of Poly(β-diketone) Polymer and Its Oxime Toward Heavy Metal Ions. *J. Appl. Polym. Sci.,* **2008**, *108*, 2415-2420.

(49). Ebraheem, K. A. K.; Hamdi, S. T. Synthesis and Properties of a Copper Selective Chelating Resin Containing a Salicylaldoxime Group. *Reactive & Functional Polymers*, **1997**, *34*, 5-10.

CHAPTER 3

WASTE PLASTICS AS ADSORBENTS FOR PER- AND POLYFLUORINATED ALKYL SUBSTANCES

3.1 Introduction

3.1.1 Background

Per- and polyfluorinated substances (PFAS) are a classification of man-made organic compounds which typically contain long alkyl chain tails with carbon-fluorine bonds accompanied by a polar functional group as the head (Figure 3.1). The variation of PFAS identity is defined by the type of functional group located on the molecule as well as the length of the fluorocarbon tail. As a result, thousands of PFAS compounds have been classified though the most prominent are presented in Figure 3.2.[1] Such unique structure allows for variation between hydrophobic and hydrophilic properties as well as high thermal stability.[2] Thus these chemicals find application in household items like nonstick cookware,[3] food packaging,[4] flame retardants,[5] and textiles.[6] Industrially, PFAS compounds are used in the aerospace and automotive industries [7] as well as the main component of Teflon products.[8]

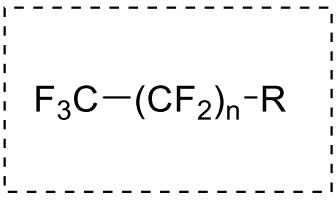

Figure 3.1: General structure of PFAS, where R may be any non-fluorinated atom, typically a polar head group.

3.1.2 PFAS Health Risks

Because of the widespread use of these chemicals and their resistance to degradation owing to the strong carbon-fluorine bond, PFAS compounds are commonly known as "forever chemicals".[9, 10] Indeed, PFAS compounds have been found in waterways and drinking water across the United States and in some cases exceed the Environmental Protection Agency's (EPA) 2016 health advisory limit of 70 parts per trillion (ppt).[11] As of 2022, the EPA has further lowered the health advisory limit for perfluorooctanoic acid (PFOA) in drinking water to 0.004 ppt and 0.02 ppt for perfluorooctane sulfonic acid (PFOS).[12] Furthermore, PFAS compounds have been detected in soil and plant life[13, 14] as well as aquatic life.[15] This penetration of PFAS pollution into seemingly every aspect of human life may have adverse health effects. Notably, recent studies have indicated that PFOA may be linked to kidney and testicular cancers.[16] Additionally, immune suppression and obesity are thought to be linked to PFAS exposure at a young age.[17, 18]

In addition to the alarming effects that exposure to PFAS may have on the health of the human population, a 2012 study from the Centers for Disease Control (CDC) found varying concentrations of PFAS present in the blood of 97% of Americans, some with concentrations as high as 4 parts per billion (ppb).[19] Though no concentration of PFAS in the human body has been deemed "acceptable" yet, these results should not be dismissed. Therefore, it is essential that in addition to prevention of the use of PFAS for manufacturing, methods to capture existing PFAS within waterways throughout the United States and other parts of the world be developed.

Carboxylic Acids

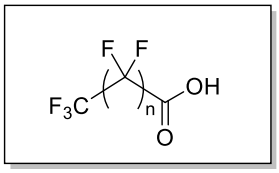

n = 3 *Perfluoropentanoic acid (PFPeA)*

n = 5 *Perfluoroheptanoic acid (PFHpA)*

n = 6 *Perfluorooctanoic acid (PFOA)*

Sulfonic Acids

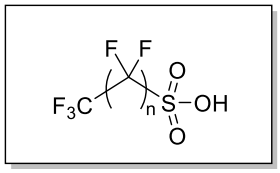

n = 3 *Perfluorobutane sulfonic acid (PFBS)*

n = 5 *Perfluorohexane sulfonic acid (PFHxS)*

n = 7 *Perfluorooctane sulfonic acid (PFOS)*

Sulfonamides

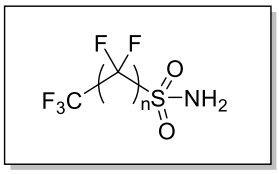

n = 3 *Perfluorobutanesulfonamide (FSBA)*

n = 7 *Perfluorooctanesulfonamide (PFOSA)*

Phosphonic Acids

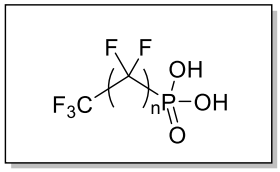

n = 5 *Perfluorohexyl phosphonic acid (PFHxPA)*

n = 7 *Perfluoroocryl phosphonic acid (PFOPA)*

Figure 3.2: Common linear chain PFAS classified by functional head group.

3.1.3 PFAS Mitigation

Due to the potential health risks posed by PFAS and their presence in the environment, current research has focused on methods for the capture and removal of these chemicals from waterways. Effective techniques which have been demonstrated for the capture of PFAS include adsorption to an inert material, or filtration by membrane or ion resin exchange.[20] Other removal methods such as chlorination,[21] UV treatment,[22] and advanced oxidation processes[23] have also shown success, however these methods are not deemed viable due to long contact times, and formation of unwanted radical species.[24]

Of the separation methods mentioned, use of membranes is beneficial for removal of both long and short chain PFAS,[25] and are remarkably efficient since no adsorption is occurring.[20, 26] Despite this, membranes are prone to degradation and real-world application in water treatment is costly.[20, 27] Likewise, ion-exchange methods are efficient and good for removal of long chain PFAS and anionic species,[20, 28, 29] but can be costly to regenerate and exclude shorter chain PFAS during filtration.[20, 30, 31]

Materials used for PFAS adsorption make use of the electrostatic and hydrophobic interactions on the polar head and carbon-fluorine tail, respectively, in order to adhere to the material's surface.[32] As such, typical adsorbents often possess high surface area, small particle size, and varying surface charge.[33] Activated carbon is one such material which fits these criteria and thus is widely used as a PFAS adsorbent. Although excellent for adsorption to long chain PFAS,[34] activated carbon is of limited use for smaller PFAS molecules and can be ineffective around other organic molecules.[20, 35] Other adsorbents such as metal-organic frameworks (MOFs),[36] or silica[37] may also be used, though these materials are not entirely environmentally-friendly themselves.

3.1.4 Waste Plastic Adsorbents

Although various materials previously discussed herein have shown effectiveness in adsorption capability to PFAS and thus offer promising removal and mitigation routes, many of these materials must be synthesized, purchased, or regenerated after use through costly methods.[20] Thus, it would be ideal for materials used as PFAS adsorbents to come from both abundant and reusable sources. One potential material suiting these specifications are waste plastics. Though non-renewable, plastics such as polyethylene and polypropylene account globally for 36% and 21% of non-fiber plastics, respectively.[38] Of

all plastics produced, only 10 % are recycled,[38] and in the United States approximately 69 % are stored in a land-fill.[39] Because of the overabundance of these materials, the explosion in production and use, and the limited space available within the planet, it is imperative that either a viable disposal route or application of such landfilled materials is developed.

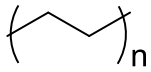

Polyethylene (PE)

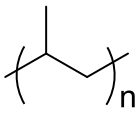

Polypropylene (PP)

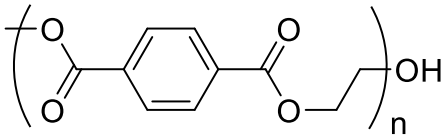

Polyethylene Terephthalate (PET)

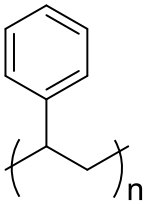

Polystyrene (PS)

Figure 3.3: Chemical structures of waste plastics commonly used as pollutant adsorbents.

Given the associated risks that rising PFAS concentrations have in both the environment and humans, as well as the seemingly permanent presence of waste plastics, it would be ideal if both problems could be mitigated or reduced simultaneously. The use of waste plastics for the adsorption and removal of PFAS in waterways is one such application which theoretically would find use for landfilled plastics as well. Indeed, early research suggests that such an application is possible. PFAS adsorption studies have been conducted using adsorbents such as polyethylene, polystyrene, polyethylene terephthalate, and polypropylene among others (Figure 3.3).[40, 41, 42] Good uptake of PFAS and other

contaminants such as polychlorinated biphenyls (PCBs) and even heavy metals is observed, with polyethylene and polystyrene showing the most promising adsorption capability.[43] Factors which for such varying adsorption abilities include the solution pH, salinity, polymer identity and shape, as well as microbe presence.[44] Among the factors influencing adsorption capability, it has been suggested that surface area may play a critical role though knowledge in this area is limited.[44, 45]

3.1.5 Project Goals

The primary aim of this project was to investigate the ability of waste plastics such as polyethylene and polypropylene to adsorb PFAS pollutants in solution. Specific inquiries focus on what effect the surface area of the plastic plays in its overall adsorption capability, with the hypothesis that a smaller particle with a larger surface area should adsorb a greater degree of PFAS. Surface modification is to be achieved either by chemical means (oxidation of polymer chains) or by mechanical means (milling or grinding). Determination of PFAS adsorption is to be accomplished using liquid chromatography mass spectroscopy (LC/MS) to determine concentration of the solution before and after exposure to the plastic. Therefore, the beginning stages of the project will primarily focus on the establishment of a reliable LC/MS method to determine PFAS concentration and thus plastic adsorption capability.

3.2 Results and Discussion

3.2.1 Polyethylene & PFOA Initial Adsorption Determination

Three variations of polyethylene and their adsorption capabilities to PFOA were chosen. The first variation was that of low-density polyethylene (LDPE) and the next two

being ultra-high molecular weight polyethylene (UHMWPE), and UHMWPE after seven minutes of ball milling. Initial solutions of PFOA were made to a concentration of 500 ppm, then after exposure to the plastic, were diluted to a concentration of 61-63 ppm after thoroughly washing the filtered polymers for any loosely bound PFOA. Aliquots of both solutions were sent for LC/MS analysis with the difference in PFOA concentration to be attributed to any which may be bound to the plastic. Along with the aliquots, a series of PFOA standards ranging from 50 to 500 ppm were sent for analysis in order to determine the concentration.

Sample	Concentration (ppm)	Peak Area
UHMWPE (I)	500	$9.9*10^8$
UHMWPE (F)	61[a]	$2.5*10^8$
Milled UHMWPE (I)	500	$11*10^8$
Milled UHMWPE (F)	63[a]	$2.3*10^8$
LDPE (I)	500	$9.6*10^8$
LDPE (F)	63[a]	$2.4*10^8$
PFOA Standard 1	50	$5.1*10^7$
PFOA Standard 2	100	$10*10^7$
PFOA Standard 3	200	$2.0*10^8$
PFOA Standard 4	400	$3.3*10^8$
PFOA Standard 5	500	$3.2*10^8$

Table 3.1: Plastic samples and associated PFOA solution concentrations with given peak area obtained from LC/MS chromatogram. All solutions were run in DI water. (I): Initial solution before plastic exposure, (F): final solution after plastic exposure. [a]Theoretical concentration.

Concentrations of solutions of PFOA before and after exposure to plastic and their associated areas of the PFOA peak from the LC/MS chromatogram are shown in Table 1. It should be noted that initial solutions of PFOA before exposure to the plastic have a higher peak area than the solutions after exposure. Normally this would imply a decrease in concentration of the PFOA in solution, which could then be attributed to adsorption to the plastic. In this case, since the plastics were washed to remove any loosely bound PFOA, and this wash added to the final solutions, the final concentrations are in fact lowered by this process. Therefore, the decrease in peak area cannot be attributed to PFOA lost to adsorption alone without knowledge of the exact concentration value. This variable was to be determined by use of known standards of PFOA, though upon implementation the initial PFOA solutions do not fit into the calibration range (Figure 3.4).

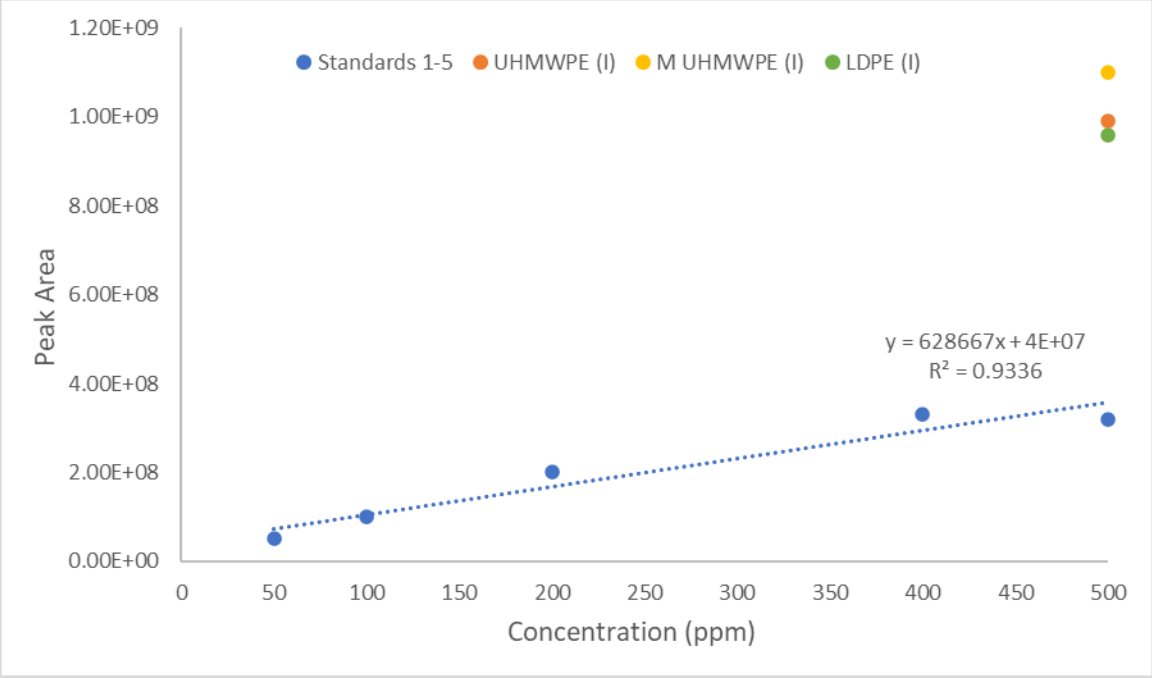

Figure 3.4: Calibration curve created from PFOA standards of known concentration along with initial PFOA solutions before exposure to plastic. Peak area is retrieved from LCMS and corresponds to the area of the PFOA peak in the chromatograph.

One possible explanation for these discrepancies can be observed in the standards themselves. At a concentration of 500 ppm the associated peak area no longer falls within a linear incline. This may suggest that concentrations exceeding 400 ppm surpass the instrument's detection limit. This might explain the exceptionally high peak areas for the three initial solutions, all of which are 500 ppm and do not align with the standard of the same concentration. It is also possible that the rather low solubility of PFOA in water plays a role in some of discrepancies, as well the possibility of micelle formation due to hydrophobic interactions of the alkyl chain.

3.2.2 Polyethylene & PFOA Adsorption in Methanol

After the first adsorption investigation of LDPE and PFOA, standard concentrations were lowered to a range of 100 to 300 ppm with the hopes that any such instrument detection limit errors would be eliminated. The adsorption potential of LDPE was studied again with some adjustments to experimental procedure. Plastics were not washed after exposure to the PFOA solutions and as such, no dilutions were made to the final solution. Furthermore, experiments were conducted in methanol rather than DI water to eliminate the possibility of PFOA solubility issues or micelle formation.

Results listed in Table 3.2 indicate a calibration curve which is less linear than the previous adsorption experiment shown in Figure 3.4. However, the initial solutions of PFOA at a concentration of 300 ppm align closer to the standards of the same value (Figure 3.5). This may be a result of lowering the concentration away from the supposed instrument detection limit, although both initial solution peak area values still vary slightly. Such variations prevent the exact determination of a meaningful concentration value from the calibration plot. PFOA solutions exposed to LDPE in methanol appear to have a decrease

in PFOA peak area in comparison to aliquots from the initial solution. Since the polymers were not washed and the final solution was not diluted, the change in peak area could be attributed to adherence to the plastic. It may also be the case however that PFOA is being adsorbed to the glass from the reaction flask, or even the cotton used to filter the polymer from the final solution. It may be more likely that the latter two are plausible explanations for the missing PFOA in the final solution. This is supported by the use of a control, which contained no LDPE in the PFOA solution. Analysis of this control solution indicated a decrease in PFOA peak area in the final solution. This implies either PFOA is adhering to another surface instead of the plastic which is accounting for the difference in concentration, or the two values fall within instrument error.

Sample	Concentration (ppm)	Peak Area
PFOA Standard 1	100	$5.4*10^6$
PFOA Standard 2	150	$9.2*10^6$
PFOA Standard 3	200	$9.1*10^6$
PFOA Standard 4	250	$9.8*10^6$
PFOA Standard 5	300	$1.4*10^7$
LDPE (I)	200	$1.0*10^7$
LDPE (F)	-	$8.3*10^6$
Control (I)	200	$1.2*10^7$
Control (F)	-	$5.0*10^6$

Table 3.2: Standards of known PFOA concentration along with initial and final solutions of PFOA before and after exposure to LDPE. PFOA control solutions with no LDPE were also analyzed both in methanol.

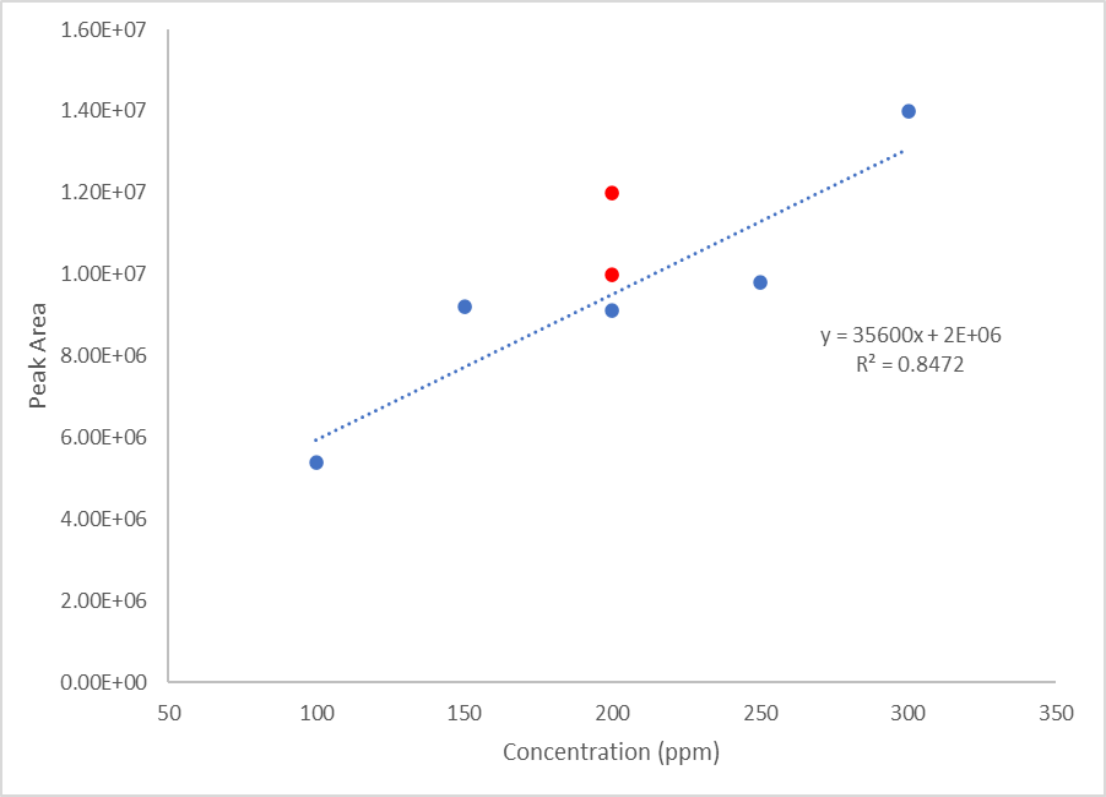

Figure 3.5: Calibration curve for standards of known PFOA concentration with initial PFOA solutions of 300 ppm included.

3.2.3 Calibration Curve Refinement

After a series of seemingly inconsistent PFOA peak areas from standards of known concentrations which prevented the exact determination of experimental concentration values, the next step of the project focused on establishing a reliable analysis method. PFOA standards in both methanol and water with concentrations ranging from 1 to 20 ppm were run in triplicate, then given peak areas were averaged and standard error was calculated (Table 3.3). Upper and lower peak area bounds appear within reasonable ranges and average peak areas align in a linear fashion (Figure 3.6). It should be noted that standards run in methanol appear to deviate from linearity more so than those in water.

It is possible that due to the volatility of methanol, solvent may have evaporated if samples are left to sit long enough thus changing concentration and therefore peak area. Regardless, it is likely necessary to run future samples in DI water and in triplicate or greater. Despite linearity it is still unknown whether or not such a calibration plot can be reliably applied to samples of unknown PFOA concentration. As such the next series of experiments aim at ensuring that control samples of known PFOA concentration can be accurately determined using the calibration method established here, then samples of unknown PFOA concentration after exposure to plastic may be determined.

Sample	Conc. (ppm)	Solvent	Avg. Peak Area	Error (upper)	Error (lower)
STD 1	20	DI H_2O	$1.18*10^8$	$1.15*10^8$	$1.15*10^8$
STD 2	15	DI H_2O	$9.60*10^7$	$9.63*10^7$	$9.55*10^7$
STD 3	10	DI H_2O	$6.15*10^7$	$6.20*10^7$	$6.10*10^7$
STD 4	5	DI H_2O	$3.00*10^7$	$3.05*10^7$	$2.97*10^7$
STD 5	1	DI H_2O	$7.80*10^6$	$8.06*10^6$	$7.54*10^6$
STD 6	20	MeOH	$1.08*10^8$	$1.09*10^8$	$1.07*10^8$
STD 7	15	MeOH	$7.75*10^7$	$7.84*10^7$	$7.66*10^7$
STD 8	10	MeOH	$6.45*10^7$	$6.51*10^7$	$6.40*10^7$
STD 9	5	MeOH	$2.49*10^7$	$2.55*10^7$	$2.43*10^7$
STD 10	1	MeOH	$9.69*10^6$	$1.02*10^7$	$9.18*10^6$

Table 3.3: PFOA peak area values for standards of known PFOA concentrations in both methanol and DI water.

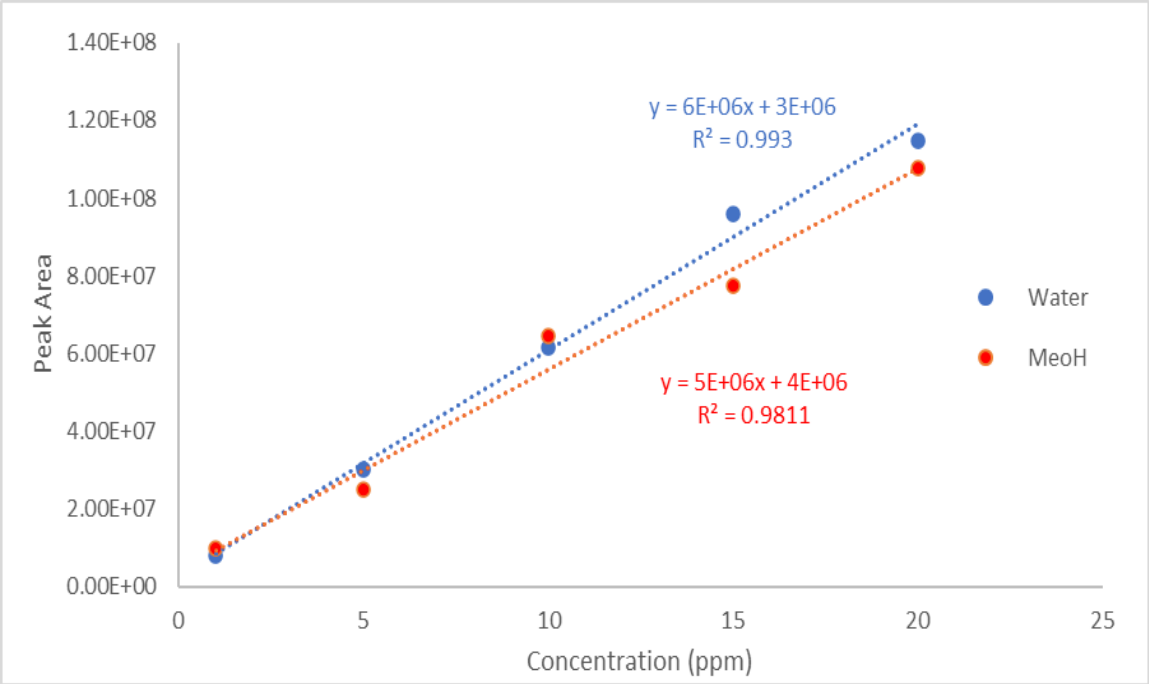

Figure 3.6: Calibration curve for standards of known PFOA concentration in DI water (blue) and methanol (red), run in triplicate.

3.3 Conclusion

This project sought to investigate the effectiveness of waste plastic as adsorbents for PFAS pollutants. Specifically, plastics such as polyethylene were hypothesized to be most effective at adsorption when surface area is maximized. Such surface area modification was to be achieved through use of milling or oxidation, with only the former being implemented with success. Initially, solutions of PFOA with concentrations of 500 ppm were combined with plastic samples consisting of milled high molecular weight, low density, and ultra-high molecular weight polyethylene. Analysis of the solutions before and after exposure to plastic did not yield results which are comparable to standards of known PFOA concentration. With the possibility of previous PFOA concentrations possibility infringing on the instrument's detection limit, concentration the experiments were

conducted in was lowered. After samples again gave PFOA peak area values which did not fall within the values of the calibration curve, focus was shifted to the establishment of a reliable analysis method. After running standards of lower concentration in triplicate, a linear and seemingly reliable calibration plot was obtained. Future experiments will involve confirming the reliability of said calibration plot by applying samples with known and unknown concentrations of PFOA. After confidence in the analysis method is established, plastics of differing surface areas achieved through varied milling times and their adsorption potential may be studied.

3.4 Experimental

3.4.1 General Methods

All chemicals and solvents were purchased commercially unless otherwise noted. No additional purification methods were taken. PFOA samples were analyzed through use of a Waters Acquity SQD liquid chromatography-mass spectroscopy instrument by researchers at the University of Pennsylvania. Peak area was determined by integration of the PFOA chromatograph peak.

3.4.2 UHMWPE and LDPE PFOA Adsorption

PFOA was added to three sperate vials, (12.4 mg, 0.03mmol) along with 25 mL of DI water to create solutions with a concentration of 500 ppm. An initial 1 mL aliquot of these solutions was taken for analysis. Additionally, a series of PFOA standards were also created in DI water, with concentrations of 50, 100, 200, 400 and 500 ppm. 25 mg of polymer was added to each vial and stirred overnight. Solution filtered using a Hirsch

funnel into a 200 mL volumetric flask. The plastic was washed with DI water and the plastic free PFOA solution was diluted to the mark. An aliquot was then sent for analysis.

3.4.3 Polyethylene PFOA Adsorption in Methanol

PFOA solutions were created by dissolving (10 mg, 0.024 mmol) of PFOA in 50 mL of methanol, then an initial aliquot of 1 mL was taken for analysis. A series of standards with known concentrations of PFOA consisting of 100, 150, 200, 250, and 300 ppm were created in methanol. To the first PFOA sample, 20 mg of LDPE was added. The second sample contained no plastic and served as a control. Both solutions were stirred at room temperature for 24 hours, after which an aliquot was taken and passed through a cotton pipette, then sent for analysis.

3.4.4 Triplicate PFOA Standard Calibration Curve

PFOA standards of concentrations 20, 15, 10, 5 and 1 ppm were created by fractional dilutions of a 20 ppm standard (10 mg PFOA/500mL solvent) detailed in Table 3.4. Identical standards were made for both water and methanol as the solvent. Each standard was run in triplicate and peak areas were averaged before plotting. Standard deviation of each peak area was calculated using the stdev.s excel formula. Standard error was found by use of Equation 3.1 Where σ is the standard deviation and n is the number of samples.

$$\sigma_{\bar{x}} = \frac{\sigma}{\sqrt{n}} \qquad \textbf{(3.1)}$$

Upper and lower peaks area bounds were found by adding average peak area to the standard error and subtraction of peak area by standard error, respectively.

Initial Conc. (ppm)	Dilution	Stock (mL)	Solvent (mL)	Final Conc. (ppm)
20	3/4	75	25	15
20	1/2	25	25	10
20	1/5	10	40	5
20	1/20	10	190	1

Table 3.4: Fractional dilutions made from a stock solution of 20 ppm PFOA and their respective final concentrations. Each was done in both methanol and DI water.

3.5 References Cited

(1). Ghisi, R.; Vamerali, T.; Manzetti, S. Accumulation of Perfluorinated Alkyl Substances (PFAS) in Agricultural Plants: A Review. *Environmental Research*, **2019**, *169*, 326-341.

(2). Kucharzyk, K. H.; Darlington, R.; Benotti, M.; Deeb, R.; Hawley, E. Novel Treatment Technologies for PFAS Compounds: A Critical Review. *Journal of Environmental Management*, **2017**, *204*, 757-764.

(3). Prevedouros, K.; Cousins, I. T.; Buck, R. C.; Korezeniowski, S. H. Sources, Fate and Transport of Perfluorocarboxylates *Environ. Sci. Technol.*, **2006**, *40* (1), 32-44.

(4). Trier, X.; Granby, K.; Christensen, J. H. Polyfluorinated Surfactants (PFS) in Paper and Board Coating for Food Packaging. *Environmental Science and Pollution Research*, **2011**, *18*, 1108-1120.

(5). Clarity, C.; Trowbridge, J.; Gerona, R.; Ona, K.; McMaster, M.; Bessoneau, V.; Rudel, R.; Buren, H.; Morello-Frosch, R. Associations Between Polyfluoroalkyl Substance and Organophosphate Flame Retardant Exposures and Telomere Length in a Cohort of Women Firefighters and Office Workers in San Francisco. *Environmental Health*, **2021**, *20* (90).

(6). Schellenberger, S.; Liagkouridis, I.; Awad, R.; Khan, S.; Plassmann, M.; Peters, G.; Benskin, J. P.; Cousins, I. T. An Outdoor Aging Study to Investigate the Release of Per- And Polyfluoroalkyl Substances (PFAS) from Functional Textiles. *Environ. Sci. Technol.*, **2022**, *56*, 3471-3479.

(7). Gluege, J.; Scheringer, M; Cousins, I. T.; DeWitt, J. C.; Goldenman, G.; Herzke, D.; Lohman, R.; Ng, C. A.; Trier, X.; Wang, Z. An Overview of the Uses of Per- and Polyfluoroalkyl Substances (PFAS). *Environ. Sci.: Processes Impacts*, **2020**, *22*, 2345-237.3.

(8). Meegoda, J. N.; Kewalramani, J. A.; Li, B.; Marsh, R. W. A Review of the Applications, Environmental Release, and Remediation Technologies of Per- and Polyfluoroalkyl Substances. *Int. J. Environ. Res. Public Health*, **2020**, *17*, 8117.

(9). Mahinroosa, R.; Senevirathna, L. A Review of the Emerging Treatment Technologies for PFAS Contaminated Soils. *Journal of Environmental Management*, **2020**, *255*, 109896.

(10). Brennan, N. M.; Evans, T. A.; Fritz, M. K.; Peak, S. A. von Holst, H. E. Trends in the Regulations of Per- and Polyfluoroalkyl Substances (PFAS): A Scoping Review. *Int. J. Environ. Res. Public Health*, **2021**, *18*, 10900.

(11). Hu, X. C.; Andrews, D. Q.; Lindstrom, A. B.; Bruton, T. A.; Schaider, L. A.; Grandjean, P.; Lohmann, R.; Carignan, C. C.; Blum, A.; Balan, S. A.; Higgins, C. P.; Sunderland, E. M. Detection of Poly- and Perfluoroalkyl Substances (PFASs) in U.S. Drinking Water Linked to Industrial Sites, Military Fire Training Areas, and Wastewater Treatment Plants. *Environ. Sci. Technol. Lett.*, **2016**, *3*, 344-350.

(12). Lifetime Drinking Water Health Advisories for Four Perfluoroalkyl Substances. *Fed. Reg.*, **2022**, *87* (118), 36848-36849.

(13). Herzke, D.; Huber, S.; Bervoets, L.; D'Hollander, W. D.; Hajslova, J.; Pulkrabova, J.; Brambilla, G.; De Filippis, S. P.; Klenow, S.; Heinemeyer, G.; de Voogt, P. Perfluorinated Alkylated Substances in Vegetables Collected in Four European Countries; Occurrence and Human Exposure Estimations. *Environmental Science and Pollution Research*, **2013**, *20*, 7930-7939.

(14). D'Hollander, W.; Herke, D.; Huber, S.; Hajslova, J.; Pulkrabova, J.; Brambilla, G.; De Filippis, S. P.; Bervoets, L.; de Voogt, P. Occurrence of Perfluorinated Alkylated Substances in Cereals, Salt, Sweets and Fruit Items Collected in Four European Countries. *Chemosphere*, **2015**, *129*, 179-185.

(15). Ahrens, L.; Bundschuh, M. Fate and Effects of Poly- and Perfluoroalkyl Substances in the Aquatic Environment: A Review. *Environmental Toxicology and Chemistry*, **2014**, *33* (9), 1921-1929.

(16). Barry, V.; Winquist, A.; Steenland, K. Perfluorooctanoic Acid (PFOA) Exposures and Incident Cancers among Adults Living Near a Chemical Plant. *Environ. Health Perspect.*, **2013**, *121* (11-12), 1313-1318.

(17). Grandjean, P.; Anderson, E. W.; Budtz-Jorgenson, E.; Nielsen, F.; Molbak, K.; Weihe, P.; Heilmann, C. Serum Vaccine Antibody Concentration in Children Exposed to Perfluorinated Compounds. *JAMA*, **2012**, *307* (4), 391-397.

(18). Braun, J. M.; Chen, A.; Romano, M. E.; Calafat, A. M.; Webster, G. M.; Yolton, K.; Lanphear, B. P. Prenatal Perfluoroalkyl Substance Exposure and Child Adiposity at 8 Years of Age: The HOME Study. *Obesity*, **2016**, *24*, 231-237.

(19). Lewis, R. C.; Johns, L. E.; Meeker, J. D. Serum Biomarkers of Exposure to Perfluoroalkyl Substances in Relation to Serum Testosterone and Measures of Thyroid Function Among Adults and Adolescents from NHANES 2011–2012. *Int. J. Environ. Res. Public Health*, **2015**, *12*, 6098-6114.

(20). Das, A.; Ronen, A. A Review on Removal and Destruction of Per- and Polyfluoroalkyl Substances (PFAS) by Novel Membranes. *Membranes*, **2022**, *12*, 662.

(21). Loganathan, B. G.; Sajwan, K. S.; Sinclair, E.; Kumar, K. S.; Kannan, K. Perfluoroalkyl Sulfonates and Perfluorocarboxylates in Two Wastewater Treatment Facilities in Kentucky and Georgia. *Water Research*, **2007**, *41*, 4611-4620.

(22). Olatunde, O. C.; Kuvarega, A. T.; Onwudiwe, D. C. Photo Enhanced Degradation of Polyfluoroalkyl and Perfluoroalkyl Substances. *Heliyon*, **2020**, e05614.

(23). Mitchell, S. M.; Ahmad, M.; Teel, A. L.; Watts, R. J. Degradation of Perfluorooctanoic Acid by Reactive Species Generated through Catalyzed H_2O_2 Propagation Reactions. *Environ. Sci. Technol. Lett.*, **2014**, *1*, 117-121.

(24). Metz, J.; Zuo, P.; Wang, B.; Wong, M. S.; Alvarez, P. J. J. Perfluorooctanoic Acid Degradation by UV/Chlorine. *Environ. Sci. Technol. Lett.*, **2022**, *9*, 673-679.

(25). Ateia, M.; Arifuzzaman, M.; Pellizzeri, S.; Attia, M. F.; Tharayil, N.; Anker, J. N.; Karanfil, T. Cationic Polymer for Selective Removal of GenX and Short-Chain PFAS from Surface Waters and Wastewaters and ng/L Levels. *Water Research*, **2019**, *163*, 114874.

(26). Franke, V.; Ullberg, M.; McCleaf, P.; Walinder, M.; Koehler, S. J.; Ahrens, L. The Price of Really Clean Water: Combining Nanofiltration with Granular Activated Carbon and Anion Exchange Resins for the Removal of Per- And Polyfluoralkyl Substances (PFASs) in Drinking Water Production. *ACS EST Water*, **2021**, *1*, 782-795.

(27). Chen, X.; Vanagamudi, A.; Wang, J.; Jegatheesan, J.; Mishra, V.; Sharma, R.; Gray, S. R.; Kujawa, J.; Kujawski, W.; Wicaksana, F.; Dumee, L. F. Direct Contact Membrane Distillation for Effective Concentration of Perfluoroalkyl Substnaces – Impact of Surface Fouling and Material Stability. *Water Research*, **2020**, *182*, 116010.

(28). Yu, Q.; Zhang, R.; Deng, S.; Huang, J.; Yu, G. Sorption of Perfluorooctane Sulfonate and Perfluorooctanoate on Activated Carbons and Resin: Kinetic and Isotherm Study. *Water Research*, **2009**, *43*, 1150-1158.

(29). Liu, Y.; Sun, M. Ion Exchange and Resin Regeneration to Treat Per- and Polyfluoroalkyl Ether Acids and Other Emerging PFAS in Drinking Water. *Water Research*, **2021**, *207*, 117781.

(30). Sukeesan, S.; Boontanon, S. K.; Boontanon, N.; Fujii, S. Regeneration of Ion-Exchange Resins and Granular Activated Carbon with the Sonochemical Technique for Enabling Adsorption of Aqueous Per- and Polyfluoroalkyl Substances. *IOP Conf. Ser.: Earth Environ. Sci.* **2022**, *973*, 012004.

(31). Wang, R.; Ching, C.; Dichtel, W. R.; Helbling, D. E. Evaluating the Removal of Per- and Polyfluoroalkyl Substances from Contaminated Groundwater with Different Adsorbents Using a Suspect Screening Approach. *Environ. Sci. Technol. Lett.* **2020**, *7*, 954-960.

(32). Wu, C.; Klemes, M. J.; Trang, B.; Dichtel, W. R.; Helbling, D. E. Exploring the Factors that Influnce the Adsorption of Anionic PFAS on Conventional and Emerging Adsorbents in Aquatic Matrices. *Water Research*, **2020**, *182*, 115950.

(33). Park, M.; Wu, S.; Lopez, I. J.; Chang, J. Y.; Karanfil, T.; Snyder, S. A. Adsorption of Perfluoroalkyl Substances (PFAS) in Groundwater by Granular Activated Carbons: Roles of Hydrophobicity of PFAS and Carbon Characteristics. *Water Research*, **2020**, *170*, 115364.

(34). Murray, C. C.; Marshall, R. E.; Liu, C. J.; Vatankhah, H.; Bellona, C. L. PFAS Treatment with Granular Activated Carbon and Ion Exchange Resin: Comparing Chain Length, Empty Bed Contact Time, and Cost. *J. Water Process Eng.*, **2021**, *44*, 102342.

(35). Murray, C. C.; Vatankhah, H.; McDonough, C. A.; Nickerson, A.; Hedtke, T. T.; Cath, T. Y.; Higgins, C. P.; Bellona, C. L. Removal of Per- and Polyfluoroalkyl Substances Using Super-Fine Powder Activated Carbon and Ceramic Membrane Filtration. *Journal of Hazardous Materials*, **2019**, *366*, 160-168.

(36). Li, R.; Alomari, S.; Islamoglu, T.; Farha, O. K.; Fernando, S.; Thagard, S. M.; Holsen, T. M.; Wriedt, M. Systematic Study on the Removal of Per- and Polyfluoroalkyl Substances from Contaminated Groundwater Using Metal−Organic Frameworks. *Environ. Sci. Technol.*, **2021**, *55*, 15162-15171.

(37). Stebel, E. K.; Pike, K. A.; Nguyen, H.; Hartmann, H. A.; Klonowski, M. J.; Lawrence, M. G.; Collins , R. M.; Hefner, C. E.; Edmiston, P. L. Adsorption of Short-Chain to Long-Chain Perfluoroalkyl Substances Using Swellable Organically Modified Silica. *Environ. Sci. Water Res. Technol.* **2019**, *5*, 1854-1866.

(38). Geyer, G.; Jambeck, J. R.; Law, K. L. Production, Use, and Fate of All Plastics Ever Made. *Sci. Adv.*, **2017**, *3*, e1700782.

(39). Environmental Protection Agency, *Containers and Packaging: Product – Specific Data.* **2023**, https://www.epa.gov/facts-and-figures-about-materials-waste-and-recycling/containers-and-packaging-product-specific#PlasticC&P

(40). Llorca, M.; Schirinzi, G.; Martinez, M.; Barcelo, D.; Farre, M. Adsorption of Perfluoroalkyl Substances on Microplastics Under Environmental Conditions. *Environmental Pollution*, **2018**, *235*, 680-691.

(41). Ateia, M.; Zheng, T.; Calace, S.; Tharayil, N.; Pilla, S.; Karanfil, T. Sorption Behavior of Real Microplastics (MPs): Insights for Organic Micropollutants Adsorption on a Large Set of Well-Characterized MPs. *Science of the Total Environment*, **2020**, *720*, 137634.

(42). Teuten, E. L.; Rowland, S. J.; Galloway, T. S.; Thompson, R. C. Potential for Plastics to Transport Hydrophobic Contaminants. *Environ. Sci. Technol.* **2007**, *41*, 7759-7764.

(43). Alimi, O. S.; Budarz, J. F.; Hernandez, L. M.; Tufenkji, N. Microplastics and Nanoplastics in Aquatic Environments: Aggregation, Deposition, and Enhanced Contaminant Transport. *Environ. Sci. Technol.* **2018**, *52*, 1704-1724.

(44). Joo, S. H.; Liang, Y.; Kim, M.; Byun, J.; Choi, H. Microplastics with Adsorbed Contaminants: Mechanisms and Treatment. *Environmental Challenges*, **2021**, *3*, 100042.

(45). Scott, J. W.; Gunderson, K. G.; Green, L. A.; Rediske, R. R.; Steinman, A. D. Perfluoroalkylated Substances (PFAS) Associated with Microplastics in a Lake Environment. *Toxics*, **2021**, *9*, 106.

CHAPTER 4

EFFECTS OF PER- AND POLYFLUORINATED ALKYL SUBSTANCES ON PHOSPHOLIPID BILAYER MORPHPOLOGY

4.1 Introduction

4.1.1 Background

Per- and polyfluorinated alkyl substances (PFAS) have widely been linked to adverse health effects such as cancer,[1, 2] immune deficiencies,[3, 4] metabolic issues,[5] and possible neurodevelopmental complications.[6, 7] Despite this information, the exact mechanism for cellular uptake of PFAS is still undergoing research.[8, 9, 10] Such information pertaining to PFAS introduction into the body is critical to informed decision-making regarding prevention and or limiting exposure to these compounds. It is suspected, for instance, that PFAS head group and fluorocarbon chain length play a critical role in cellular uptake and morphology changes.[11, 12] As such, particular PFAS possessing chemical features known to facilitate cellular uptake should be should be avoided accordingly.

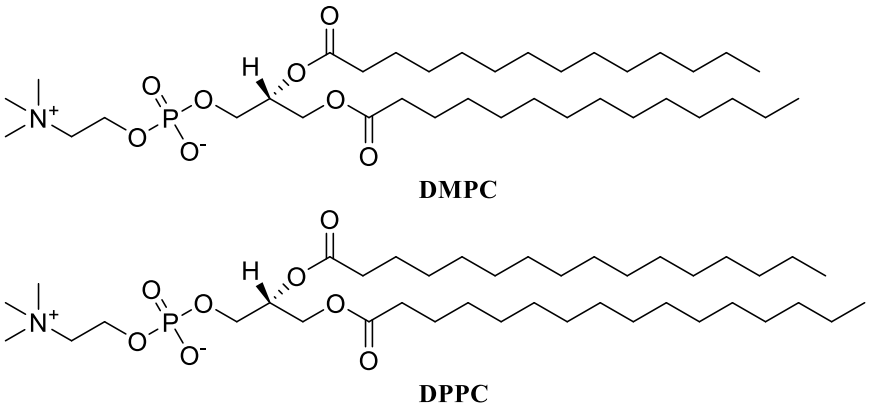

Figure 4.1: Phospholipids DPPC and DMPC.

Current research regarding PFAS uptake into membranes focuses primarily on the effect PFAS have on phospholipid bilayers such as morphology change and membrane incorperation.[13, 14] Phospholipids such as 1,2-dipalmitoyl-sn-glycero-3-phosphocholine (DPPC) and 1,2-dimyristoyl-sn-glycero-3-phosphocholine (DMPC) are often selected as the lipid of choice for PFAS bilayer studies,[15-18] due to the location of their phase transition temperatures (23 °C and 42 °C respectively)[19] and their presence in animal cell membranes.[20] Although it is known that PFAS incorporation into bilayers alters liposome morphology,[21, 22, 23] it is essential that characterization methods encompassing this occurrence are developed.

4.1.2 PFAS and Membrane Bilayer Interactions

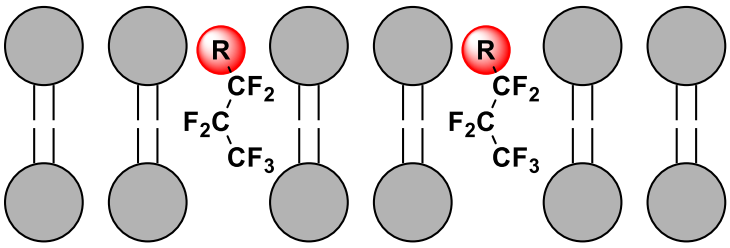

Figure 4.2: Representation of the likely orientation of PFAS within a phospholipid bilayer. The group "R" represents a polar functional group. Fluorocarbon tail is shortened for sizing purposes.

In the presence of water, phospholipids may form into bilayers by orienting the hydrophilic head towards the polar medium with the hydrophobic alkyl tails aligned with each other, away from the polar medium (Figure 4.2). These bilayers may then align into liposomes of varying sizes and layers. The most common of which fall into the classification of small unilamellar vesicles (SUVs) of up to 100 nm in diameter, large unilamellar vesicles (LUVs) from 100 – 250 nm in diameter, and multilamellar vesicles

(MLVs) ranging from 100 – 400 nm in diameter (Figure 4.3).[24] Given the structural similarities between many PFAS molecules and phospholipids such as DPPC and DMPC, the observation of such high lipophilicity can be rationalized. It is likely that hydrophobic interactions between the non-polar lipid alkyl tails and the PFAS fluorocarbon chain, as well as potential hydrogen bonding by the polar lipid head and PFAS functional group are responsible for such affinity.[15, 25]

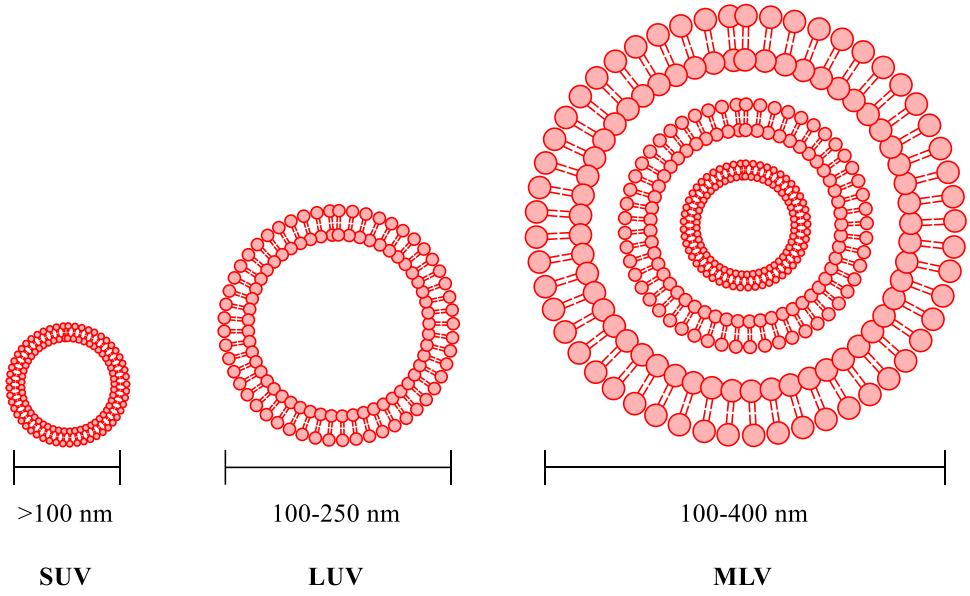

Figure 4.3: Common liposomes formed by phospholipids and their associated diameters and bilayer compositions.

Incorporation of PFAS into lipid membranes has been observed to cause a variety of effects on overall membrane properties. These include increased permeability,[26] increased fluidity,[27] and alteration of overall stability of the bilayer.[28] Although such membrane effects by PFAS are known, studies regarding membrane degradation over time and associated PFAS concentration thresholds are scarce. Furthermore, the mechanism of

PFAS penetration into the bilayer, as well as the effect of bilayer thickness and lipid identity on PFAS lipophilicity remain largely unknown.[21]

4.1.3 PFAS and Bilayer Interactions: Characterization Methods

In order to observe the effects PFAS have on the fluidity, permeability and stability of the lipid bilayer, reliable methods of characterization must be employed. Several of these methods exist and have been applied to varying degrees of success. For instance, fluorescence anisotropy has been used to investigate the partitioning of perfluorobutane sulfonate into phosphatidylcholine membranes, and exhibited disruption of the bilayers.[29] Membrane permeability of lipid bilayers in the presence of perfluorooctanoic acid (PFOA) and perfluorooctanesulfonic acid (PFOS) has also been investigated using cyclic voltammetry.[30] Less common techniques such as neutron reflectometry have also been applied in studies regarding membrane stability in the presence of PFAS.[11]

One of the most widely used analytical techniques for observation of PFAS interactions with lipid bilayers is likely differential scanning calorimetry (DSC). This technique allows for the observation of phase transition temperatures of lipid vesicles, giving insight on their morphology such as crystallinity of the membrane and other thermotropic behavior.[31, 32] Such information is of great use when studying the effects guest molecules have on the structure and characteristics of membranes, hence the popularity of the technique within PFAS research.

4.1.4 Project Goals

This project aims to investigate the effects of PFAS, specifically PFOA and PFOS, on the morphology of liposomes consisting of DPPC and DMPC phospholipids.

Specifically, the effect which PFAS has on the membrane fluidity and stability of varying sizes of liposome diameter and bilayer thickness. Such information is a critical addition to the knowledge pertaining to the mechanism by which PFAS enters cells and therefore is essential to our understanding of health risks pertaining to PFAS.

Varying concentrations of PFOA and PFOS are incorporated into bilayers of DPPC or DMPC SUVs and MLVs and the associated effects on the membrane are studied. The time in which membranes deteriorate after incorporation of PFAS is also to be determined. Investigation of such effects is achieved primarily through use of DSC, which will allow for observation of any membrane stiffening in the presence of PFAS, and for the monitoring of the overall integrity of the liposome. Such structural integrity of the membrane may also be verified by use of dynamic light scattering (DLS), which is also used to determine the approximate diameter of the vesicles.

4.2 Results and Discussion

4.2.1 DMPC and DPPC MLV Phase Transition Studies

Initial understanding of PFAS effects on liposome morphology and membrane integrity began by establishing variation of the phase transitions of MLV liposomes at altering ratios of PFAS concentration. MLVs synthesized from both DMPC and DPPC were implemented, along with both PFOS and PFOA. Lipid to PFAS ratios varied from as low as 10:1 to as high as 75:1, with the most observable changes in phase transition temperature occurring as the ratio approached 1:1. DPPC MLVs with incorporated PFOA show a slight decrease in temperature as PFOA ratio increases (Table 4.1 and Figure 4.4). This trend is more observable however, when PFOS is implemented instead of PFOA.

Lipid	PFAS	Eq (Lipid:PFAS)	Phase Transition (°C)
DPPC	PFOA	10:1	40.4
DPPC	PFOA	15:1	39.6
DPPC	PFOA	25:1	40.5
DPPC	PFOA	35:1	40.6
DPPC	PFOA	50:1	40.7
DPPC	PFOA	75:1	40.7
DPPC	PFOA	100:0	41.1

Table 4.1: Phase transitions temperatures of DPPC MLVs in the presence of varying ratios of PFOA.

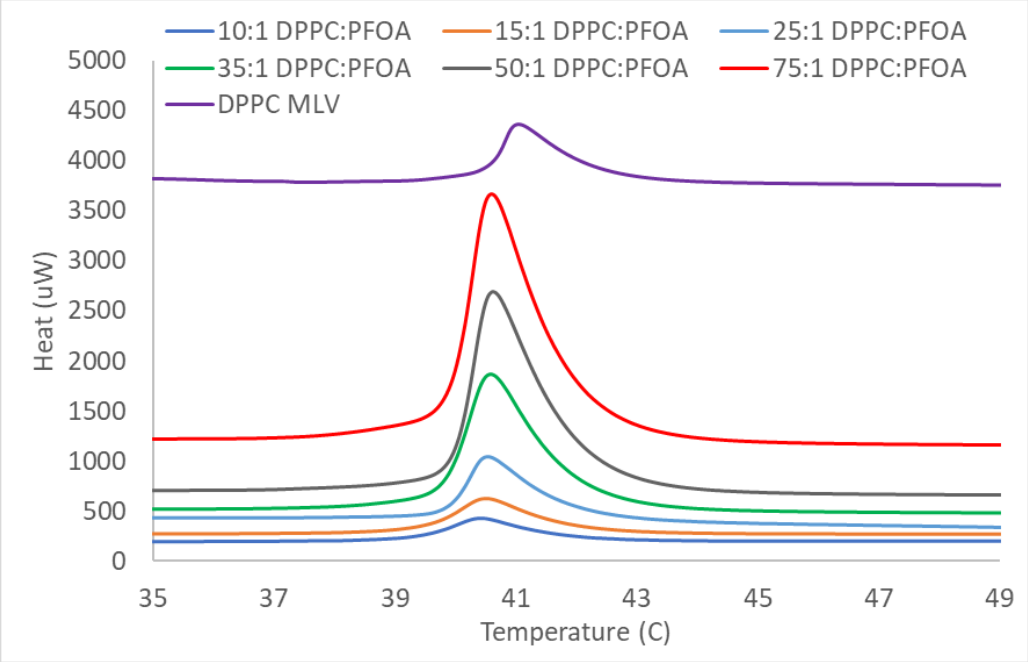

Figure 4.4: DSC trace for DPPC MLVs with varied ratios of PFOA. Data is staggered on the y-axis for visual convenience.

In the case of PFOS, the decrease in phase transition is more noticeable as the ratio of PFAS increases. For instance, at 75:1 equivalents of DPPC to PFOS, phase transition occurs at a temperature of 40.7 °C, this being only a slight difference from the transition of pure DPPC at 41.1 °C. At a final ratio of 10:1, phase transition occurs at a temperature of 39.1°C for a total difference of 1.6 °C or 2 °C from pure DPPC MLVs (Table 4.2). In comparison with DPPC phase transitions obtained in the presence of PFOA which give a total difference 0.3 °C from 75:1 to 10:1 or 0.7 °C from 100:0 to 10:1, a clear trend can be observed (Figure 4.5). One possible explanation for this discrepancy could be the identity of the functional group on the PFAS. The sulfonic acid group present on PFOS may exhibit slightly more steric repulsion than the carboxylic acid group present on PFOS. Such steric repulsion induced by PFOS may affect the morphology of the lipid bilayer by distorting the phospholipid packing more so than that of PFOA. A morphological change such as this would be likely be observable through a more drastic phase transition change as more PFOS is incorporated.

Lipid	PFAS	Eq (Lipid:PFAS)	Phase Transition (ºC)
DPPC	PFOS	10:1	39.1
DPPC	PFOS	15:1	39.6
DPPC	PFOS	25:1	39.8
DPPC	PFOS	35:1	40.1
DPPC	PFOS	50:1	40.4
DPPC	PFOS	75:1	40.7
DPPC	PFOS	100:0	41.1

Table 4.2: Phase transition temperatures of DPPC MLVs in the presence of varying ratios of PFOS.

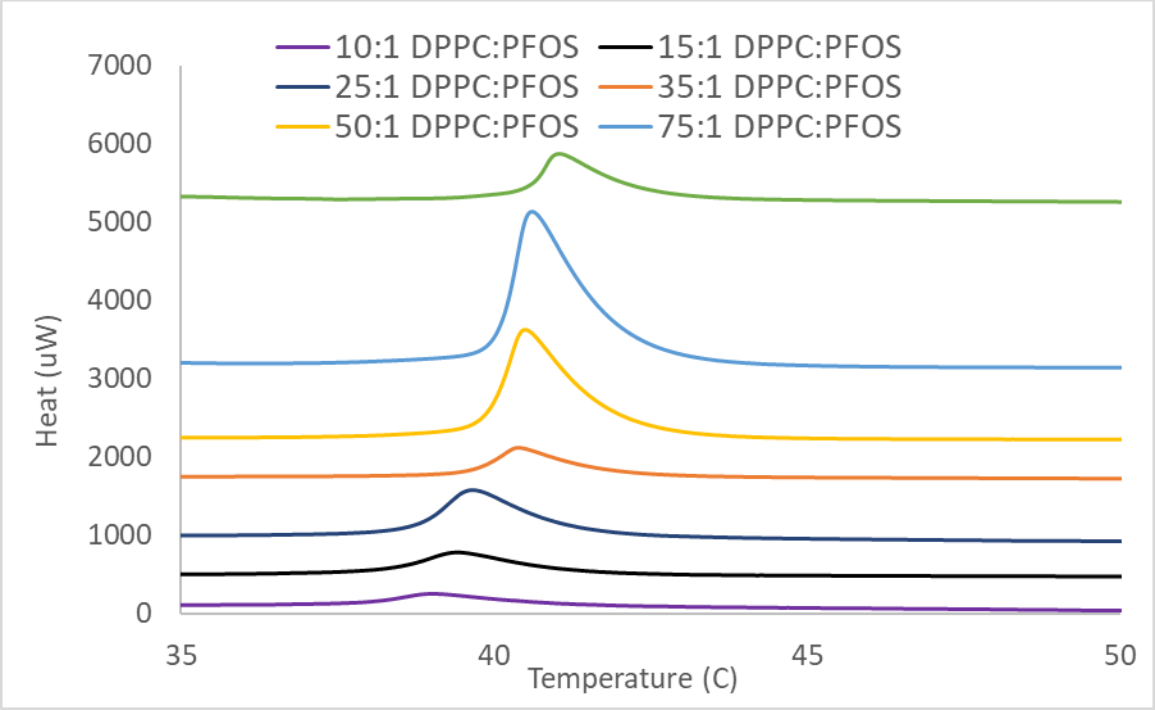

Figure 4.5: DSC trace for DPPC MLVs with varied ratios of PFOS. Data is staggered on the y-axis for visual convenience.

A similar trend can be observed when MLVs are formed from DMPC rather than DPPC. DMPC MLVs were subject to PFOA incorporation at concentrations ranging from 10:1 to 75:1 equivalents of lipid to PFAS. MLVs with no incorporation of PFOA give a phase transition of 23.4 °C, this is then lowered to a temperature of 23.1 °C at 75:1 and finishes at 22.5 °C at 10:1 for a total difference of 0.9 °C (Table 4.3 and Figure 4.6). This is a slightly larger downward trend in phase transition temperature than those observed with DPPC and PFOA (0.7 °C), suggesting that chain length of the phospholipid may have a slight effect in addition to any steric disruption produced by PFAS head group. Despite studies which have suggested the contrary for membrane permeability and lipid chain length towards PFAS.[33]

Lipid	PFAS	Eq (Lipid:PFAS)	Phase Transition (°C)
DMPC	PFOA	10:1	22.5
DMPC	PFOA	15:1	22.6
DMPC	PFOA	25:1	22.7
DMPC	PFOA	35:1	23.3
DMPC	PFOA	50:1	23.2
DMPC	PFOA	75:1	23.1
DMPC	PFOA	100:0	23.4

Table 4.3: Phase transition temperatures of DMPC MLVs in the presence of varying ratios of PFOA.

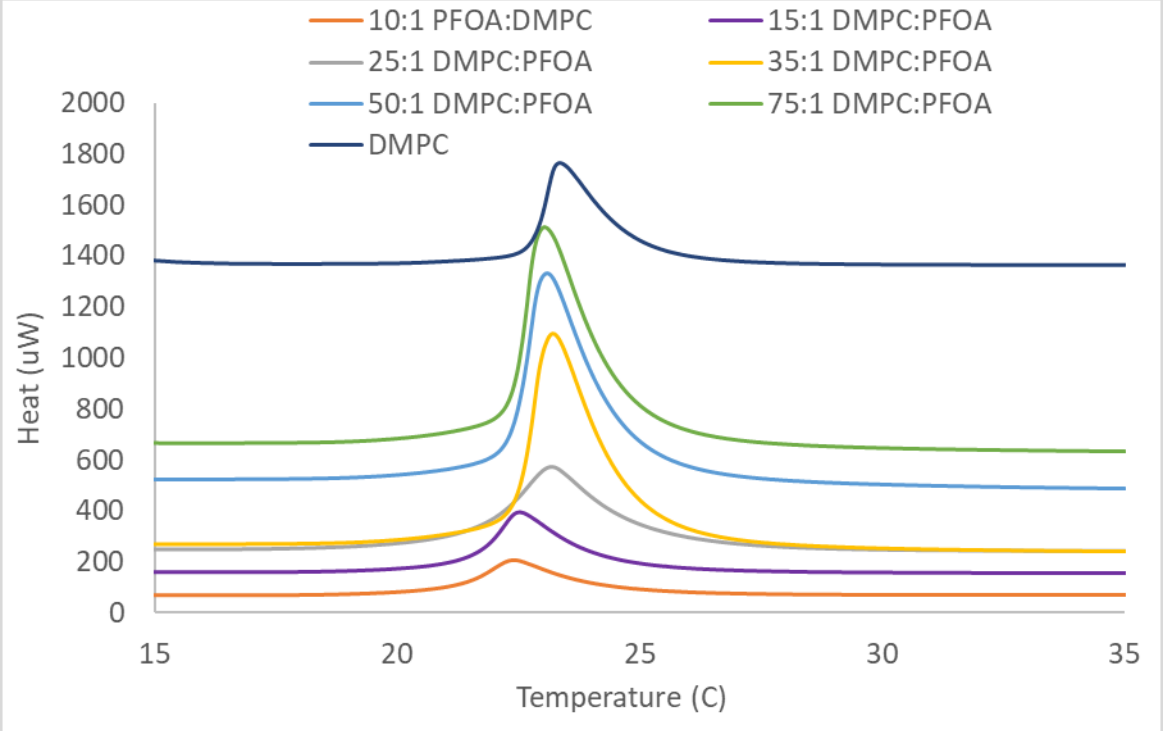

Figure 4.6: DSC trace for DMPC MLVs with varied ratios of PFOA. Data is staggered on the y-axis for visual convenience.

MLVs formed by use of DMPC in the presence of PFOA exhibited phase transitions similar to their DPPC MLVs counterparts. At 75:1 equivalents of lipid to PFAS, a phase transition of 23.1 °C was observed. This decreased to a temperature of 20.8 °C at 10:1 equivalents for a total decrease of 2.3 °C or 2.6 °C from pure DMPC MLVs at 23.4°C (Table 4.4 and Figure 4.7). Though similar trends are exhibited with both DPPC and DMPC in the presence of PFOA vs PFOS, a larger decrease in phase transition temperature is observed when DMPC is implemented. In addition to PFAS head group playing a role in potential membrane effects these data may also suggest lipid chain length plays small but measurable effect on morphology change.

Lipid	**PFAS**	**Eq (Lipid:PFAS)**	**Phase Transition (°C)**
DMPC	PFOS	10:1	20.8
DMPC	PFOS	15:1	21.8
DMPC	PFOS	25:1	22.5
DMPC	PFOS	35:1	22.8
DMPC	PFOS	50:1	23.1
DMPC	PFOS	75:1	23.0
DMPC	PFOS	100:1	23.1
DMPC	PFOS	100:0	23.4

Table 4.4: Phase transition temperatures of DMPC MLVs in the presence of varying ratios of PFOS.

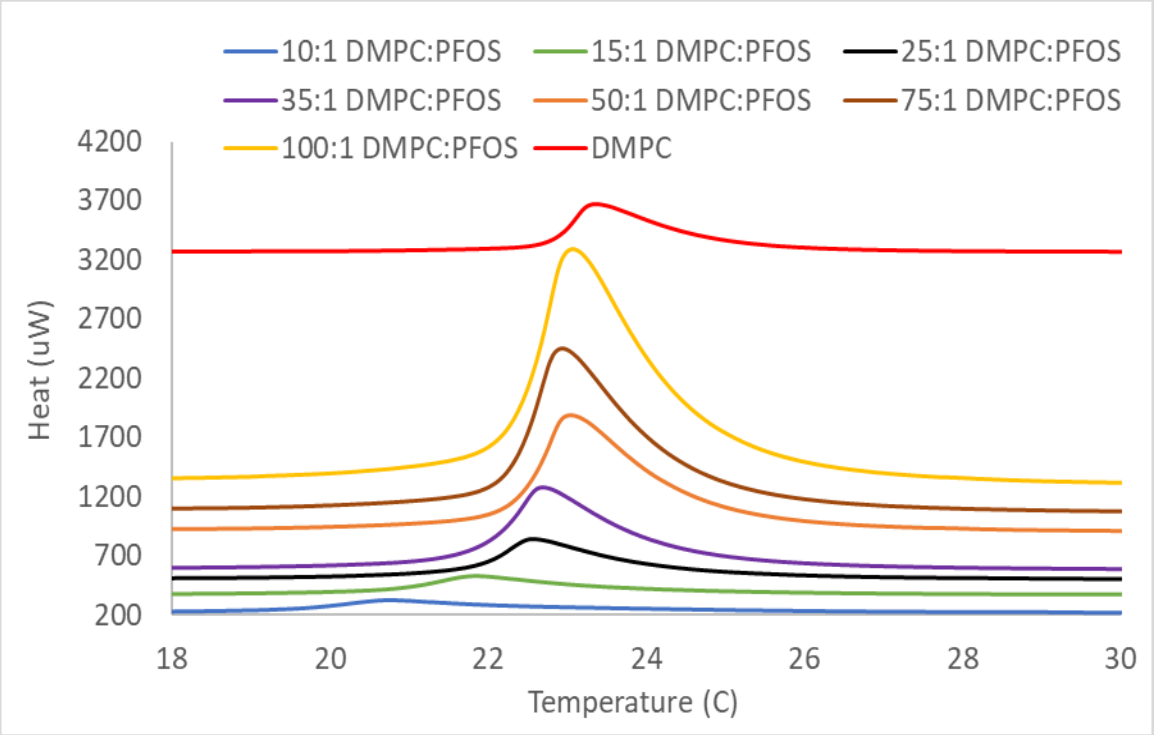

Figure 4.7: DSC trace for DMPC MLVs with varied ratios of PFOS. Data is staggered on the y-axis for visual convenience.

4.2.2 DMPC and DPPC SUV Phase Transition Studies

In addition to DMPC and DPPC MLVs with multiple bilayers, the effect which PFAS have on single bilayer SUV morphology was also investigated. PFOS and PFOA are used for DPPC and DMPC, respectively. DPPC SUVs with incorporated ratios of PFOS ranging from 10:1 to 60:1 equivalents of lipid to PFOS were created and associated phase transitions measured. DPPC SUVs with no PFOS give a phase transition temperature of 41.2 °C, then decrease to 40.8 °C at 60:1, finishing at 10:1 with a broad peak centering at approximately 39.9 °C (Table 4.5 and Figure 4.8).

Eq (Lipid:PFAS)	Phase Transition (°C)	Size (nm)
10:1	39.9 (Broad)	159
20:1	40.5	146
40:1	40.7	137
50:1	40.8	141
60:1	40.8	157
100:0	41.2	180

Table 4.5: Phase transition temperatures of DPPC SUVs with varying ratios of PFOS.

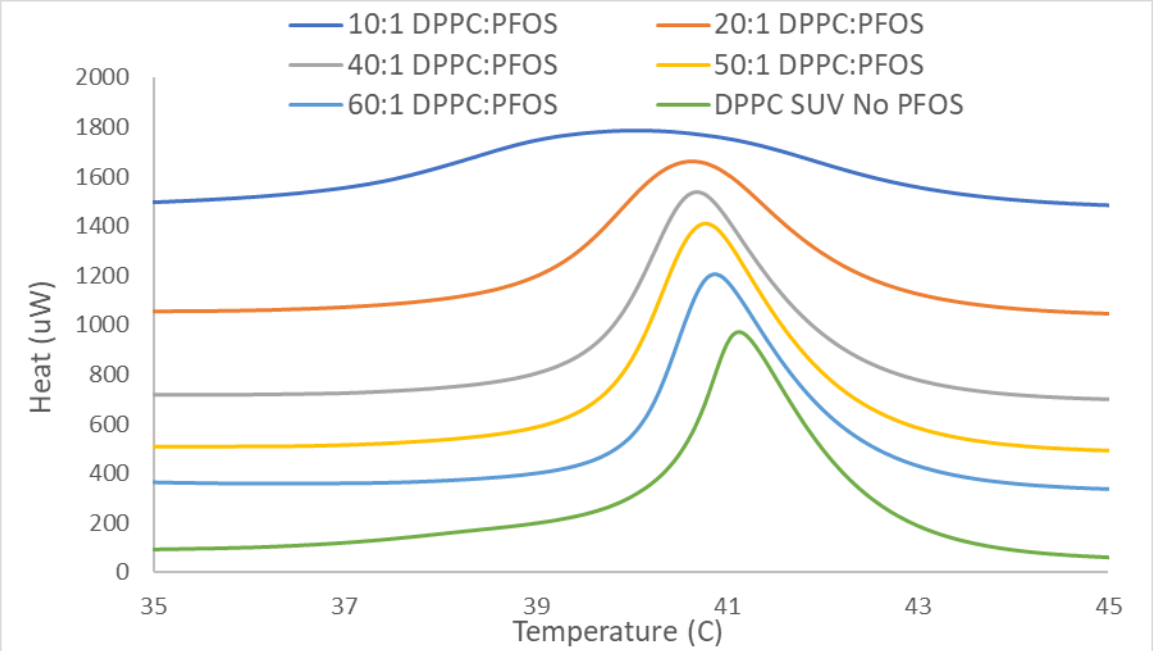

Figure 4.8: DSC trace for DPPC SUVs with varied ratios of PFOS. Data is staggered on the y-axis for visual convenience.

DMPC SUV phase transition temperatures were also measured in the presence of varying ratios of PFOA, again ranging from 10:1 to 60:1 equivalents of lipid to PFOA. Pure DMPC was observed to give a phase transition temperature of 24.2 °C, then decreases to 23.5°C at 60:1 and reaches 22.3 °C at 10:1 equivalents for a total difference of 1.9 °C (Table 4.6 and Figure 4.9). In comparison to the temperature difference of 1.3 °C from DPPC SUVs, it would appear again that DMPC liposomes have a greater shift in overall phase transition temperature upon PFAS incorporation.

Eq (Lipid:PFAS)	Phase Transition (°C)	Size (nm)
10:1	22.3	198
20:1	23.1	83.6
30:1	23.3	78.5
40:1	23.5	59.1
50:1	23.7	55.0
60:1	23.5	99.1
100:0	24.2	74.0

Table 4.6: Phase transition temperatures of DMPC SUVs at varying ratios of PFOA.

Other than the identity of the lipid and PFAS, the size of the vesicle itself appears to play a role in the degree of phase transition temperature shift. MLVs containing multiple phospholipid bilayers within the vesicle appear to have a lesser observable shift in temperature in comparison to their single bilayer SUV counterparts. This is evident when

comparing the total temperature difference of 0.9 °C from DMPC MLVs from no PFOA incorporation to 10:1 equivalents to those of DMPC SUVs, which give a total difference of 1.9 °C. Thus, it may be the case that incorporation of PFAS into a smaller vesicle has a more observable effect on the overall morphology.

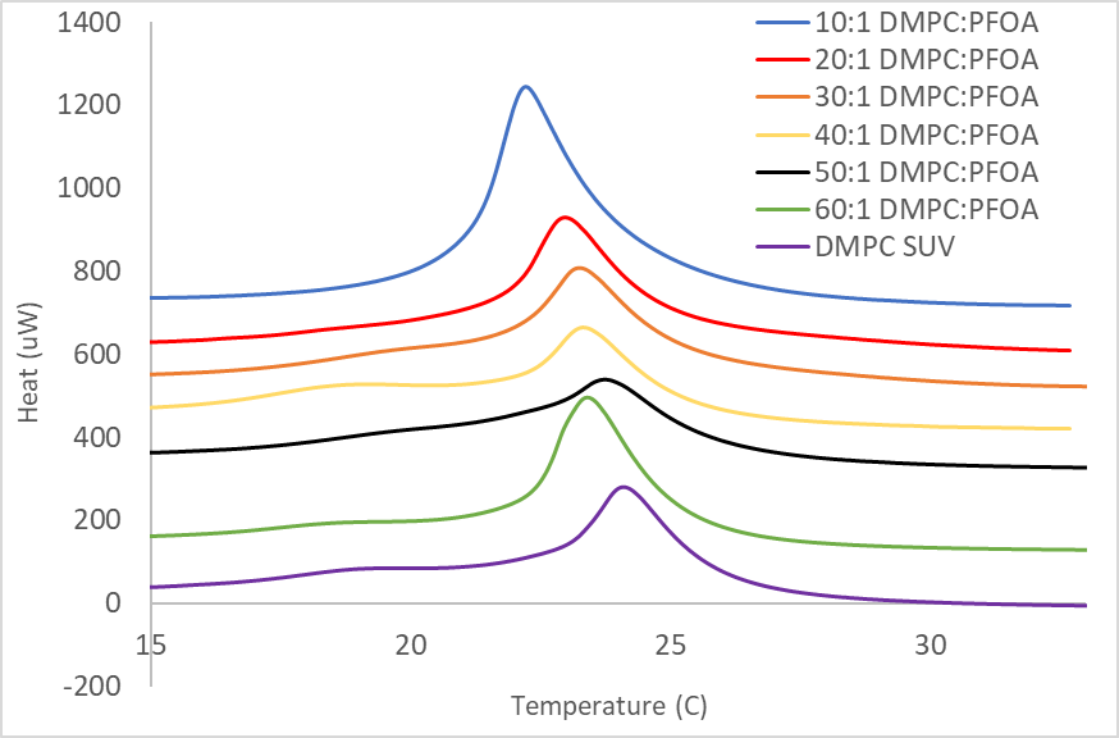

Figure 4.9: DSC trace for DMPC SUVs with varying ratios of PFOA. Data is staggered on the y-axis for visual convenience.

4.2.3 PFOS Uptake Kinetics of Lipid MLVs and SUVs

In addition to the effects of PFAS on lipid vesicle morphology, the time in which the contaminant is taken up into the membrane was also of interest. PFOS is selected rather than PFOA due to its greater observed effect on phase transition discussed previously. Initially, MLVs were synthesized separately from PFOS, which was then added to the

vesicles such that 25:1 lipid:PFAS would result. The resulting phase transition temperature was measured over time in order to gauge the uptake of PFOS (Figure 4.10).

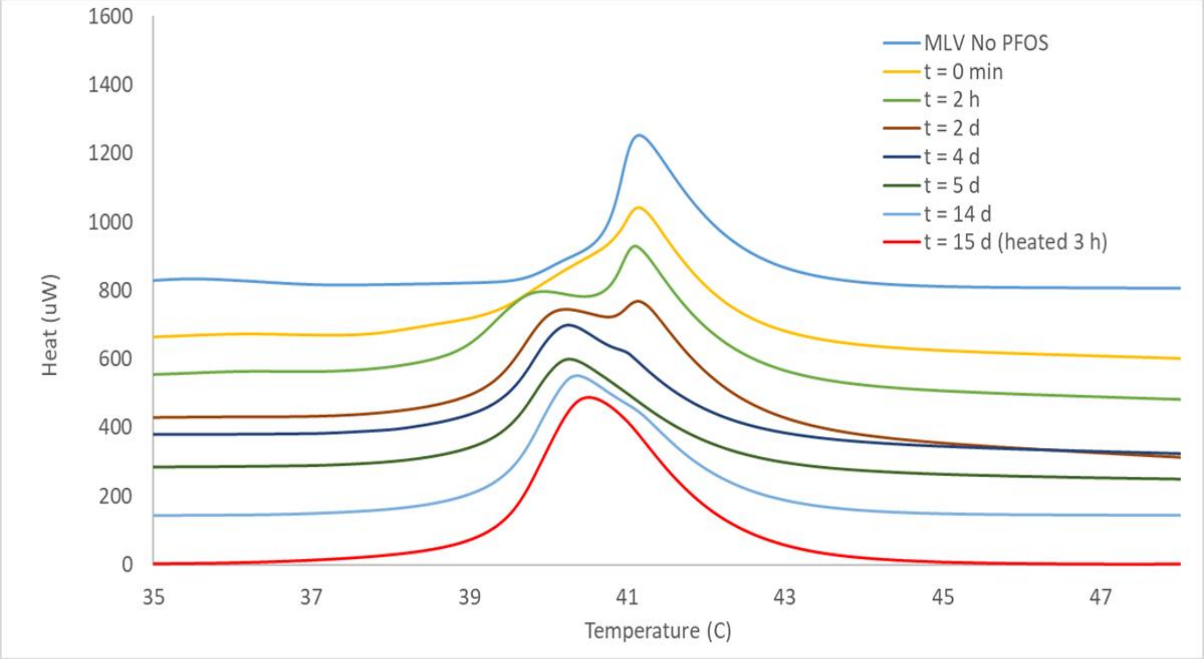

Figure 4.10: DSC traces over time of DPPC MLVs after addition of PFOS. Data is staggered on the y-axis for visual convenience.

DPPC MLVs with no addition of PFOS gave a phase transition temperature of 41.2 °C. After 2 hours of PFOS addition, two peaks can be observed with one overlapping at a temperature which corresponds to the MLV peak with no PFOS added, the other appearing at 40.0 °C. The later lower temperature peak is likely vesicles with PFOS beginning to accumulate, whereas the higher temperature peak may be vesicles which are still uncontaminated. The intensity of the lower temperature peak appears to increase as time passes, signifying that more PFOS is being incorporated into the vesicles. For instance, after four days at room temperature, the higher temperature peak appears drastically

reduced to a small shoulder. After 15 days at room temperature plus an additional three hours of heating at 45 °C, the DSC traces shows only the lower temperature peak indicating that all vesicles have been incorporated with PFOS.

The effect which multiple levels of bilayers plays into the uptake time of PFAS was also explored. As such, single bilayer DMPC SUVs were synthesized and added to a solution of PFOA such that a 40:1 lipid to PFAS ratio was achieved. The resulting phase transition of the PFOA incorporated vesicles occurs at a temperature of 23.2 °C, which is shifted from an initial temperature of 24.2 °C. such a shift occurs immediately after exposure to PFOA, as subsequent measurements of the PFOA incorporated SUVs yield overlapping peaks at a temperature of 23.2 °C indicating that likely all of the vesicles in solution have been subject to PFOA penetration (Figure 4.11).

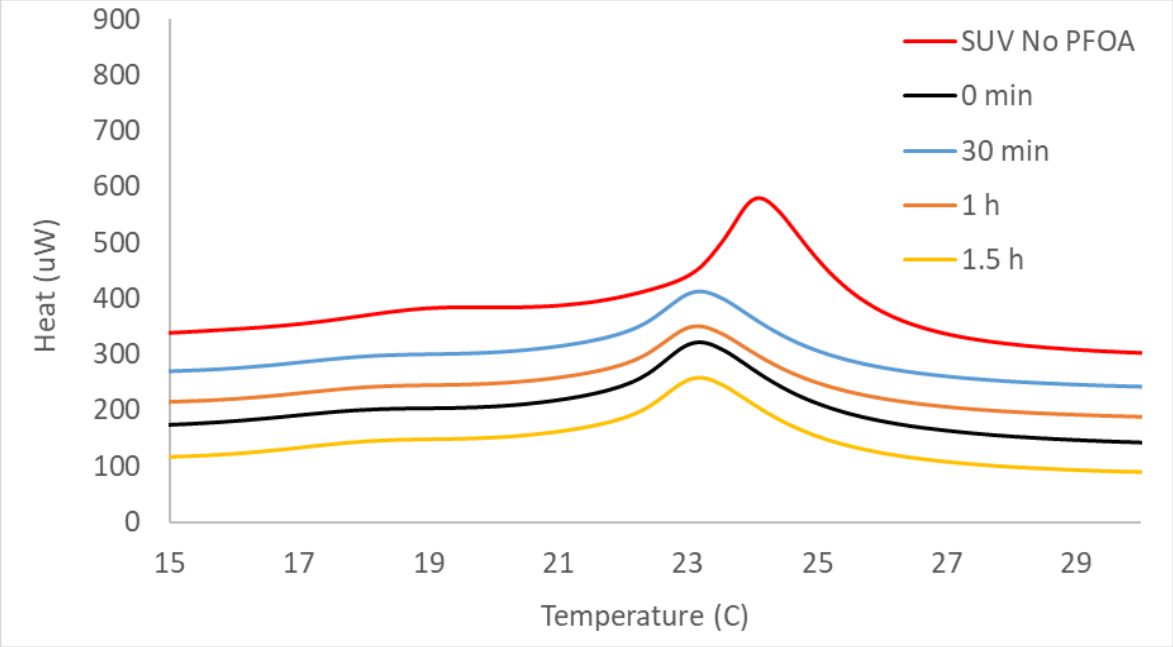

Figure 4.11: DSC traces over time of DMPC SUVs after addition of PFOS. Data is staggered on the y-axis for visual convenience.

The fast uptake of PFOA into SUVs as observed here is logical due to the presence of only one bilayer. It is likely that PFAS enters SUVs at a faster rate than in MLVs, where they must traverse multiple membranes. Furthermore, it may be that because SUVs are significantly smaller and contain only one bilayer, they require less PFAS incorporation in order to make any observable change in vesicle morphology.

4.2.4 Lipid Vesicle Stability in the Presence of PFOS

The stability of lipid SUVs after exposure to PFOS was also studied. This was accomplished by synthesizing SUVs from DPPC lipids and exposing them to PFOS such that a ratio of 1:1 lipid to PFAS was achieved. Vesicles were allowed to sit at room temperature and the corresponding phase transition temperatures of the SUV before PFOS addition, after PFOS addition overnight and three days after PFOS addition were measured (Figure 4.12).

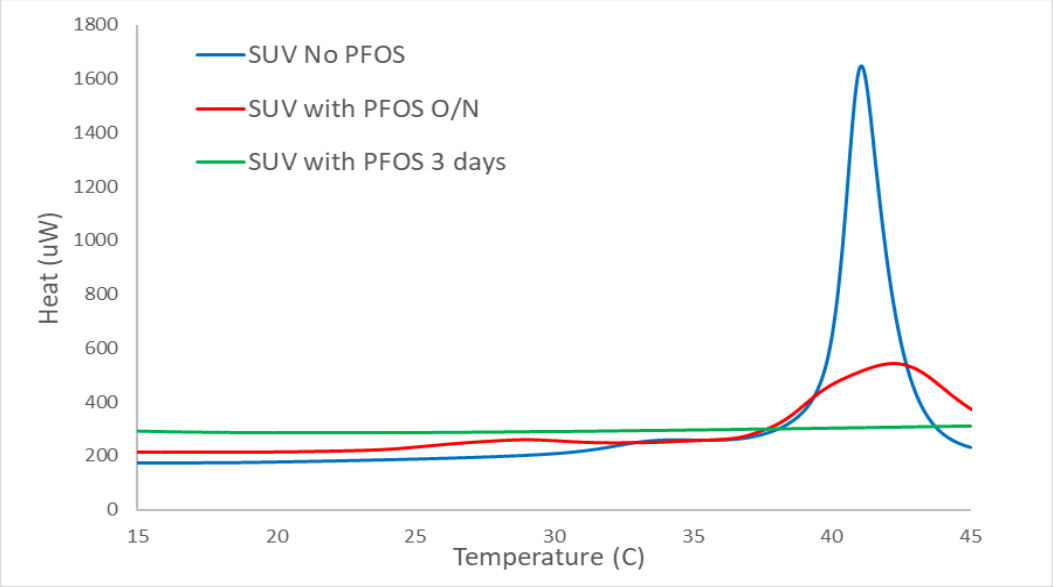

Figure 4.12: DSC trace of DPPC SUVs at varying times after incorporation of 1:1 equivalents of lipid to PFOS.

From the DSC trace, it can be observed that PFOS addition to the SUV causes a significant decrease in the intensity and sharpness of the initial peak, after sitting at room temperature overnight. Oddly, the downward shift in temperature is not observed in this case. However, the decrease in peak intensity may be indicative of vesicles deforming due to the large concentration of PFOS. After three days, there appears to be no peak present in the DSC trace which would seemingly imply all the vesicles in solution have incorporated an amount of PFOS which has disrupted the stability of the bilayers. Further insight may be gained from the approximate diameters of the vesicles over the course of the experiment.

Sample	Phase Transition (°C)	Average Size (nm)
SUV No PFOS	41.1	289
SUV with PFOS O/N	42.1	216
SUV with PFOS 3 days	No Peak	2051

Table 4.7: Phase transition temperatures and average diameters of DPPC SUVs before and after PFOS addition.

Initially, SUVs with no added PFOS gave an average diameter of 289 nm, then decreased to a diameter of 216 nm after addition of PFOS overnight. Measurement of the PFOS SUV sample after 3 days at room temperature gave a larger average vesicle size of 2051 nm (Table 4.7). A visual depiction of the DLS plot is shown in Figure 4.13, where it can be observed that SUV peaks near 100 nm mostly disappear after three days of PFOS addition. What remains are peaks located above 1000 nm, which are also present in the

initial SUV plot. It is unclear if these are larger liposomes or impurities such dust. Regardless, SUV peaks clearly lessen after addition of PFOS, corresponding with the DSC data suggesting membrane fouling by PFOS incorporation over time.

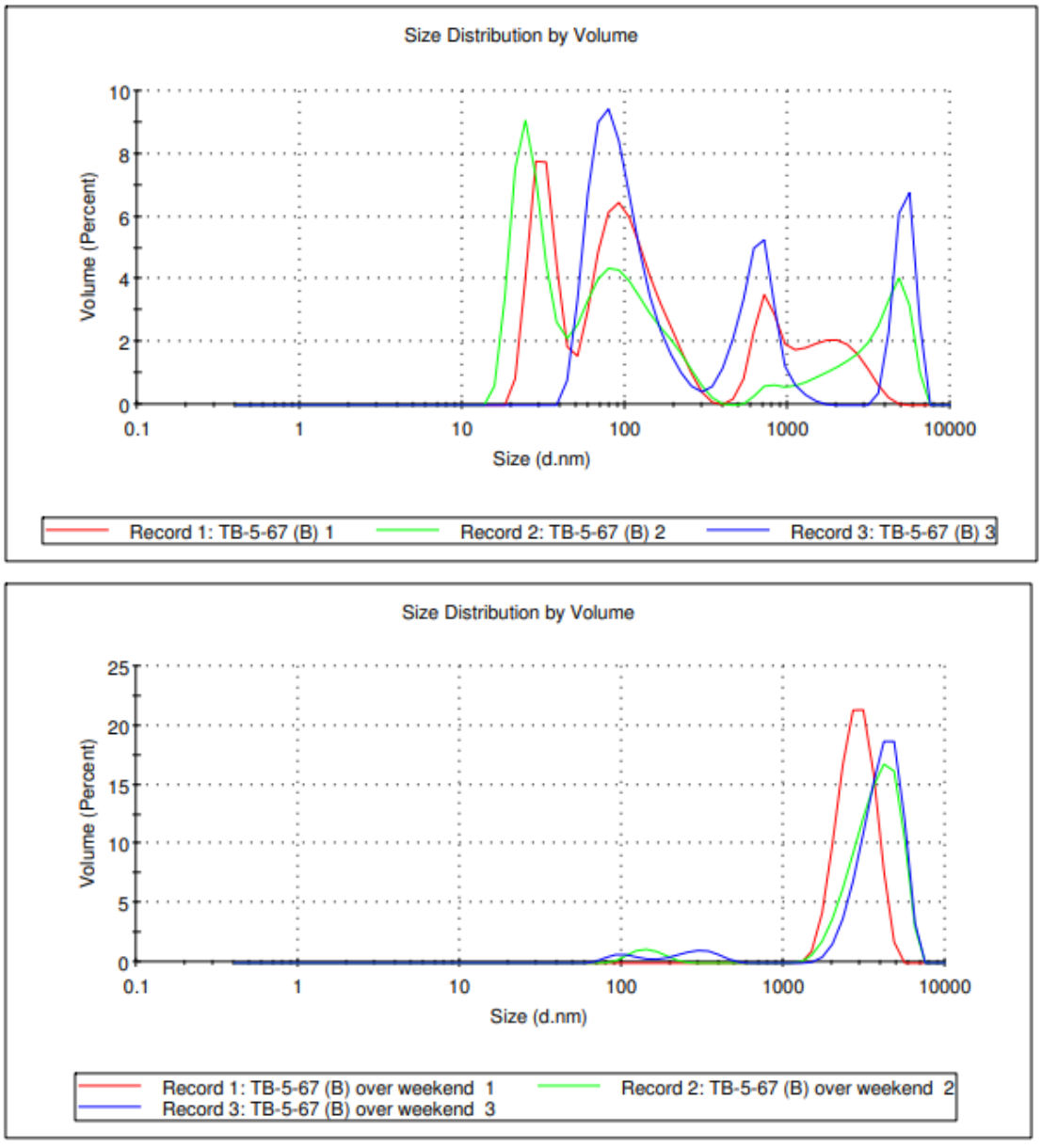

Figure 4.13: (Top): DLS plot of DPPC SUVs before PFOS addition. (Bottom): DLS plot of DPPC SUVs after PFOS addition over a period of three days.

Additional experiments regarding SUV stability in the presence of PFOS were also conducted. These included the monitoring of phase transition temperature over time of a DPPC SUV aliquot with a 1:2 ratio of lipid:PFAS. The aliquot was left in the DSC cell and measurements were taken at various time intervals. Thus, the lipid vesicles within this aliquot were cycled from a temperature of 5 °C to 55 °C throughout the experiment. The resulting data indicates that after 23 hours and 10 heating cycles, SUVs are deformed by PFOS and no longer show phase transitions (Figure 4.14).

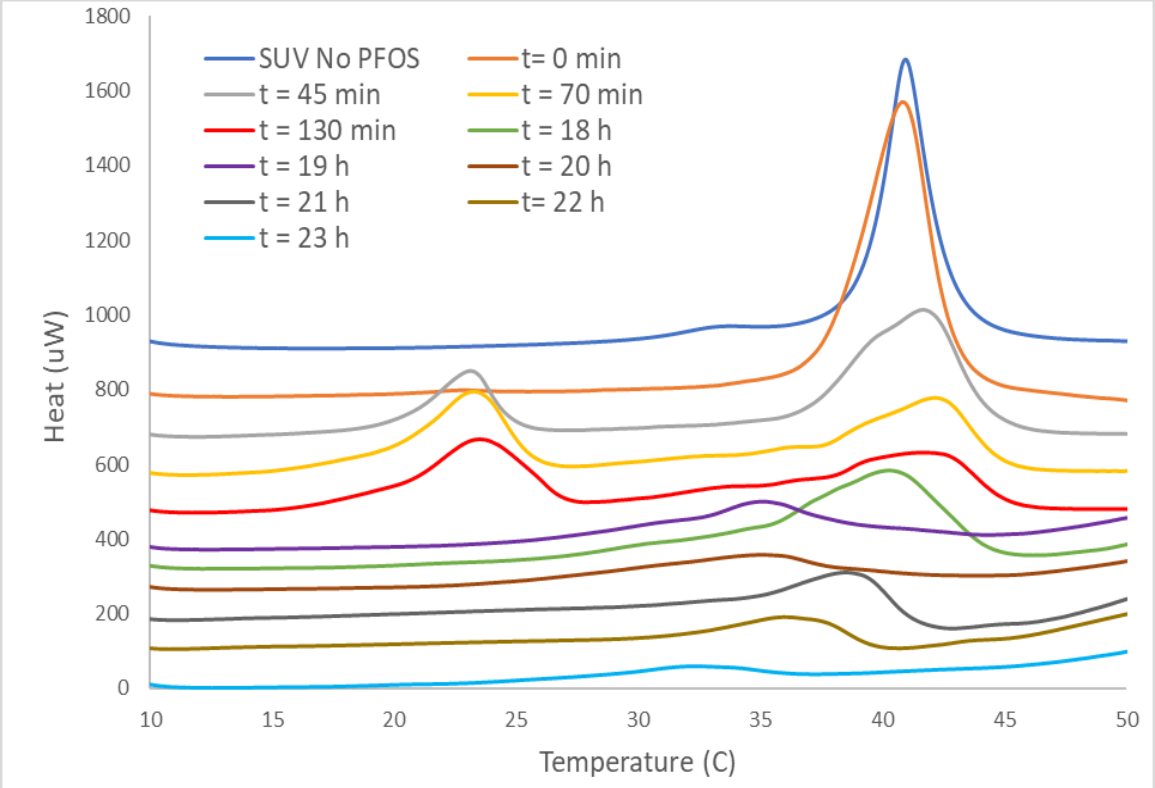

Figure 4.14: DSC trace over time of DPPC SUV aliquot with 1:2 equivalents of lipid:PFAS. Data is staggered on the y-axis for visual convenience.

As observed in previous experiments with stability of SUVs and PFOS, there is not a drastic shift in peak temperature. Rather, a decrease of peak intensity and sharpness over time, which signifies the deterioration of the lipid vesicle. It should be noted that vesicle

deformation occurs significantly faster when the sample undergoes continuous heating cycles than when left at room temperature. This is likely a result of increased membrane permeability upon heating past the phase transition temperature, which allows more PFOS to enter the vesicle therefore accelerating deformation. Furthermore, from 45 minutes to 130 minutes another peak can be observed at 23.3 °C in addition to the primary DPPC phase transition at 41 °C. This is likely a pre-transition of the lipid which is thought to be the result of ripple-like disruptions within the bilayer.[34] Such disorder is likely caused by the incorporation of large amounts of PFOS which more than likely distort said bilayers.

4.3 Conclusion

This project sought to explore the effects of PFAS on liposome vesicles of varying sizes and bilayer composition. Specifically, what effect the incorporation of PFAS have on the phase transition temperatures of DPPC and DMPC lipid vesicles. In addition, the overall vesicle membrane stability, and permeability were also studied. Additional inferences were drawn between the identity of the PFAS and the phospholipid chain length. It was found that incorporation of PFAS into lipid MLVs and SUVs shifts the phase transition to a lower temperature as PFAS concentration increases. Furthermore, the identity of the PFAS functional group appears to make a difference in the overall downward trend in temperature shift. Chain length of the lipid also appears to factor, with DMPC liposomes and PFOS displaying the most observable trend. The uptake of PFAS into lipid membranes was found to occur significantly faster in SUVs rather than MLVs likely due to the total levels of bilayers. In addition to membrane permeability towards PFAS, the stability of the vesicles in the presence of large concentrations of PFAS was also studied. Deformation of lipid vesicles was shown to occur at a much faster rate when heated

then when left at room temperature, likely due to increased membrane permeability resulting from heating the lipid over the phase transition temperature. Ultimately, the work discussed herein contributes to overall understanding of PFAS interactions with cellular membranes and broader adsorption capabilities to macromolecules.

4.4 Experimental

4.4.1 General Methods

All chemicals were purchased commercially unless noted otherwise. No additional purification methods were taken. Phase transition temperature of lipid vesicles were measured through a TA Instruments model 6300 Nano DSC at a heating rate of 2 °C per minute. Lipid vesicle size was determined by use of DLS on a Malvern Zetasizer Nano ZS instrument. Lipid vesicles were sized accordingly via an extrusion kit from Avanti Polar Lipids with associated membrane filters.

4.4.2 Synthesis of DMPC and DPPC MLVs

A representative procedure for the synthesis of DMPC and DPPC MLVs with incorporated PFAS is as follows. The lipid and PFAS were added to a 20 mL vial at the appropriate molar ratio. The solids were dissolved in chloroform, then a stream of air was passed over the solution to evaporate the solvent. The resulting film was then dried under vacuum. The lipid/PFAS film was hydrated with a solution of 0.1 mM NaCl in water at a temperature above the lipid phase transition temperature (DMPC: 25 °C, DPPC: 45 °C). Resulting solutions were then analyzed by DSC.

4.4.3 Synthesis of DMPC and DPPC SUVs

A representative procedure for the synthesis of DMPC and DPPC SUVs with incorporated PFAS is as follows. The lipid and PFAS were added to a 20 mL vial such that the appropriate molar ratio was reached. The solids were dissolved in chloroform, then a stream of air was passed over the solution to evaporate the solvent. The resulting film was dried under vacuum, then hydrated with a 0.1 mM NaCl solution above the lipid phase transition temperature. The resulting solution underwent three cycles of freezing and thawing in a dry ice acetone bath. SUVs were formed by passing the lipid solution through an extruder containing appropriate membrane pore sizes above the lipid phase transition temperature. The resulting SUV diameter was verified through DLS, and phase transition temperature obtained through DSC.

4.4.4 PFOS Uptake Kinetics of DPPC MLVs

DPPC (15 mg, 0.02 mmol) was added to a 20 mL vial and dissolved in 5 mL of chloroform. A stream of air was passed over the solution to evaporate the solvent. The resulting film was dried under vacuum, then hydrated with a 0.1 mM solution of NaCl in water and heated to 45 °C. 1 mL of a 0.8 mM solution of PFOS (0.0008 mmol) added to the lipid vesicles, then phase transition temperature was measured through DSC over time. After 15 days, the solution was heated at 45 °C for three hours then measured again.

4.4.5 PFOS Uptake Kinetics of DMPC SUVs

1 mL (25 mg, 0.04 mmol) of a 25 mg/mL DMPC solution in chloroform was placed under a stream of air to evaporate the solvent. The resulting lipid film was dried under vacuum then hydrated with 0.1 mM solution of NaCl in water at 25 °C. The lipid solution

underwent three freeze thaw cycles in a dry ice acetone bath, then sonicated in a water bath at 30 °C until a clear solution resulted. Vesicle size was verified though DLS. 1 mL of a 1 mM solution of PFOA (0.001 mmol) was added to the lipid solution and DSC measurements were taken every 30 minutes for two hours.

4.4.6 Stability of DPPC SUVs in the Presence of PFOS at Room Temperature

DPPC (15 mg, 0.02 mmol) was added to a 20 mL vial and dissolved in 1 mL of chloroform. A stream of air was passed over the solution to evaporate the solvent. The resulting film was dried under vacuum, then hydrated with 0.1 mM NaCl at 45 °C. The lipid solution then underwent three freeze thaw cycles in a dry ice acetone bath. The lipid vesicles were extruded using a 200 nm membrane filter, then DSC and DLS measurements were taken. PFOS (10 mg, 0.02 mmol) was added and DSC measurements were taken after letting the solution sit overnight, then over the course of three days.

4.4.7 Stability of DPPC SUVs in the Presence of PFOS During Heat Cycles

DPPC (15mg, 0.02 mmol) was dissolved in 1 mL of chloroform then solvent was evaporated by passing a stream of air over the solution. The resulting film was dried under vacuum then hydrated with 0.1 mM NaCl at 45 °C. The lipid solution underwent three freeze thaw cycles in a dry ice acetone bath then was extruded using a 200 nm membrane filter. Only 1 mL of lipid solution remained after extrusion (5 mg, 0.007 mmol). To this, PFOS (7 mg, 0.014 mmol) was added to make a 1:2 lipid:PFAS solution. A 0.650 mL aliquot of this solution was taken for DSC analysis. A total of 10 heat cycles were conducted over the course of 24 hours with a temperature range of 5 °C. to 50 °C.

4.5 References Cited

(1). Barry, V.; Winquist, A.; Steeland, K. Perfluorooctanoic Acid (PFOA) Exposures and Incident Cancers Among Adults and Living Near a Chemical Plant. *Environmental Health Perspectives*, **2013**, *121* (11-12), 1313-1318.

(2). Vieira, V. M.; Hoffman, K.; Shin, H. M.; Weinberg, J. M.; Webster, T. F.; Fletcher, T. Perfluorooctanoic Acid Exposure and Cancer Outcomes in a Contaminated Community: Geographic Analysis. *Environmental Health Perspectives*, **2013**, *121* (3), 318-323.

(3). DeWitt, J. C.; Peden-Adams, M. M.; Keller, J. M.; Germolec, D. R. Immunotoxicity of Perfluorinated Compounds: Recent Developments. *Toxicologic Pathology*, **2012**, *40* (2), 300-311.

(4). Dong, G. H.; Tung, K. Y.; Tsai, C. H.; Liu, M. M.; Wang, D.; Liu, W.; Jin, Y. H.; Hsieh, W. S.; Lee, Y. .; Chen, P. C. Serum Polyfluoroalkyl Concentrations, Asthma Outcomes, and Immunological Markers in a Case-Control Study of Taiwanese Children. *Environmental Health Perspectives*, **2013**, *121* (4), 507-513.

(5). Cardenas, A.; Gold, D.. R.; Hauser, R.; Kleinman, K. P.; Hivert, M. F.; Calafat, A. M.; Ye, X.; Webster, T. F.; Horton, E. S.; Oken, E. Plasma Concentrations of Per- and Polyfluoroalkyl Substances at Baseline and Associations with Glycemic Indicators and Diabetes Incidence Among High-Risk Adults in Diabetes Prevention Program Trial. *Environmental Health Perspectives*, **2017**, *125* (10), 107001.

(6). Wang, X.; Li, B; Zhao, W. D.; Liu, Y. J.; Shang, D. S.; Fang, W. G.; Chen, Y. H. Perfluorooctane Sulfonate Triggers Tight Junction "Opening" in Brain Endothelial Cells via Phosphatidylinositol 3-Kinase. *Biochemical and Biophysical Research Communications*, **2011**, *410* (2), 258-263.

(7). Johansson, N.; Fredriksson, A.; Eriksson, P. Neonatal Exposure to Perfluorooctane Sulfonate (PFOS) and Perfluorooctanoic Acid (PFOA) Causes Neurobehavioral Defects in Adult Mice. *Neurotoxicology*, **2008**, *29*, 160-169.

(8). Camdzic, M.; Aga, D. S.; Atilla-Gokcumen, E.; G. Cellular Interactions and Fatty Acid Transporter CD36-Mediated Uptake of Per- and Polyfluorinated Alkyl Substances (PFAS). *Chem. Res. Toxicol.*, **2022**, *35*, 694-702.

(9). Rosenmai, A. K.; Ahrens, L.; le Godec, T.; Lundqvist, J.; Oskarsson, A. Relationship Between Peroxisome Proliferator-Activated Receptor Alpha Activity and Cellular Concentration of 14 Perfluoralkyl Substances in HepG2 Cells. *J. Appl. Toxicol.*, **2018**, *38*, 219-226.

(10). Garcia, D. S.; Sjodin, M.; Hellstrandh, M.; Norinder, U.; Nikiforova V.; Lindberg, L.; Wincent, E.; Bergman, A.; Cotgreave, I.; Kos, V. M. Cellular Accumulation and Lipid Binding of Perfluorinated Alkylated Substances (PFASs) – A Comparison with Lysosomotropic Drugs. *Chemico-Biological Interactions*, **2018**, *281*, 1-10.

(11). Nouhi, S.; Ahrens, L.; Pereira, H. C; Hughes, A. V.; Campana, M.; Gutfreund, P.; Palsson, G. K.; Vorobiev, A.; Hellsing, M. S. Interactions of Perfluoroalkyl Substances with a Phospholipid Bilayer Studied by Neutron Reflectometry. *Journal of Colloid and Interface Science*, **2018**, *511*, 474-481.

(12). Krafft, M. P.; Riess, J. G. Per- and Polyfluorinated Substances (PFASs): Environmental Challenges. *Current Opinion in Colloid & Interface Science*, **2015**, *20* (3), 192-212.

(13). Fitzgerald, N. J. M.; Wargenau, A.; Sorenson, C.; Pedersen, J.; Tufenkji, N.; Novak, P. J.; Simick, M. F. Partitioning and Accumulation of Perfluoroalkyl Substances in Model Lipid Bilayers and Bacteria. *Environ. Sci. Technol.*, **2018**, *52*, 10433-10440.

(14). Xie, W.; Kania-Korwel, I.; Bummer, P. M.; Lehmler, H. J. Effect of Potassium Perfluorooctanesulfonate, Perfluorooctanoate and Octanesulfonate on the Phase Transition of Dipalmitoylphosphatidylcholine (DPPC) Bilayers. *Biochimica et Biophysica Acta*, **2007**, *1768*, 1299-1308.

(15). Lehmler, H. J.; Bummer, P. M. Mixing of Perfluorinated Carboxylic Acids with Dipalmitoylphosphatidylcholine. *Biochimica et Biophysica Acta*, **2004**, *1664*, 141-149.

(16). Wang, H.; Zhang, X.; Liu, X.; Liu, J. Stabilization of Liposomes by Perfluorinated Compounds. *ACS Omega*, **2018**, *3*, 15353-15360.

(17). Lehmler, H. J.; Xie, W.; Bothun, G. D.; Bummer, P. M.; Knutson, B. L. Mixing of Perfluorooctanesulfonic Acid (PFOS) Potassium Salt with Phosphatidylcholine (DPPC). *Colloids Surf B Biointerfaces*, **2006**, *51* (1), 25-29.

(18). Matyszewska D.; Tappura, K.; Oradd, G.; Bilewicz, R. Influence of Perfluorinated Compounds on the Properties of Model Lipid Membranes. *J. Phys. Chem. B*, **2007**, *111*, 9908-9918.

(19). Sujatha, J.; Mishra, A. K. Phase Transitions in Phospholipid Vesicles: Excited State Prototropism of 1-Napthol as a Novel Probe Concept. *Langmuir*, **1998**, *14*, 2256-2262.

(20). Ardail, D.; Privat, J. P.; Egert-Charlier, M.; Levrat, C.; Lerme, F.; Louisot, P. Mitochondrial Contact Sites. *Journal of Biological Chemistry*, **1990**, *265* (31), 18797-18802.

(21). Shen, Z.; Ge. J.; Ye, H.; Tang, S.; Li, Y. Cholesterol-like Condensing Effect of Perfluoroalkyl Substances on a Phospholipid Bilayer. *J. Phys. Chem. B*, **2020**, *124*, 5415-5425.

(22). Bruening, B.; Farago, B. Perfluorooctanoic Acid Rigidifies a Model Lipid Membrane. *Phys. Rev. E*, **2014**, *89*, 040702.

(23). Jbeily, M.; Baerenwald, R.; Joerg, K.; Saalwaechter, K.; Ferreira, T. M. Cholesterol-like Effects of a Fluorotelomer Alcohol Incorporated in Phospholipid Membranes. *Scientific Reports*, **2018**, *8*, 2154

.

(24). Gomez, A. G.; Hosseinidoust, A. Liposomes for Antibiotic Encapsulation and Delivery. *ACS Infect. Dis.*, **2020**, *6* (5), 896-908.

(25). Inoue, T.; Iwanaga, T.; Fukushima, K.; Shimozawa, R. Effect of Sodium Octanoate and Sodium Perfluorooctanoate on Gel-to-liquid-crystalline Phase Transition of Dipalmitoylphosphatidylcholine Vesicle Membrane. *Chemistry and Physics of Lipids*, **1988**, *46*, 25-30.

(26). Fitzgerald, N. J. M.; Simick, M. F.; Novak, P. J. Perfluoroalkyl Substances Increase the Membrane Permeability and Quorum Sensing Response in *Aliivibrio fischeri*. *Environ. Sci. Technol. Lett.*, **2018**, *5*, 26-31.

(27). Toni, L. D.; Nisio, A. D.; Rocca, M. S.; Pedrucci, F.; Garolla, A.; Dall'Acqua, S.; Guidolin, D.; Ferlin, A.; Foresta, C. Comparative Evaluation of the Effects of Legacy and New Generation Perfluoroalkyl Substances (PFAS) on Thyroid Cells *In Vitro*. *Front. Endocrinol.*, **2022**, *13*, 915096.

(28). Toni, L. D.; Radu, C. M.; Sabovic, I.; Nisio, A. D.; Dall'Acqua, S.; Guidolin, D.; Spampinato, S.; Campello, E.; Simioni, P.; Foresta, C. Increased Cardiovascular Risk Associated with Chemical Sensitivity to Perfluoro-Octanoic Acid: Role of Impaired Platelet Aggregation. *Int. J. Mol. Sci.*, **2020**, *21*, 399.

(29). Oldham, E. D.; Xie, W.; Farnoud, A. M.; Fiegel, J.; Lehmler, H. J. Disruption of Phosphatidylcholine Monolayers and Bilayers by Perfluorobutane Sulfonate. *J. Phys. Chem. B.* **2012**, *116*, 9999-10007.

(30). Jing, P.; Rodgers, P. J.; Amemiya, S. High Lipophilicity of Perfluoroalkyl Carboxylate and Sulfonate: Implications for Their Membrane Permeability. *J. Am. Chem. Soc.* **2009**, *131*, 2290-2296.

(31). McElhaney, R. N. Differential Scanning Calorimetric Studies of Lipid-Protein Interactions in Model Membranes. *Biochimica et Biophysica Acta*, **1986**, *864*, 361-421.

(32). McElhaney, R. N. The Use of Differential Scanning Calorimetry and Differential Thermal Analysis in Studies of Model and Biological Membranes. *Chemistry and Physics of Lipids*, **1982**, *30*, 229-259.

(33). Xie, W.; Ludewig, G.; Wang, K.; Lehmler, H. J. Model and Cell Membrane Partitioning of Perfluorooctanesulfonate is Independent of the Lipid Chain Length. *Colloids Surf B Biointerfaces*, **2010**, *76* (1), 128.

(34). Riske, K. A.; Barroso, R. P.; Vequi-Suplicy C. C.; Germano, R.; Henriques, V. B.; Lamy, M. T. Lipid Bilayer Pre-Transition as the Beginning of the Melting Process. *Biochimica et Biophysica Acta*, **2009**, *1788*, 954-963.